

Nasa CR-65358

M-58-65-3 14 APRIL 1966

M-58-65-3

FACILITY FORM 802

ACCESSION NUMBER	N66 25564	(THRU)	
(PAGES)	142	(CODE)	
(NASA CR OR TMX OR AD NUMBER)	CR-65358	(CATEGORY)	06

PHASE III FINAL REPORT

DESIGN AND FABRICATION OF
A TRACE CONTAMINANT REMOVAL SYSTEM FOR APOLLO

GPO PRICE \$

CFSTI PRICE(S) \$

Hard copy (HC) \$4.00

Microfiche (MF) 1.00

Prepared for National Aeronautics and Space Administration Under Contract No. NAS 9-3415

LIBRARY COPY

APR 15 1966

MANNED SPACECRAFT CENTER
HOUSTON, TEXAS

Lockheed

MISSILES & SPACE COMPANY

A GROUP DIVISION OF LOCKHEED AIRCRAFT CORPORATION

SUNNYVALE, CALIFORNIA

M-58-65-3 14 APRIL 1966

M-58-65-3

PHASE III FINAL REPORT

**DESIGN AND FABRICATION OF
A TRACE CONTAMINANT REMOVAL SYSTEM FOR APOLLO**

Prepared for National Aeronautics and Space Administration Under Contract No. NAS 9-3415

LIBRARY COPY

APR 15 1966

Lockheed

MISSILES & SPACE COMPANY

A GROUP DIVISION OF LOCKHEED AIRCRAFT CORPORATION

SUNNYVALE, CALIFORNIA

MANNED SPACECRAFT CENTER
HOUSTON, TEXAS

FOREWORD

This report describes the work accomplished between September 1965 and February 1966 by the Lockheed Missiles and Space Company (LMSC) under Contract NAS 9-3415 "Design and Fabrication of a Trace Contaminant Removal System for Apollo."

The work reported herein constitutes Phase III of a three phase program for the Crew Systems Division of the NASA Manned Spacecraft Center.

The Phase I effort encompassed theoretical and experimental efforts in sorption and catalysis; engineering analysis, optimization, and prototype hardware design, and test planning for final evaluation of the hardware.

The Phase II effort encompassed the fabrication, assembly, and successful experimental evaluation of the prototype hardware.

The Phase III effort, reported herein, encompassed experiments (1) to verify the "potential-plot" approach for prediction of sorbent capacity, (2) to determine the low temperature CO conversion efficiency of two catalysts when exposed to a typical catalyst poison (H_2S), and (3) to determine the oxidation efficiency of one catalyst for multiple contaminants including CO, H_2 , and CH_4 at temperatures in the 450-550° F range. In addition to the above, a combined theoretical and experimental effort was conducted in an attempt to correlate the results of "retention-time" and "flow-type" experiments, to facilitate future predictions of sorbent performance characteristics.

Mr. J. M. Smith was manager of the program at LMSC. The "potential-plot" absorption, carbon monoxide oxidation, and adsorption correlation investigations were directed by Dr. E. V. Ballou, assisted by Drs. F. G. Borgardt and A. J. Robell. Mr.

T. M. Olcott directed the experimental work on catalyst oxidation efficiency in the presence of multiple contaminants. Professor R. Merrill, University of California Department of Chemical Engineering collaborated with Dr. Robell on the prediction of breakthrough curve characteristics.

The contract monitor was Mr. M. Owen, Environmental Control Development Section, Crew Systems Division, NASA Manned Spacecraft Center.

ABSTRACT

Experiments were conducted to obtain points on a "potential-plot" for 15 contaminants on four sorbent materials. Two experiments were conducted to establish the CO conversion efficiencies of 1% Pt - 1% Pd and 0.5% Pd catalysts in the presence of H_2S at approximately the space-cabin maximum allowable concentration. Additional experiments were conducted to determine the simultaneous oxidation efficiencies of the 0.5% Pd catalyst for CO, H_2 , CH_4 and other contaminants in the temperature range of 450-550° F. Studies and experiments were also conducted to explore the possible correlation of contaminant retention-time with both saturation capacity and dynamic contaminant removal behavior.

CONTENTS

Section		Page
	FOREWORD	iii
	ABSTRACT	v
	ILLUSTRATIONS	ix
	TABLES	xiii
1	INTRODUCTION	1-1
	1.1 Introduction	1-1
	1.2 Summary	1-1
2	POTENTIAL-PLOT VERIFICATION	2-1
	2.1 Objectives	2-1
	2.2 Apparatus	2-4
	2.3 Procedure	2-7
	2.4 Results	2-7
	2.5 Discussion	2-8
3	RETENTION-TIME CORRELATION AND DYNAMIC BEHAVIOR PREDICTIONS	3-1
	3.1 Retention-Time Versus Saturation Capacity	3-1
	3.2 Correlation of Retention-Time Data With Dynamic Break- through Curves	3-6
4	CATALYST TESTS—CO CONVERSION AND H ₂ S POISONING	4-1
	4.1 Objectives	4-1
	4.2 Apparatus	4-1
	4.3 Procedure	4-3
	4.4 Results	4-3
	4.5 Discussion	4-3
5	CATALYST TESTS—OXIDATION EFFICIENCY OF 0.5% PD CATALYST	5-1
	5.1 Objectives	5-1
	5.2 Apparatus	5-1

Section	Page
5.3 Procedure	5-4
5.4 Results	5-5
5.5 Discussion	5-5
6 6.1 Conclusions	6-1
6.2 Recommendations	6-4
Appendix	
A DATA FROM DYNAMIC ADSORPTION TESTS	A-1

ILLUSTRATIONS

Figure		Page
2-1	Flow Test Apparatus—Schematic	2-5
2-2	Apparatus for Adsorption Studies	2-6
2-3	Potential Plot for BD Charcoal	2-10
2-4	Potential Plot for AC Charcoal	2-11
2-5	Potential Plot for C1 Charcoal	2-12
2-6	Potential Plot for MSA Fiber	2-13
2-7	Comparison of Sorbent Capacities	2-14
3-1	Retention—Time/Capacity Correlation for BD Charcoal	3-3
3-2	Retention—Time/Capacity Correlation for AC Charcoal	3-4
3-3	Retention—Time/Capacity Correlation for C1 Charcoal	3-5
3-4	Concentration vs. Time for a Typical Continuous-Flow Experiment	3-6
3-5	Normalized Concentration-Time Plot for a Continuous-Flow Experiment	3-7
3-6	Normalized Results for an Injection Experiment	3-8
3-7	Correlation of Injection and Flow Experiments Freon-12 on AC	3-11
3-8	Correlation of Injection and Flow Experiments Freon-12 on BD	3-12
3-9	Correlation of Injection and Flow Experiments CH ₄ on BD	3-13
3-10	Correlation of Injection and Flow Experiments CH ₄ on BD	3-14
3-11	Correlation of Injection and Flow Experiments CH ₄ on BD	3-15
3-12	Definition of W for an Injection Pulse	3-17
3-13	Definition of W _f for a Breakthrough Curve	3-17
3-14	Peclet Number vs $N_p d_p / b L$	3-19
3-15	Correction Factor, b, vs. r and ζ From Reference	3-20
3-16	C/C _i vs. Number of Plates and Dimensionless Time	3-20
3-17	Correlation of Experimental and Theoretical Breakthrough Curves Freon-12 on AC	3-23

Figure		Page
3-18	Correlation of Experimental and Theoretical Breakthrough Curves n-Butane on BD	3-25
3-19	Correlation of Experimental and Theoretical Breakthrough Curves n-Butane on BD	3-26
3-20	Correlation of Experimental and Theoretical Breakthrough Curves n-Butane on BD	3-27
4-1	Apparatus for Catalyst Studies	4-2
4-2	CO Conversion vs. Time-1% Pt, 1% Pd Catalyst	4-4
4-3	CO Conversion vs. Time, 0.5% Pd Catalyst	4-5
4-4	H ₂ S Concentration vs. Time Over 0.5% Pd Catalyst	4-6
4-5	H ₂ S Concentration vs. Time Over 0.5% Pd Catalyst	4-7
5-1	Apparatus For Oxidation Efficiency Tests Schematic Diagram	5-2
5-2	Test Apparatus for Oxidation Efficiency Tests	5-3
5-3	Methane Oxidation Efficiency in Presence of Contaminants Listed in Table 5-1	5-6
5-4	Final Oxidation Efficiency Test Results Without Freon-12	5-7
5-5	Final Oxidation Efficiency Test Results With Freon-12	5-14
A-1	Run Number 103	A-5
A-2	Run Number 104	A-6
A-3	Run Number 105	A-7
A-4	Run Number 106	A-8
A-5	Run Number 107	A-9
A-6	Run Number 108	A-10
A-7	Run Number 109	A-11
A-8	Run Number 110	A-12
A-9	Run Number 111	A-13
A-10	Run Number 112	A-14
A-11	Run Number 113	A-15
A-12	Run Number 114	A-16
A-13	Comparison of Run Numbers 108 and 114	A-17
A-14	Run Number 115	A-18
A-15	Comparison of Run Numbers 105 and 115	A-19
A-16	Run Number 116	A-20

Figure		Page
A-17	Run Number 117	A-21
A-18	Run Number 118	A-22
A-19	Run Number 119	A-23
A-20	Run Number 120	A-24
A-21	Run Number 121	A-25
A-22	Run Number 122	A-26
A-23	Run Number 123	A-27
A-24	Run Number 124	A-28
A-25	Run Number 125	A-29
A-26	Run Number 126	A-30
A-27	Run Number 127	A-31
A-28	Run Number 128	A-32
A-29	Run Number 129	A-33
A-30	Run Number 130	A-34
A-31	Run Number 131	A-35
A-32	Run Number 132	A-36
A-33	Run Number 133	A-37
A-34	Run Number 134	A-38
A-35	Run Number 135	A-39
A-36	Run Number 136	A-40
A-37	Run Number 137	A-41
A-38	Run Number 138	A-42
A-39	Run Number 139	A-43
A-40	Run Number 140	A-44
A-41	Run Number 141	A-45
A-42	Run Number 142	A-46
A-43	Run Number 143	A-47
A-44	Run Number 144	A-48
A-45	Run Number 145	A-49
A-46	Run Number 146	A-50
A-47	Run Number 147	A-51

TABLES

Table		Page
2-1	Sorbent Studies	2-2
2-2	Contaminants Studied With BD Charcoal	2-3
2-3	Summary of Breakthrough Curve Data For BD Charcoal	2-8
3-1	Summary of Runs 50, 51, and 53	3-24
5-1	Contaminants Used in Initial Oxidation Efficiency Tests	5-4
5-2	Contaminants Used in Final Oxidation Efficiency Tests	5-5
5-3	Final Oxidation Efficiency Test Results - Without Freon-12	5-8
5-4	Final Oxidation Efficiency Test Results - With Freon-12	5-9
5-5	Predicted Order of Oxidation Efficiency For Single Contaminants	5-13
A-1	Summary of Dynamic Adsorption Experiments	A-2
A-2	Injection Experiments	A-3
A-3	Injection Experiments - Flow Rate Effects	A-4
A-4	Injection Experiments - Volume Effects	A-4

Section 1
INTRODUCTION AND SUMMARY

1.1 INTRODUCTION

In the previous phases of this program, reported in Refs. 1 and 2, a number of contaminant removal techniques were investigated and sufficient data obtained to allow prototype hardware design for a contaminant removal unit for Apollo. The hardware was fabricated and subjected to a 5-day test under simulated Apollo Command Module conditions.

In the course of the above work certain performance prediction techniques were evolved and certain performance characteristics of the hardware were noted which suggested further investigations. Under Phase III these investigations were conducted to confirm the design posture of the prototype hardware.

1.2 SUMMARY

The Phase III investigations included additional experiments to verify the "potential-plot" approach for predicting the saturation capacity of sorbents for contaminants of interest; testing of 1% Pt-1% Pd and 0.5% catalysts to determine low temperature CO conversion efficiencies, prior to and in the presence of H_2S , at approximately the space-cabin maximum allowable concentration; and determination of the simultaneous oxidation efficiencies of the 0.5% Pd catalyst for CO, H_2 , CH_4 and other contaminants in the temperature range of 450-550° F. Studies and experiments were also conducted to explore the possible correlation of contaminant retention time with both saturation capacity and dynamic contaminant removal behavior.

1. "Design and Fabrication of a Trace Contaminant Control System for Apollo," M-58-65-1, Lockheed Missiles and Space Co., Sunnyvale, California, 15 March 1965.
2. "Design and Fabrication of a Trace Contaminant Control System for Apollo, Phase II," M-58-65-2, Lockheed Missiles and Space Co., Sunnyvale, California, 23 November 1965.

Section 2
POTENTIAL-PLOT VERIFICATION

2.1 OBJECTIVES

This work was undertaken to provide additional verification of the correlation reported in Ref. 1, of contaminant volume adsorbed, q , with the parameter

$$A = \frac{T}{V_m} \log_{10} \frac{P_s}{P}$$

where

- T = temperature of adsorption, ($^{\circ}\text{K}$)
- V_m = molar volume of adsorbate as a liquid at its normal boiling point
(cc liq./mole)
- P_s = vapor pressure of adsorbate at adsorption temperature
- P = partial pressure of adsorbate

The additional experimental work was to cover a wider range of the parameter A than had been accomplished in Phase I of this program; to involve more contaminant species, including sulfur containing compounds; and to deal with the four sorbents listed in Table 2-1.

Table 2-1
SORBENTS STUDIES

Manufacturer	Designation	Description	Hereafter Referred To As
Barnebey-Cheney Co.	BD	Coconut shell charcoal	BD
Barnebey-Cheney Co.	AC	Coconut shell charcoal	AC
LMSC	C1	Acid-impregnated BD charcoal	C1
Mine Safety Appliance Co.	fibrous carbon	Carburized synthetic fiber	MSA

Since the previous work had been primarily with Type BD charcoal, this sorbent was studied with the greatest number of additional contaminants in order to build the maximum data base possible. Contaminants tested on BD are presented in Table 2-2.

Table 2-2

CONTAMINANTS STUDIED WITH BD CHARCOAL

Identification No. *	Species	A	Studied In Phase I Only
42	Freon-114	14.4	X
73	Propyl Mercaptan	14.8	
8	n-Butane	17.2	
9	Butene-1	18.5	X
39	Freon-12	22.5	
82	Freon-21	23.7	
71	Propane	24.3	
84	Vinyl Chloride	27.3	
68	Propylene	27.6	
40	Freon-22	30.8	
64	Methyl Mercaptan	32	
41	Freon-23	40.4	
33	Ethylene	42.1	
62	Methane	42.1	
3	Acetylene	49.2	

Freon-114 and butene-1 were tested only in Phase I. n-butane, Freon-12, propylene and Freon-23 were tested in Phase I as well as in the work reported herein.

*For reference to Phase I work.

Contaminants were selected to cover as wide a range of the parameter A as possible and still be measurable at the SMAC.*

The sorbents AC, C1, and MSA were tested with butane, Freon-12, Freon-22, ethylene, and acetylene. The purpose of these tests was to compare the performance of these sorbents with that of BD, over a reasonable range of A.

Contaminants at concentrations approximating SMAC were flowed through beds of the sorbents and breakthrough curves determined; from these the volume adsorbed, q , — also called the retentivity or adsorptivity — was calculated. The correlation between q and the potential plot parameter A was studied.

2.2 APPARATUS

A flow system, similar to that used in Phase I of this work, was used to allow the determination of the capacities and dynamic performance of selected adsorbents under conditions simulating the expected conditions at the sorbent inlet of the Apollo system; i.e., temperature of 43.8° C, water vapor partial pressure of 15.5 torr corresponding to a relative humidity of 23%, 5 psia total pressure in an atmosphere of 0.8% CO₂ in O₂.

The flow system is shown in Figs. 2-1 and 2-2. The interconnecting tubing is 1/4 in. stainless steel with Swagelok connections to valves, gages, and meters. A Beckman solenoid-operated gas sampling valve was used to ensure sampling reproducibility.

The analytical instrument used was an F&M Scientific Co. Model 810 Research Chromatograph; a flame ionization detector was used for the work described herein.

*space cabin maximum allowable concentration.

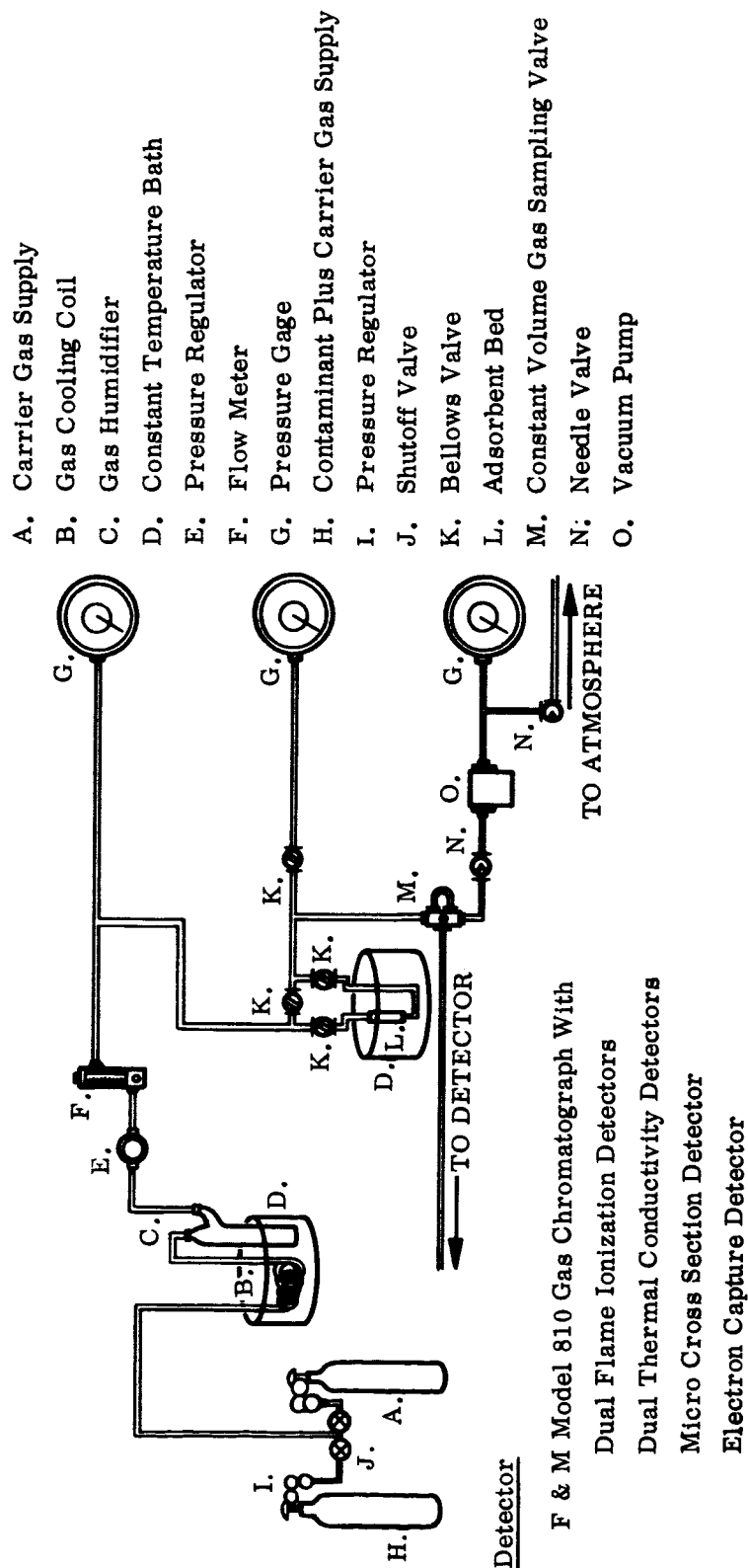


Fig. 2-1 Flow Test Apparatus - Schematic

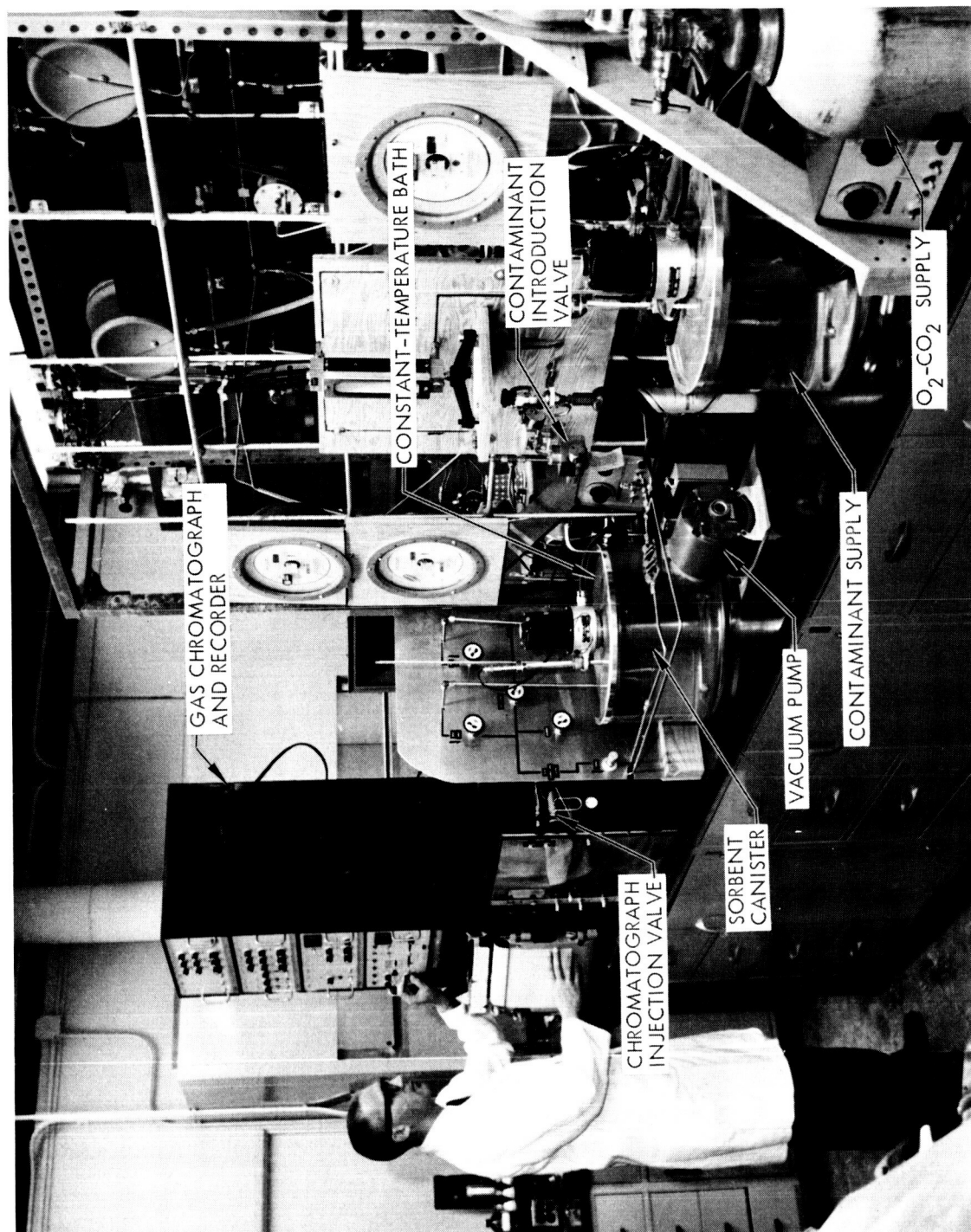


Fig. 2-2 Apparatus for Adsorption Studies

2.3 PROCEDURE

All contaminants studied were pre-mixed in cylinders of oxygen containing 0.8% CO₂, purchased from the Matheson Co.

A carrier gas of O₂ with 0.8% CO₂ and no contaminant present was used to equilibrate the adsorbent bed prior to each run.

All gases contacting the adsorbent beds were first passed through a humidifier, attaining the water vapor content mentioned above.

The adsorbent bed, immersed in a constant temperature bath, was preconditioned with flowing diluent gas at experimental conditions for approximately 1 hour. The adsorbent bed was then isolated and the contaminant-containing mixture was then diverted through a by-pass. The concentration of the contaminant was monitored by injection of constant known-volume aliquots into the gas chromatograph through the gas sampling valve. Multiplication of the area of the contaminant peak by a previously determined calibration factor gave the concentration. After the inlet concentration was established, the contaminant-carrying stream was directed into the adsorbent bed, marking time zero for the run. The effluent concentration was monitored throughout the run by the periodic injection of 2-cc samples from the effluent gas stream into the gas chromatograph. The amount of contaminant present in the effluent gas was plotted versus time to obtain the contaminant breakthrough curves. Retentivities were obtained by integrating the area defined by the breakthrough curve, the inlet concentration, and the coordinate axes.

2.4 RESULTS

All adsorption data are presented in Appendix A. A summary of the adsorption experiment conditions and results is presented in Table A-1 in the Appendix. In addition to the flow runs made for potential plot verification, some "pulse" or injection runs are also reported. These were for purposes of retention time correlation and will be discussed in a later section.

Runs which did not have significant uncertainties associated with them are plotted in the potential plot format in Figs. 2-3, 2-4, 2-5 and 2-6 for each of the four sorbents studied. Also plotted in Fig. 2-3 are adsorption data on BD from Phase I work. The data plotted in Fig. 2-3 are identified in Table 2-3. In Figs. 2-4, 2-5 and 2-6, a number opposite each point indicates the run number.

The lines designated as 1 and 2 in Figs. 2-3 through 2-6 represent the best correlations for Freon compounds (line 1) and for hydrocarbons (line 2).

The relative capacity of the four sorbents for Freons is compared in Fig. 2-7, which is a re-plot of line 1 from each of the preceding four figures. For q -values above 5×10^{-4} cc liq/g, sorbent capacity in decreasing order is: BD, AC, C1, and MSA.

2.5 DISCUSSION

In general, the data presented are considered to be quite accurate. An analysis of maximum expected errors, for example, is summarized in Fig. A-14 (run 115).

Table 2-3
SUMMARY OF BREAKTHROUGH CURVE DATA FOR BD CHARCOAL

Run No.	Contaminant	T° C	(mg/m ³)	Average Inlet Concentration (ppm)	q (cc liq/g)	A
1	Freon-12	43.8	9.95×10^3	6.0×10^3	6.66×10^{-2}	14.6
3	Freon-12	43.8	9.6×10^3	5.8×10^3	5.83×10^{-2}	14.6
150	Propyl Mercaptan	43.8	48.6	46.5	3.5×10^{-2}	14.8
5	Freon-12	43.8	2.16×10^3	1.3×10^3	2.60×10^{-2}	17.3
27	Freon-12	43.8	1.5×10^3	9.8×10^2	2.68×10^{-2}	17.6
28	Freon-12	43.8	1.44×10^3	8.7×10^2	2.59×10^{-2}	17.8
52	n-butane	43.8	35.1	44.	2.18×10^{-2}	17.9
15	Freon-12	51.0	1.82×10^3	1.1×10^3	2.27×10^{-2}	18.0

Table 2-3 (cont.)

Run No.	Contaminant	T° C	(mg/m ³)	Average Inlet Concentration (ppm)	q (cc liq/g)	A
16	Freon-12	51.0	1.66×10^3	1.0×10^3	1.84×10^{-2}	18.1
20	Freon-12	51.0	1.66×10^3	1.0×10^3	2.49×10^{-2}	18.1
53	n-butane	43.8	27.8	35.	2.69×10^{-2}	18.3
8	Freon-12	57.5	1.99×10^3	1.2×10^3	1.83×10^{-2}	18.7
10	Freon-12	57.5	1.82×10^3	1.1×10^3	1.55×10^{-2}	18.9
7	Freon-12	57.5	1.5×10^3	9.8×10^2	1.59×10^{-2}	19.0
19	Freon-12	51.0	1.41×10^3	8.5×10^2	1.46×10^{-2}	19.0
9	Freon-12	57.5	1.66×10^3	1.0×10^3	1.84×10^{-2}	19.1
23	1-butene	51.0	47.7	62.	2.17×10^{-2}	19.5
120	Freon-12	43.8	93.6	56.5	3.06×10^{-3}	22.5
144	Freon-21	43.8	83.2	50.2	7.75×10^{-3}	23.7
104	Propane	43.8	47.8	79.	3.54×10^{-3}	24.3
34	Propylene	43.8	865.0	1.5×10^2	4.26×10^{-3}	26.5
126	Vinyl Chloride	43.8	61.7	72.	4.04×10^{-3}	27.3
112	Propylene	43.8	45.6	79.	2.54×10^{-3}	27.6
146	Freon-22	43.8	66.5	56.	5.03×10^{-4}	30.8
133	Freon-22	43.8	62.8	53.	5.74×10^{-4}	30.8
151	Methyl Mercaptan	43.8	81.5	124.	2.45×10^{-3}	32.0
33	Freon-23	43.8	105.	1.1×10^2	3.74×10^{-5}	39.4
131	Freon-23	43.8	68.	71.	2.56×10^{-5}	40.4
105	Ethylene	43.8	31.0	81.	4.96×10^{-5}	42.0
129	Methane	43.8	1.87×10^3	8.55×10^3	2.01×10^{-4}	44.3
115	Ethylene	43.8	23.4	61.	2.66×10^{-5}	42.6
141	Methane	43.8	1.37×10^3	6.25×10^3	1.16×10^{-4}	44.3
109	Acetylene	43.8	21.4	60.	1.34×10^{-5}	49.2
103	Methane	43.8	168.	765.	2.33×10^{-5}	52.0

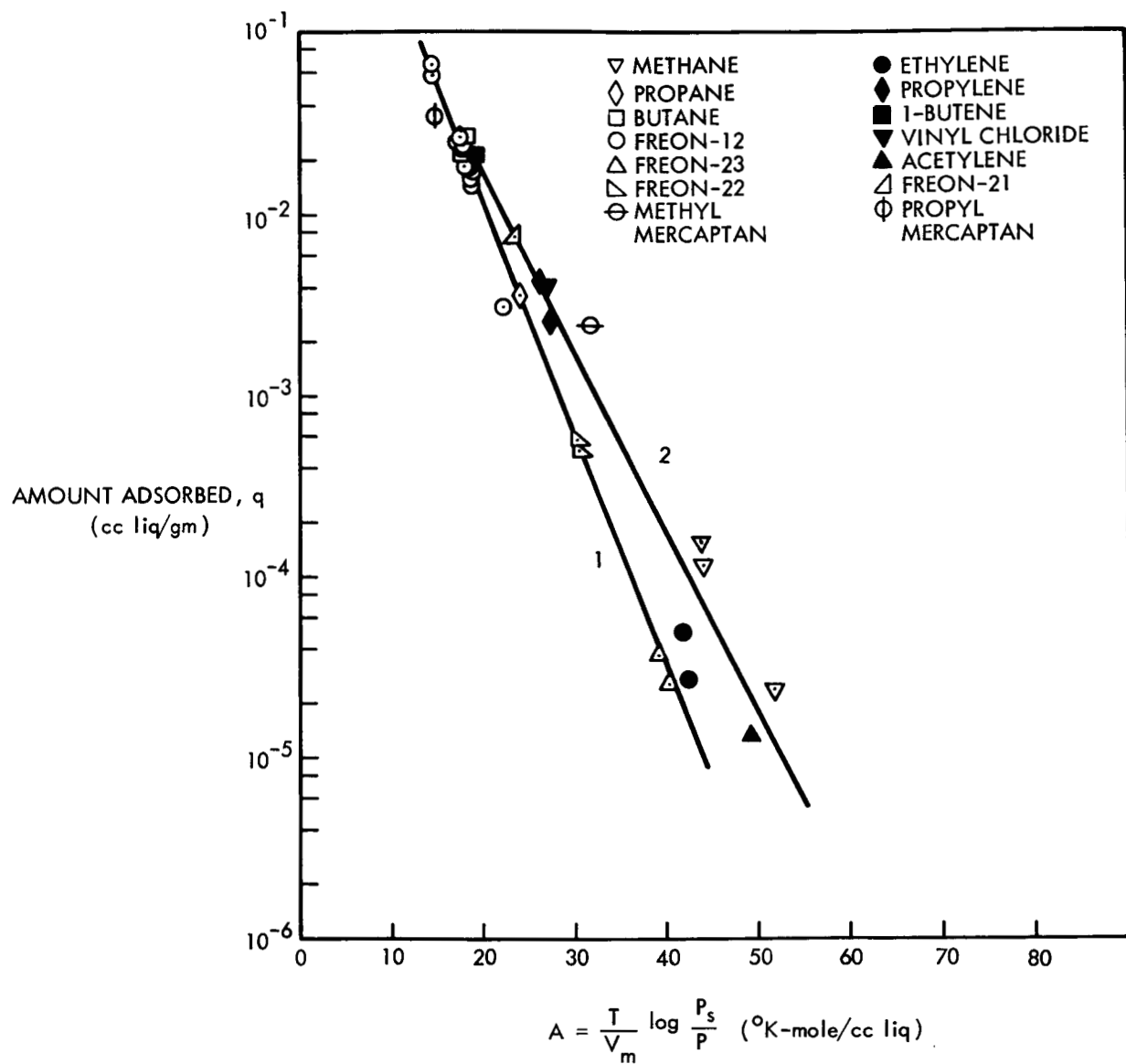


Fig. 2-3 Potential Plot for BD Charcoal

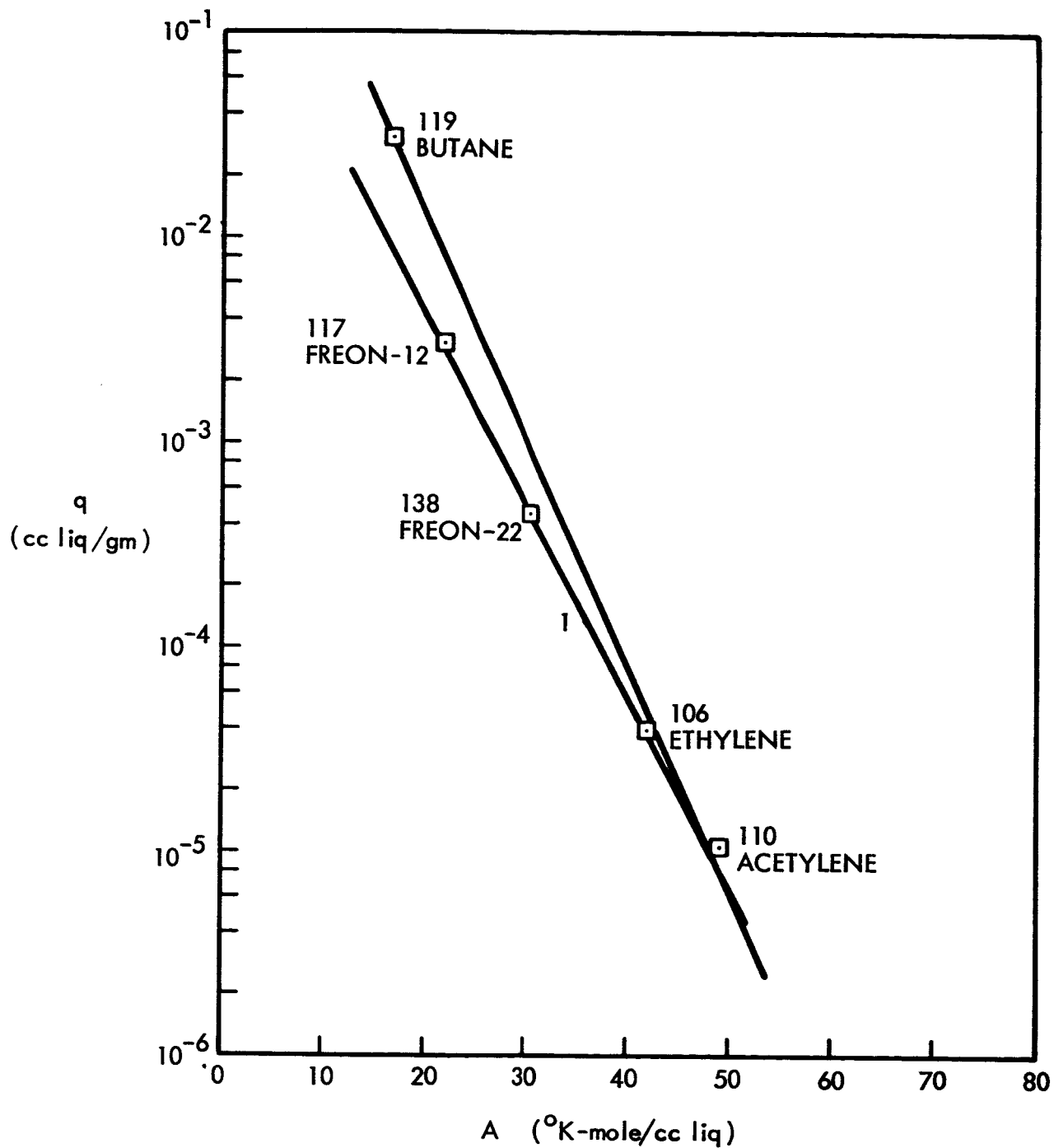


Fig. 2-4 Potential Plot for AC Charcoal

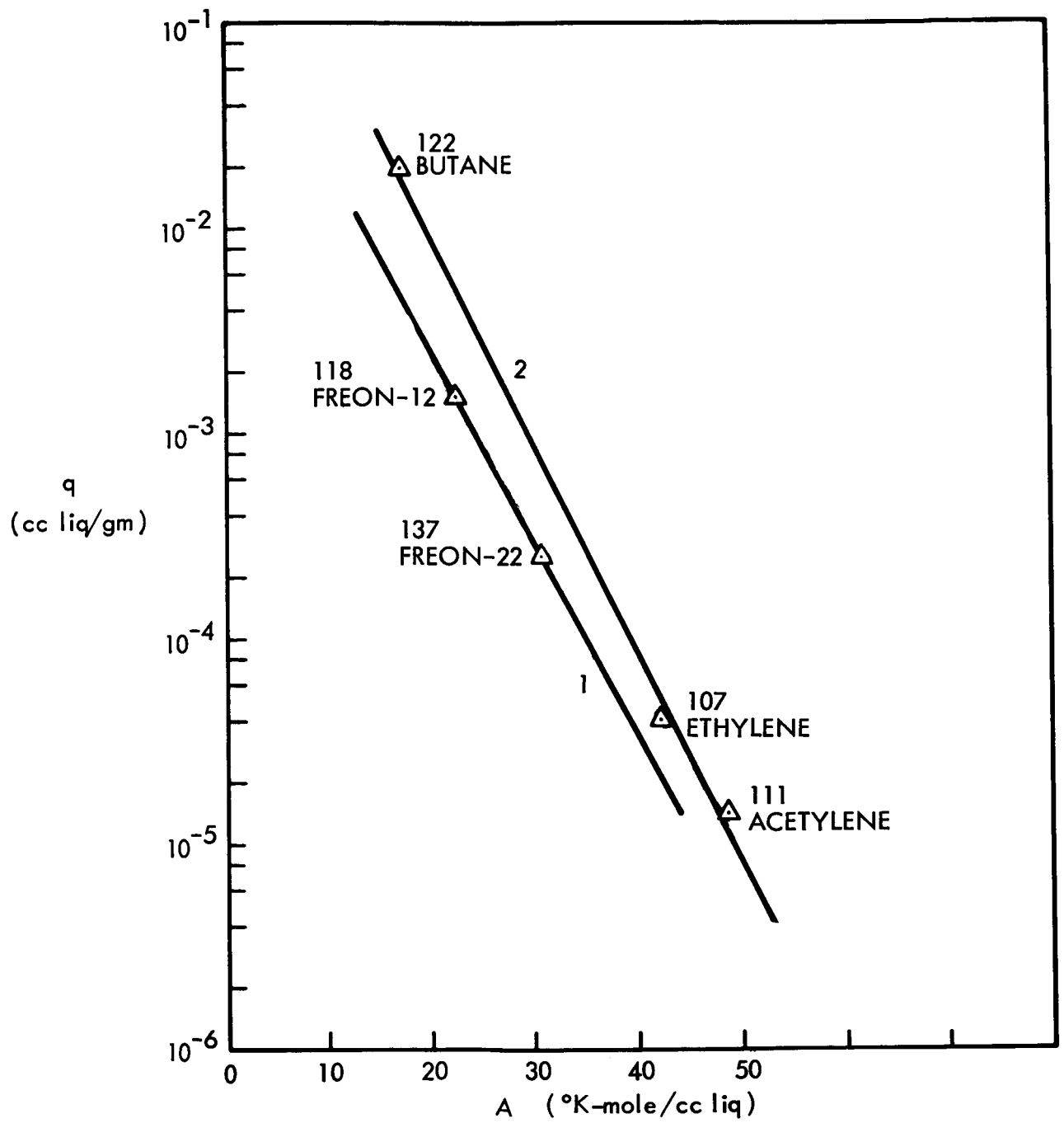


Fig. 2-5 Potential Plot for C1 Charcoal

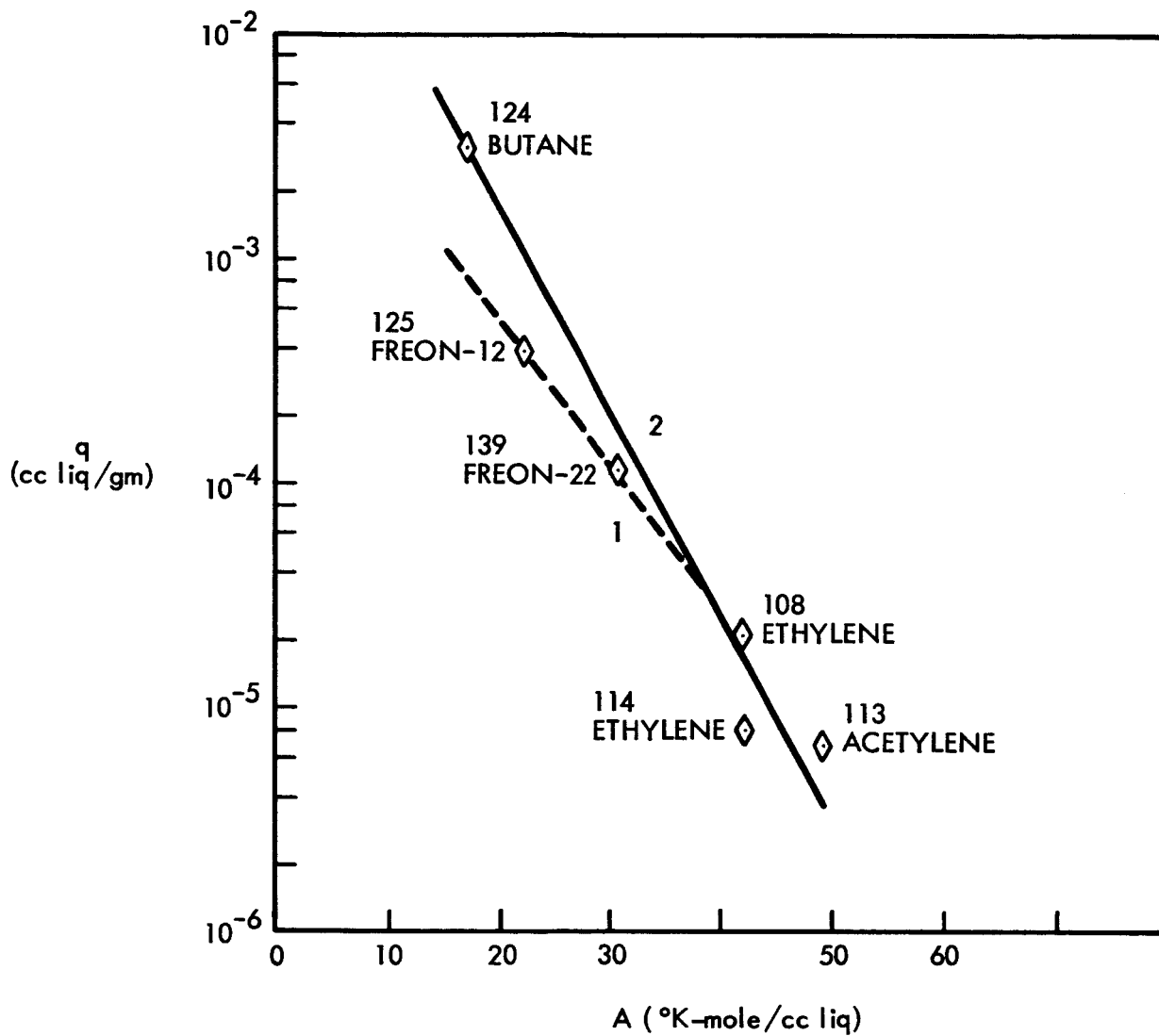


Fig. 2-6 Potential Plot for MSA Fiber

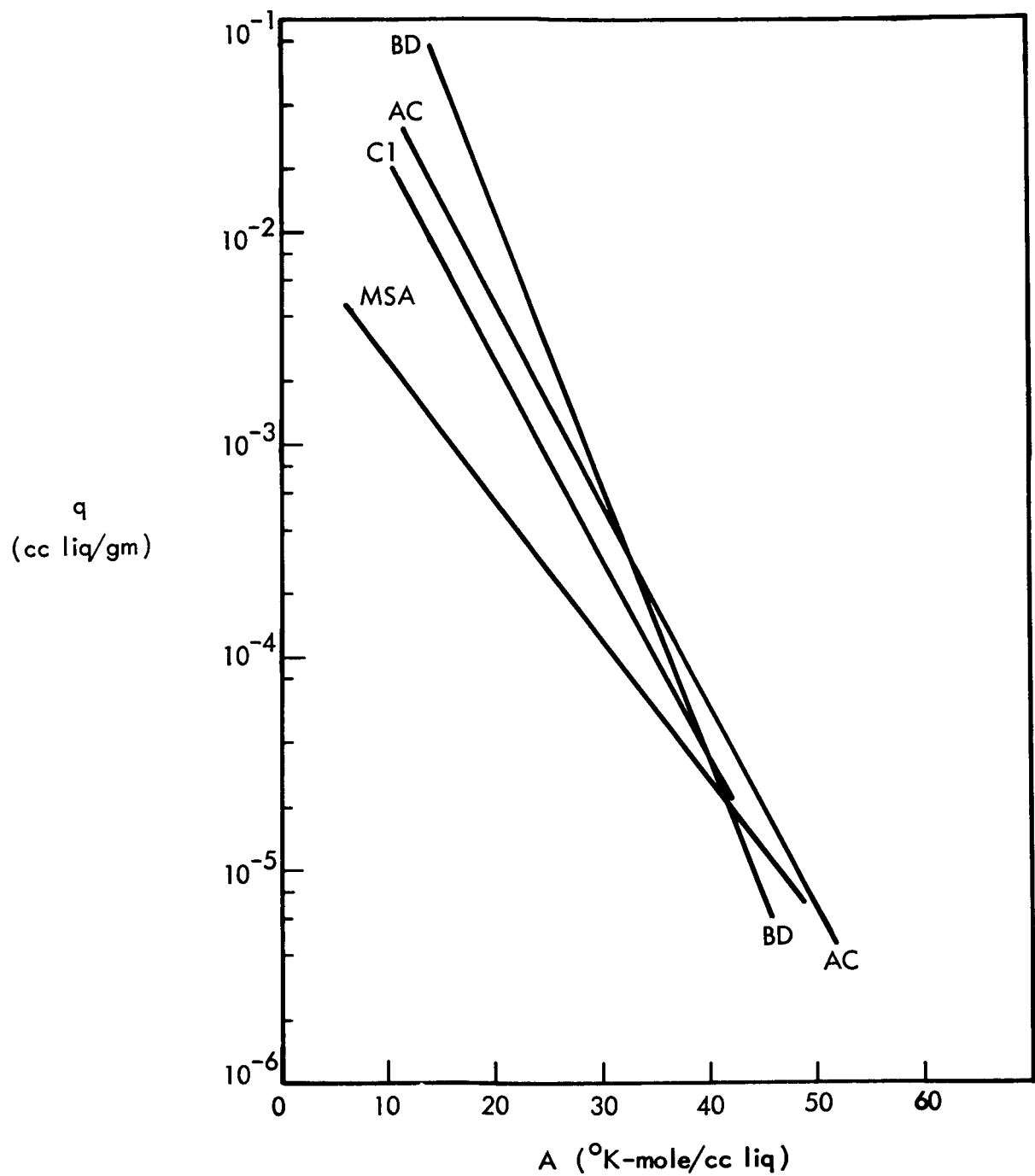


Fig. 2-7 Comparison of Sorbent Capacities

Inlet concentrations remained notably constant throughout individual runs. This is attributed to the use of pre-mixed gases rather than a variable leak valve which tends to drift with time.

An unexpected phenomenon noted in this work is apparent non-convergence, particularly in the runs with unsaturated hydrocarbons and mercaptans; that is, effluent concentration after apparent bed saturation did not reach influent concentration even after passage of considerable periods of time. See, for example, runs 106, 109, 110 and 114, made with ethylene and acetylene, and runs 150 and 151 with propyl and methyl mercaptan. Run 140, with Freon 23, was the only run where non-convergence occurred with an adsorbate other than an unsaturated hydrocarbon or a mercaptan. The only sorbent studied which did not exhibit non-convergence was C1, LMSC acid-impregnated charcoal.

Run 115, ethylene on BD, was a very long run, made to see if non-convergence remains independent of time over greatly extended periods, or is in reality a very slow secondary adsorption, polymerization, or oxidation process. The behavior shown in run 115 is indicative of the processes mentioned. The slow increase in effluent concentration is probably due to slow adsorption of the contaminant, its polymers, and/or its oxidation products.

Runs 105 and 115 were both experiments with ethylene on BD, made at different flow rates to see if the non-convergence phenomenon is dependent on flow rate. These two runs are re-plotted in Fig. A-15 with an abscissa of dimensionless time. The curve shapes are different but no marked conclusions can be drawn. Fig. A-13 is a similar plot for non-convergent runs on MSA fiber.

The processes causing non-convergence result in a sorbent removal capacity in excess of the primary adsorption defined by the potential plot. The nature of this process could be elucidated by further study, such as a quantitative analysis of the effluent gas in conjunction with gravimetric measurements.

In any event, the purpose of this work was to see if that portion of the total removal due to adsorption could be correlated by the potential plot. Accordingly, the retentivity of non-convergent runs was estimated as follows: a tangent was drawn from the final section of the breakthrough curve to the ordinate. The q-value was calculated from the area described by this tangent, the breakthrough curve, and the coordinate axes.

Some obvious malfunctions or information gaps occurred in a few runs, and these are indicated in the notes to Table A-1.

Out of 34 runs plotted in Fig. 2-3, one run (ethylene) deviates from the correlation by a factor of four. Other deviations in the low q region range as high as a factor of two. Above a q-value of 5×10^{-4} , which is the region of greatest interest for designing adsorbers for trace contaminant removal, the maximum deviation from the correlation is about 15%, except for one Freon 12 run which was not repeated for verification, and both mercaptan runs. In the case of the two mercaptan runs the wide divergence between the inlet concentration and the outlet breakthrough concentration results in q-values from these runs that are very dependent on data interpretation.

It is felt that deviations for normal runs would be decreased by the following: more rigorous pre-treatment conditions to insure a more reproducible initial surface state, more accurate calibration of chromatograph detector response as a function of concentration, better statistical sampling techniques for the selection of adsorbent bed granules, including a determination of particle size distribution, and greater uniformity in bed packing. In the case of non-convergent runs, a better understanding of the phenomenon observed is needed to interpret the relation of the data to the potential plot.

It is proposed that the data on BD charcoal as shown in Fig. 2-3 be correlated by two lines: line 1 representing Freons and line 2 representing hydrocarbons. The potential plots for the other sorbents are influenced by that for BD, to the extent that sufficient data were taken on BD to indicate the existence of two correlating lines. Granting the existence of two correlating lines, one for Freons (line 1) and one for hydrocarbons (line 2), data for sorbents AC, C1, and MSA are correlated in Figs. 2-4, 2-5, and 2-6 with, in general, negligible deviations.

Section 3

RETENTION-TIME CORRELATION
AND DYNAMIC BEHAVIOR PREDICTIONS

During previous sorbent screening work under this contract, it was noted that relative elution times and relative sorbent capacities showed some correlation. These tests were carried out in helium at elevated temperature; consequently, they are relatively simple and fast.

During the system analysis work under Phase I, it became apparent that there was limited ability to predict breakthrough curve shape as a function of flow rate, particle size and other factors, based on the number of injection and flow tests conducted.

In view of the above considerations, a study was conducted under Phase III to explore the possibility of using the high-temperature injection-type experiments, not only to screen sorbents but also to determine saturation capacities for use in defining a potential plot.

In addition, a study was conducted to develop a simpler and better method for predicting breakthrough curve shape, based on a minimum of experimental data.

3.1 RETENTION-TIME VERSUS SATURATION CAPACITY

A series of high-temperature injection experiments in helium carrier gas were conducted. Results are summarized in Tables A-2, A-3, and A-4 in Appendix A.

These tests were performed with the intent of noting the relationship between the retention times and retentivities as determined by flow experiments performed with an oxygen carrier gas also containing CO₂ and H₂O.

For flow experiments, a "stoichiometric time" t_s is defined as follows:

$$t_s = \frac{qw}{FC_i V_m} \quad (3.1)$$

where

- q = retentivity, cc liq/gram
- F = gas-phase volumetric flow rate, cc/unit time
- C_i = bed inlet concentration of contaminant, moles/cc
- V_m = molar volume of contaminant, cc liq/mole
- w = sorbent weight, gram

rearranging Eq. 3.1

$$t_s V_m \propto \frac{q}{C_i} \quad (3.2)$$

if flow rate and adsorbent weight are held constant.

It is expected that t_s , for low-temperature flow runs, is directly related to t_r , the retention time of a high-temperature elution peak, if one is in the Henry's Law (linear) region of the contaminant isotherm, if the heat of adsorption is not a function of temperature, and if a change from oxygen to helium carrier gas has a negligible effect on the adsorption mechanism.

Thus the data were analyzed to see if the quantity $(t_r V_m)$ was related to the quantity (q/C_i) . The retentivity q was not determined at the same temperature as the pulse (injection) experiments so an estimated same retentivity, q_{est} , was determined by extrapolation or interpolation of lines on the appropriate potential plot drawn through points representing flow runs performed.

The relationship between $(t_r V_m)$ and (q_{est}/C_i) is shown for BD, AC, and C1 in Fig. 3-1, 3-2, and 3-3.

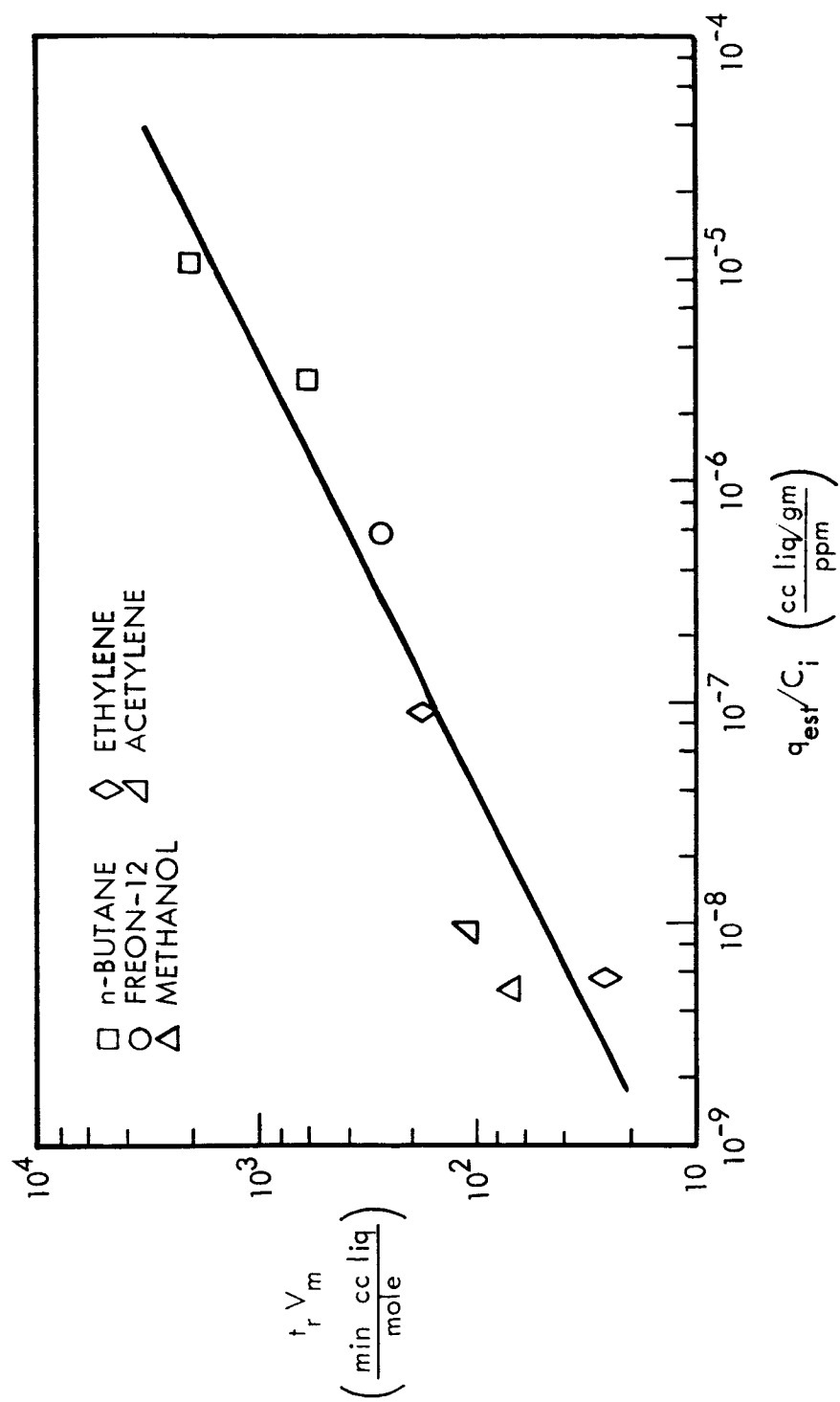


Fig. 3-1 Retention-Time/Capacity Correlation for BD Charcoal

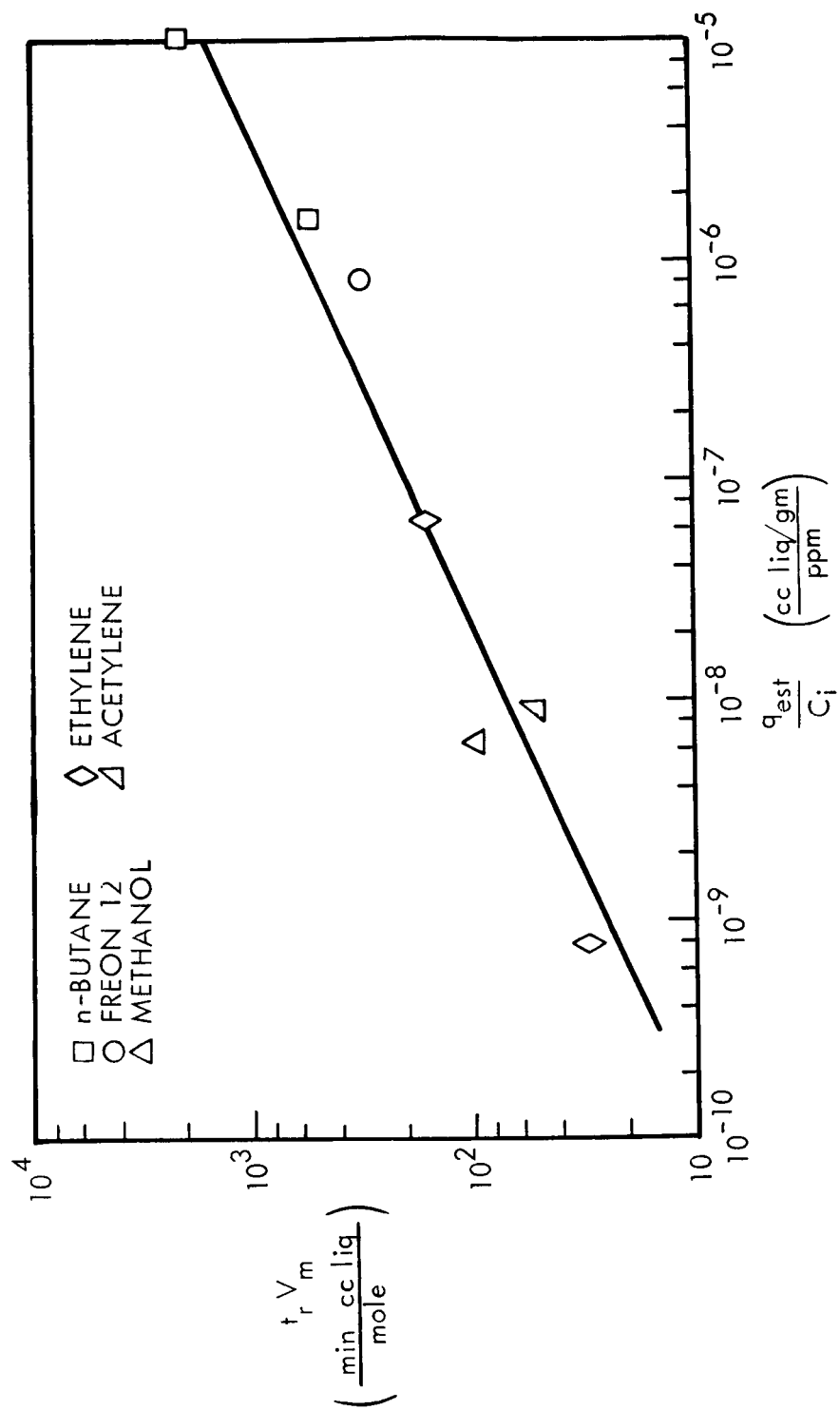


Fig. 3-2 Retention - Time/Capacity Correlation for AC Charcoal

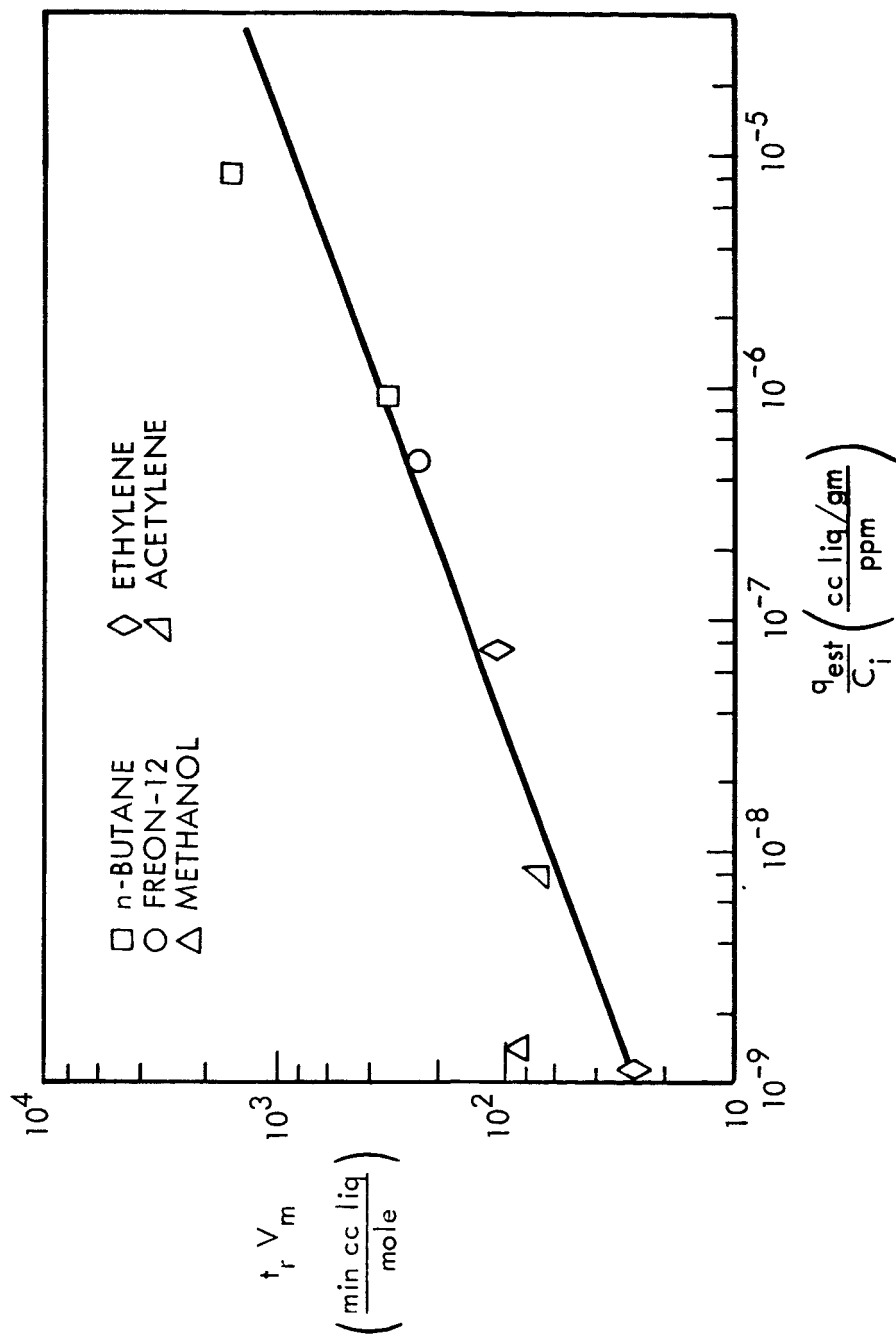


Fig. 3-3 Retention-Time/Capacity Correlation for C1 Charcoal

The parameter A used to determine q_{est} was calculated at the temperature of the pulse runs. All pulse runs were made with the same quantity injected; A was calculated on the basis of SMAC levels.

The data scatter in Figures 3-1, 3-2 and 3-3 is such that this approach apparently gives only a rough estimate of the actual capacity under the lower temperature, reduced pressure, and oxygen conditions of interest. The flow experiments, or injection experiments carried out under similar conditions, are more reliable capacity prediction tools.

3.2 CORRELATION OF RETENTION-TIME DATA WITH DYNAMIC BREAKTHROUGH CURVES

In the interest of developing techniques which will yield a maximum of design data with a minimum of experimentation, a study was undertaken to relate the results of simple, small-scale, injection-type experiments to the problem of predicting the dynamic behavior of full scale adsorption beds.

3.2.1 Theoretical Relationships Between Injection and Flow Tests

A typical breakthrough curve, from a continuous-flow experiment, is shown in Figure 3-4.

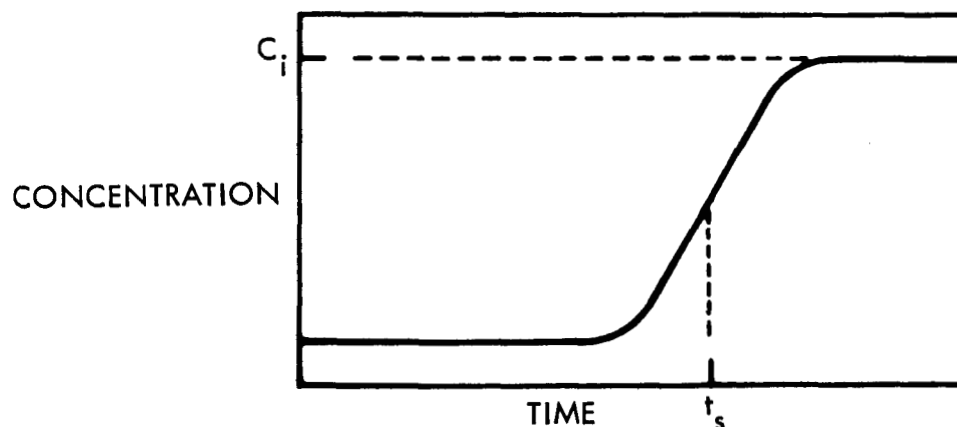


Fig. 3-4 Concentration vs. Time for a Typical Continuous-Flow Experiment

For such an experiment, the saturation capacity of the bed for the contaminant tested can be determined from equation 3.3.

$$Q = F \int_0^{\infty} [C_i - C(t)] dt \quad (3.3)$$

where

- Q = bed capacity, moles
- F = flow rate, cc/unit time
- C_i = inlet concentration, moles/cc
- C = outlet concentration, moles/cc
- t = time

Stoichiometric time, t_s , defined in equation 3.1 can also be expressed as follows:

$$t_s = \frac{Q}{FC_i} \quad (3.4)$$

Further, one can normalize the concentration by dividing by C_i , and normalize the time by dividing by t_s , as shown in Figure 3-5.

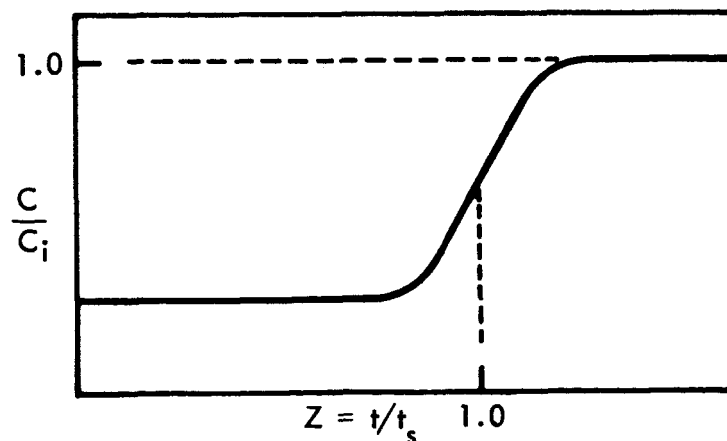


Fig. 3-5 Normalized Concentration-Time Plot for a Continuous-Flow Experiment

Injection-type experiments yield a concentration-time pulse rather than a breakthrough curve. This concentration-time pulse can also be normalized, or made dimensionless, by plotting c_p vs. Z where

$$c_p = \frac{C F t_s}{S} \quad (3.5)$$

and

S = moles of contaminant injected

$Z = t/t_s$

Figure 3-6 shows a typical normalized injection pulse.

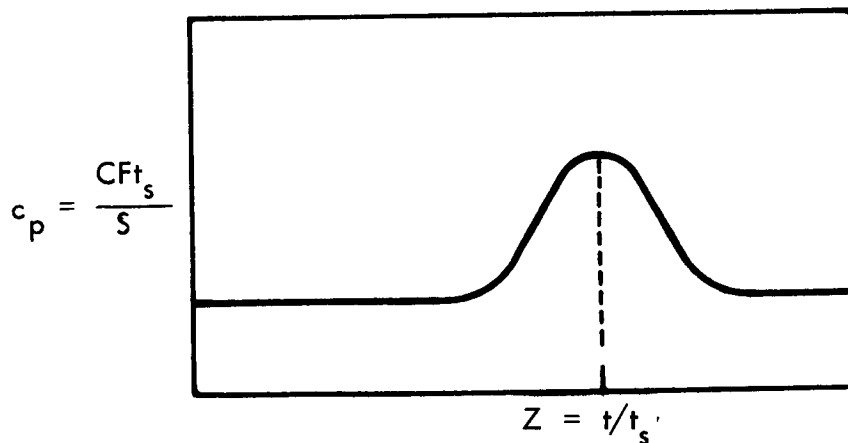


Fig. 3-6 Normalized Results for an Injection Experiment

The following mathematical relationship between the injection pulse and continuous flow curves was established in Ref. 3.

$$C(Z) = C_i \int_0^Z c_p(Z) d(Z) \quad (3.6)$$

⁽³⁾ Robell and Merrill, "Studies of Gas-Solid Interactions. IV. Dynamics of Removal Processes in Fixed Beds" LMSC report 6-76-66-3, Unpublished.

Equation 3.6 is exactly true for C_i arbitrarily large; it is a good approximation if the injection-test pulse is sharp and if the isotherm is linear.

Granting these assumptions, the breakthrough curve can be obtained by a graphical integration of the injection pulse. For symmetrical peaks and curves, time quantities are related as follows:

$$\text{retention time} = \text{breakthrough time} @ \frac{1}{2} C_i = t_s = \frac{Q}{FC_i}$$

for pulse and flow runs performed under the same conditions.

For cases where the outlet pulse is not symmetrical, the stoichiometric time is unambiguously defined from the integrated curve and may not coincide with the pulse maximum.

It is desirable to be able to measure the adsorption characteristics of solid adsorbents, either from breakthrough curves or the retention times of the elution peaks. By rearranging equation 3.4, the adsorptivity constant, K_a , may be expressed as:

$$K_a = \frac{Q}{\omega C_i} = \frac{t_s F}{\omega} \quad (3.7)$$

In the preceding discussion the stoichiometric time t_s has been defined for both flow curves and pulses. Thus, with Equation 3.7 these two types of data can be interpreted in terms of the adsorptivity coefficient.

3.2.2 Demonstration of Theoretical Relationship Between Injection and Flow Tests

In order to illustrate the validity of the integral-differential relationship, defined in equation 3.6, some elution peaks were measured at conditions nearly identical to existing breakthrough curves.

Initially, runs were made for comparison with flow experiments involving the sorption of Freon-12 on BD and AC charcoal. In both cases a fresh bed of charcoal was used for the pulse runs. The integrated pulse runs are compared to the flow runs in Figures 3-7 and 3-8, which show the stoichiometric times to differ by about 20% in each case.

Variations in the adsorption capacities (directly proportional to stoichiometric times) on the potential plot (Figure 2-3) are about 30% for the different flow runs for Freon 12 on BD charcoal. It is likely, then, that the deviations shown in Figures 3-7 and 3-8 result from normal variations in the charcoal samples and packing density variations in the beds used for the flow tests.

A second set of runs was made where the injection test was made on exactly the same bed of adsorbent as the continuous-flow test run. The comparison for methane on BD charcoal is seen in Figure 3-9 for an injection volume of $300\mu\text{l}$. The points from the integrated pulse curve follow the flow curve very closely.

In Figure 3-10 a similar comparison is made for an injection of $30\mu\text{l}$ of CH_4 . Again the agreement is good. In Figure 3-11 the same comparison is made for a $3000\mu\text{l}$ injection. Here the shape of the breakthrough curve is essentially the same as the integrated pulse curve but slightly steeper and the stoichiometric time is significantly less. Apparently the surface has begun to saturate at these partial pressures due to non-linearity in the isotherm. It is significant that the $3000\mu\text{l}$ pulse run was the first of the four runs and that the flow run was completed in sequence between the other two pulse runs. Thus the lower capacity of the $3000\mu\text{l}$ run could not have resulted from residual surface adsorption of methane.

3.2.3 Theoretical Prediction of Breakthrough Curve Characteristics

The correlation described above will allow the approximate determination of a continuous-flow breakthrough curve from the results of an injection experiment under similar conditions of flow, and identical conditions of particle size and bed length.

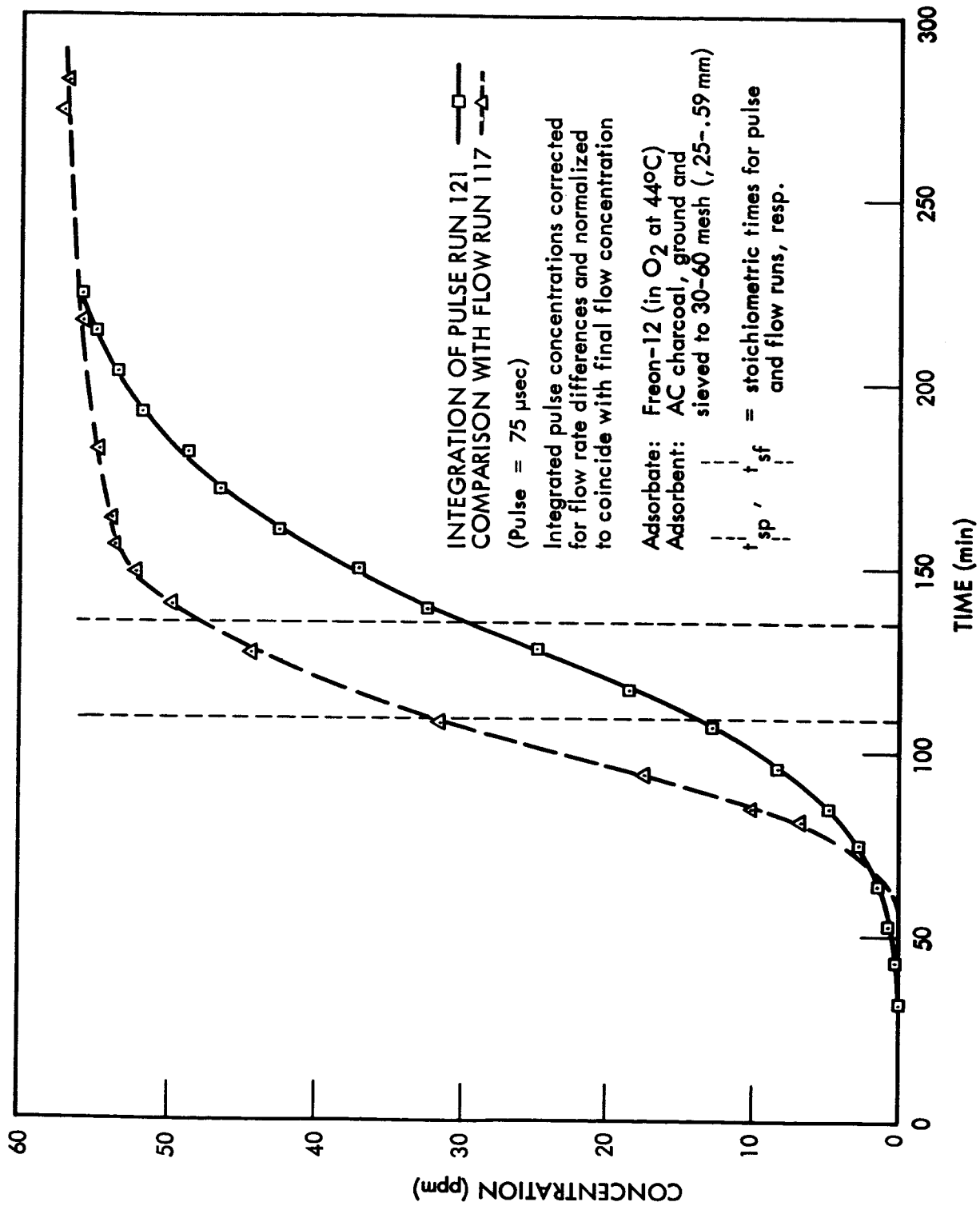


Fig. 3-7 Correlation of Injection and Flow Experiments Freon-12 on AC

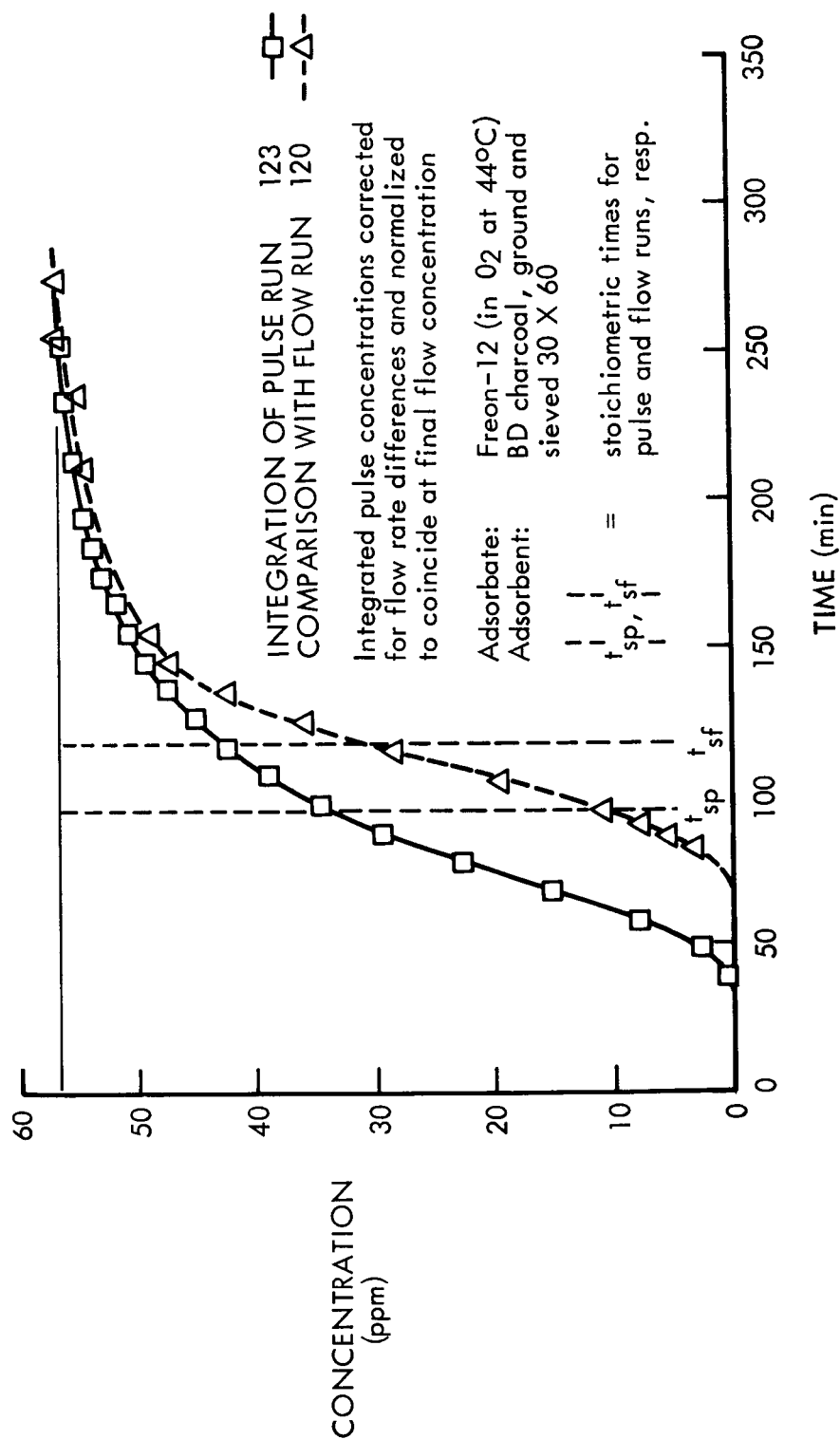


Fig. 3-8 Correlation of Injection and Flow Experiments Freon-12 on BD

INTEGRATION OF PULSE RUN 128 □
 COMPARISON WITH FLOW RUN 129 △

Integrated pulse concentrations corrected
 for flow rate differences and normalized
 to coincide at final flow concentration

Adsorbate: Methane (in O₂ at 44°)
 Pulse = 300 ul injection
 Adsorbent: BD charcoal ground and
 sieved 30 X 60
 t_{sp} t_{sf} = stoichiometric times for
 pulse and flow runs, resp.

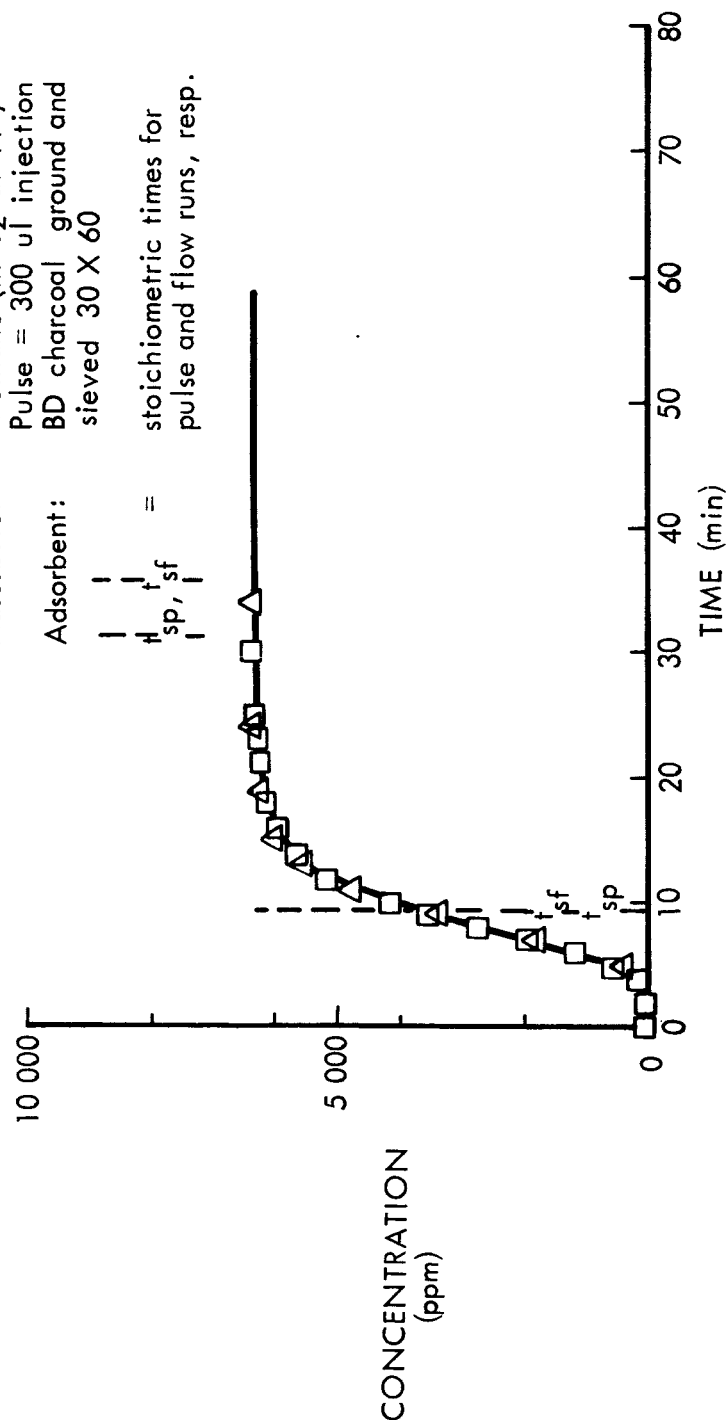


Fig. 3-9 Correlation of Injection and Flow Experiments CH₄ on BD

INTEGRATION OF PULSE RUN 130 —□—
 COMPARISON WITH FLOW RUN 129 —△—

Integrated pulse concentrations corrected
 for flow rate differences and normalized
 to coincide at final flow concentration

Adsorbate: Methane (in O₂ at 44°C)
 Pulse = 30 μl injection
 Adsorbent: BD charcoal, ground and
 sieved 30 X 60

t_{sp} t_{sf} = stoichiometric times for
 pulse and flow runs, resp.

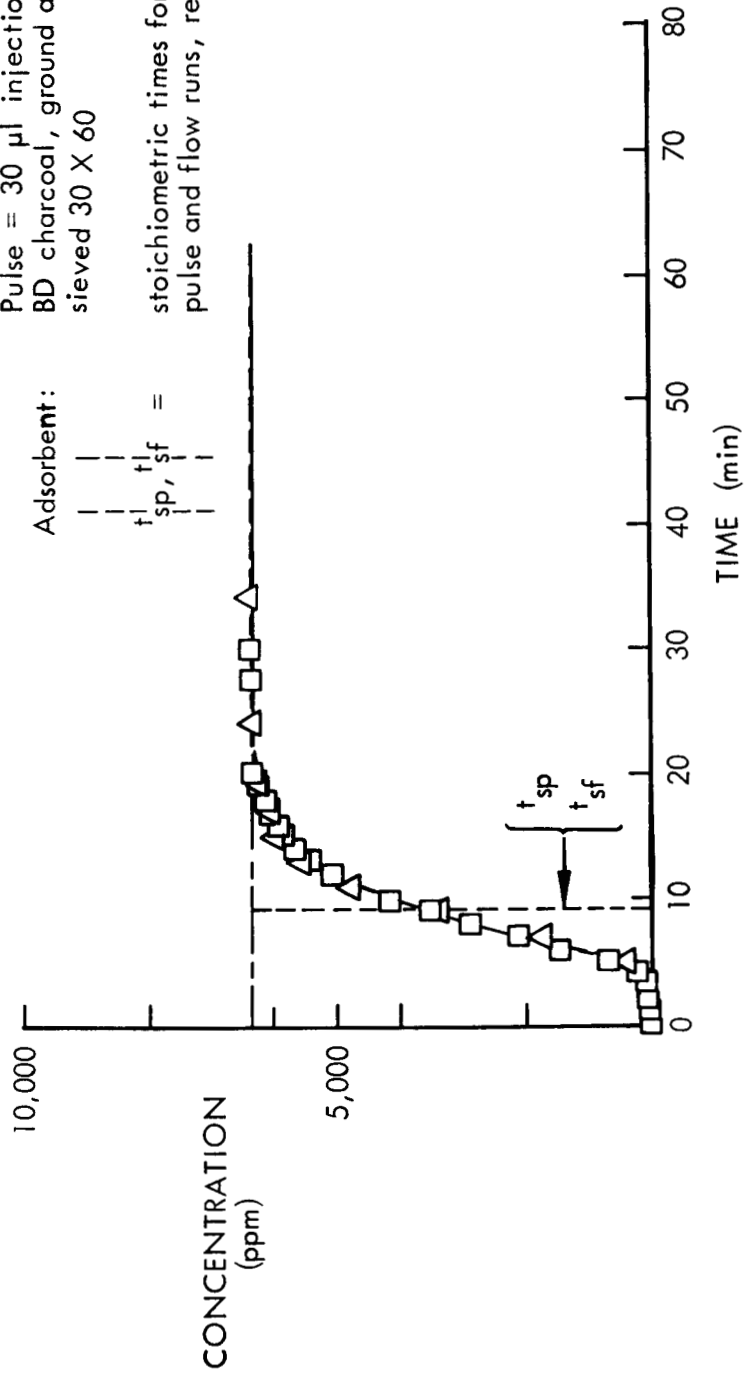


Fig. 3-10 Correlation of Injection and Flow Experiments CH₄ on BD

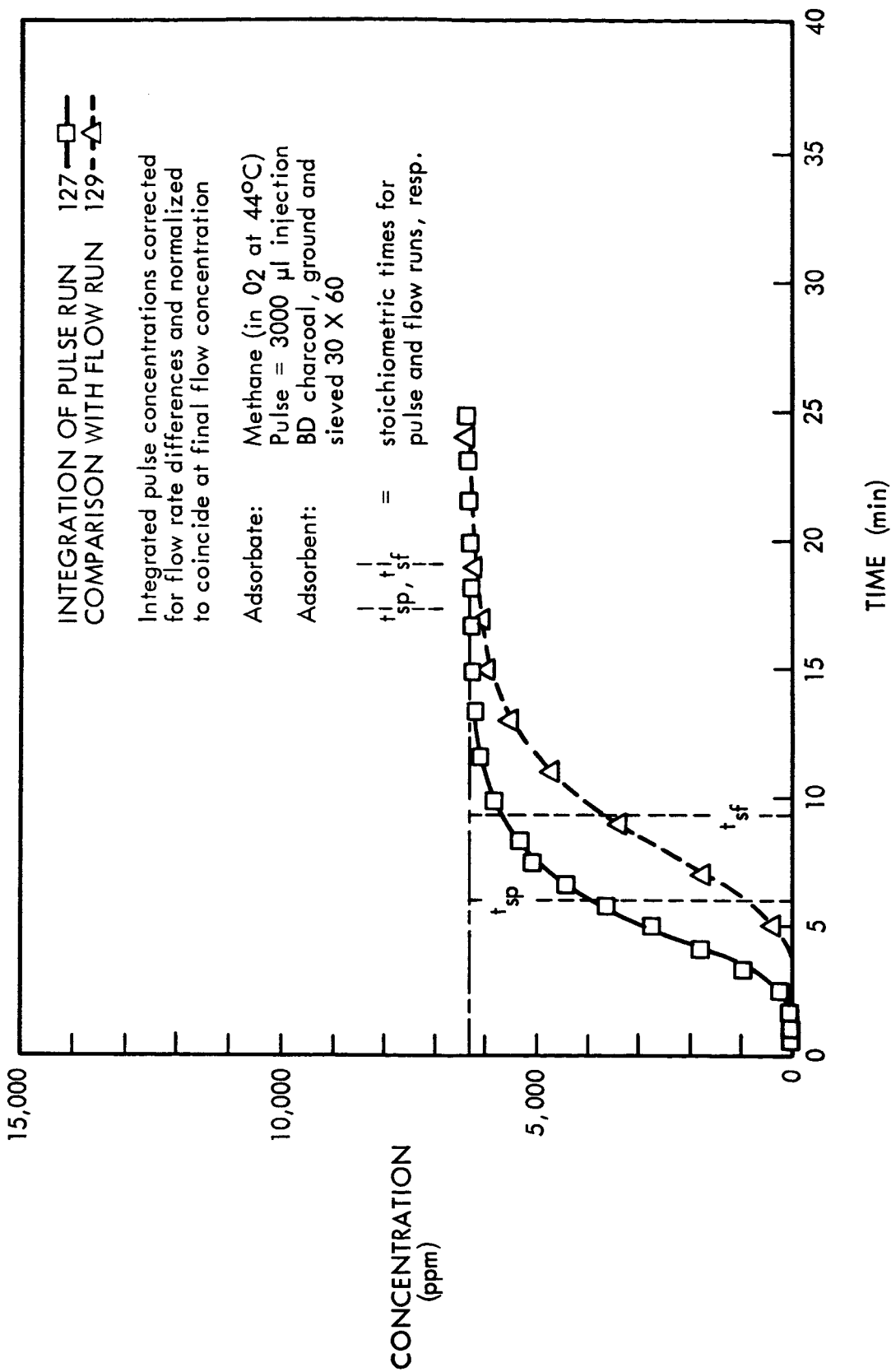


Fig. 3-11 Correlation of Injection and Flow Experiments CH₄ on BD

This in itself is a significant simplification in experimental procedure, and, consequently, a saving of cost and time.

A more powerful tool is one which will allow the prediction of the breakthrough curve for conditions of flow, particle diameter, and bed configuration other than those existing with the injection-test specimen.

Under the present study effort, a satisfactory approach to this problem has been developed, as described below.

Number of Theoretical Plates

Martin and Synge (4) considered an adsorption column as a number of "theoretical stages," each of which achieves equilibrium with the gas phase. Their results give the number of theoretical plates.

$$N_P = 16 \left(\frac{t_s}{W} \right)^2 \quad (3.8)$$

where

W = width of an injection peak

The width of the peak, W , for a pulse is defined as illustrated in Figure 3-12. If the pulse has a Gaussian shape, then the width is four times the standard deviation, σ , of the Gaussian. The width of the breakthrough curve, W_f , is defined as shown in Figure 3-13. If the derivative of the breakthrough curve has a Gaussian shape, then $W_f = \sqrt{2\pi}\sigma$. In this case then

$$W = W_f 2 \sqrt{\frac{2}{\pi}} \quad (3.9)$$

⁽⁴⁾ Martin and Synge, Biochem. J. 35 1358 (1941).

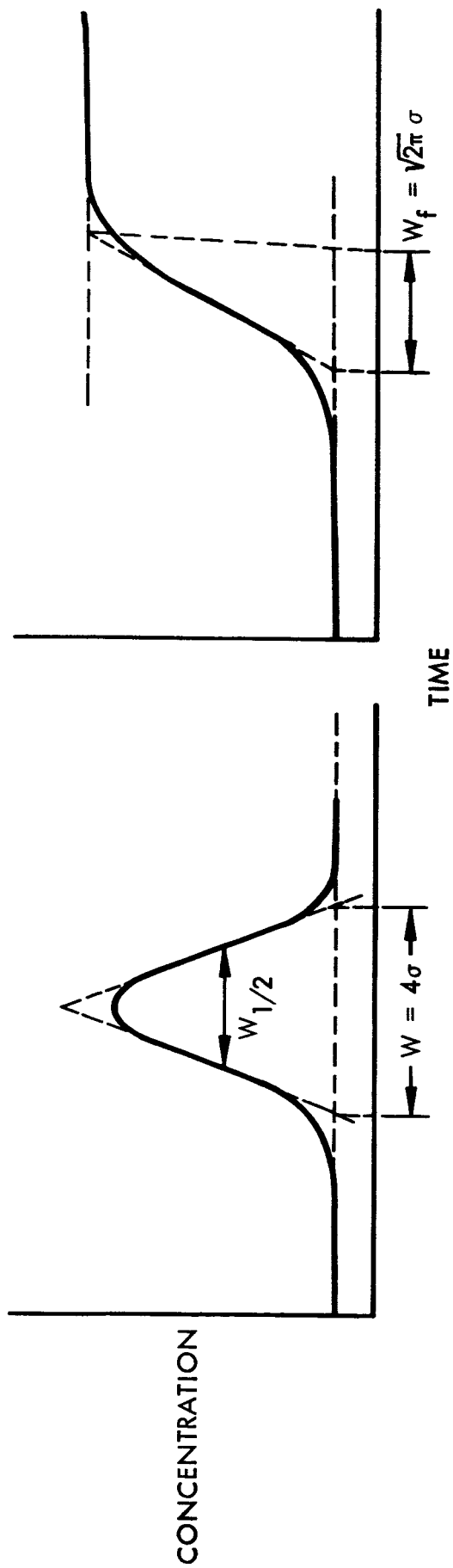


Fig. 3-12 Definition of W for an Injection Pulse

Fig. 3-13 Definition of W_f for a Breakthrough Curve

Also the width of a pulse may be calculated from the width at the half height, $W_{1/2}$, from

$$W = \sqrt{\frac{2}{\ln 2}} W_{1/2} \quad (3.10)$$

Vermeulen and co-workers (5) have proposed correlations based on the differential equation describing a mass balance across a differential element of bed volume perpendicular to flow, assuming no radial concentration or velocity gradients. A fundamental dimensionless group arising from this equation (see Ref. 3) is the Peclet number

$$Pe = \frac{d_p u}{D_f} \quad (3.11)$$

where

- d_p = particle diameter
- u = superficial gas-phase velocity
- D_f = contaminant diffusivity in the gas phase

Vermeulen proposed that the Peclet number correlates with the group $(N_p/b)(d_p/L)$ as shown in Figure 3-14(6), where L = bed length and b is the correction factor shown in Figure 3-15.

At low Peclet numbers the width, W_f , of a breakthrough curve depends largely on axial gas phase diffusion. Increasing the flow rate will decrease the effect of axial

(5) Vermeulen, Adv. in Chem. Eng., Academic Press Inc., N.Y., 1958, vol. 2.
 Heister and Vermeulen, Chem. Eng. Prog. 10 505 (1952)
 Heister, Vermeulen, and Klein, Chemical Engineer's Handbook, Perry, Chilton and Kirkpatrick (eds), McGraw-Hill, N.Y., 1963, section 16.

(6) Private communication from T. Vermeulen.

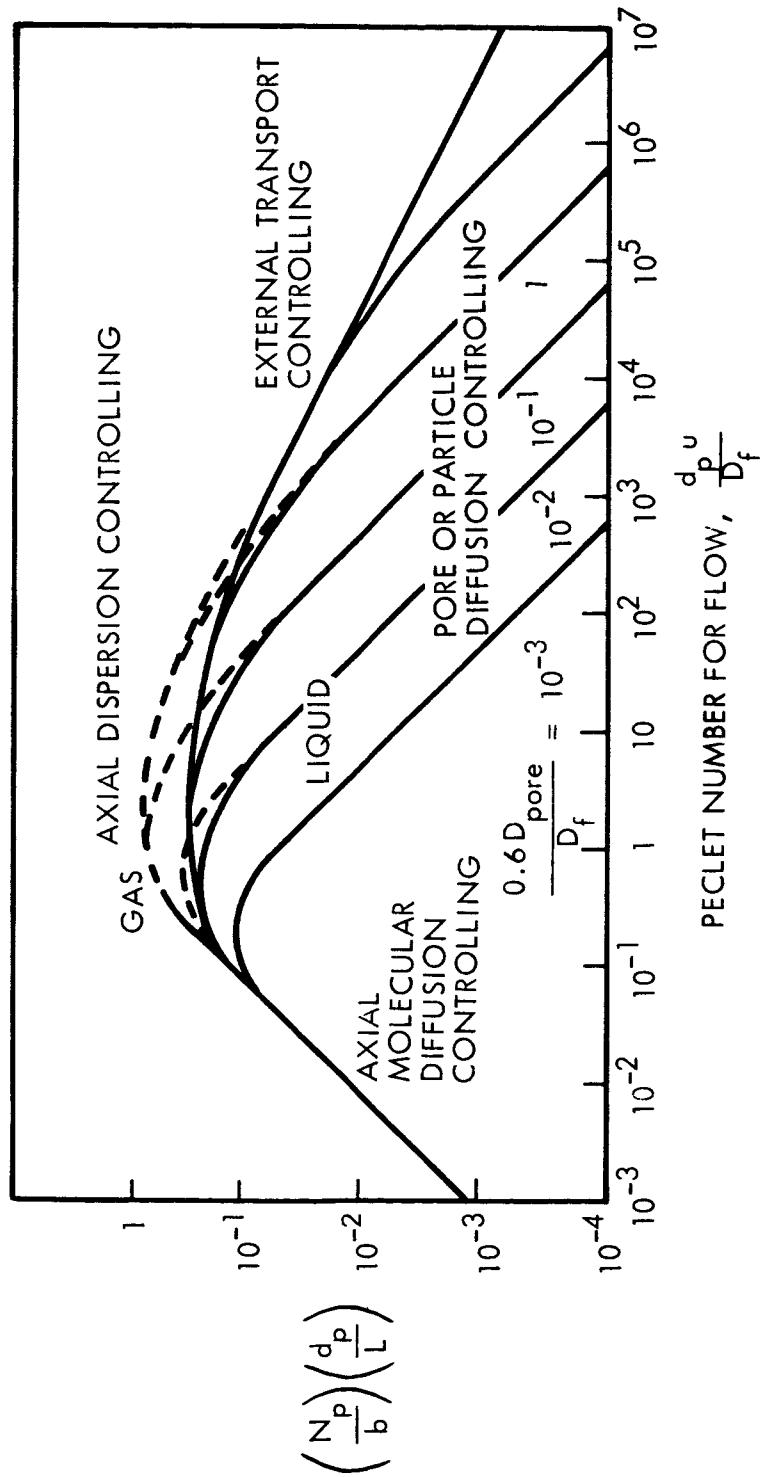


Fig. 3-14 Peclet Number vs $\frac{N_p}{b} \frac{d_p}{L}$

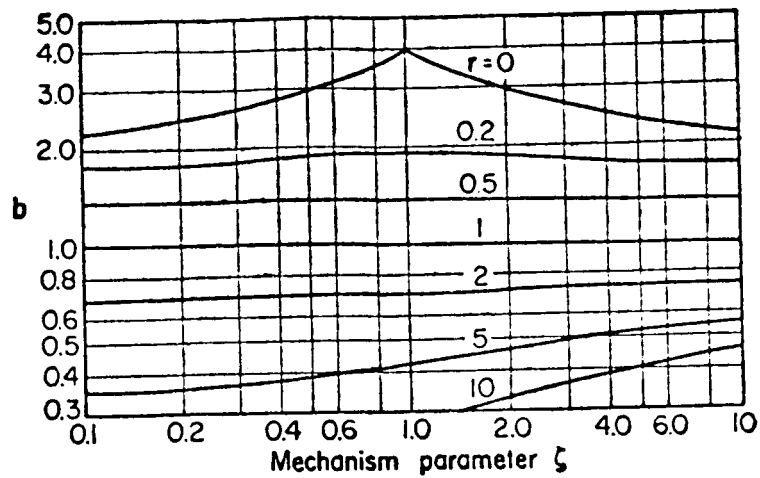


Fig. 3-15 Correction Factor, b , vs. r and ζ From Reference

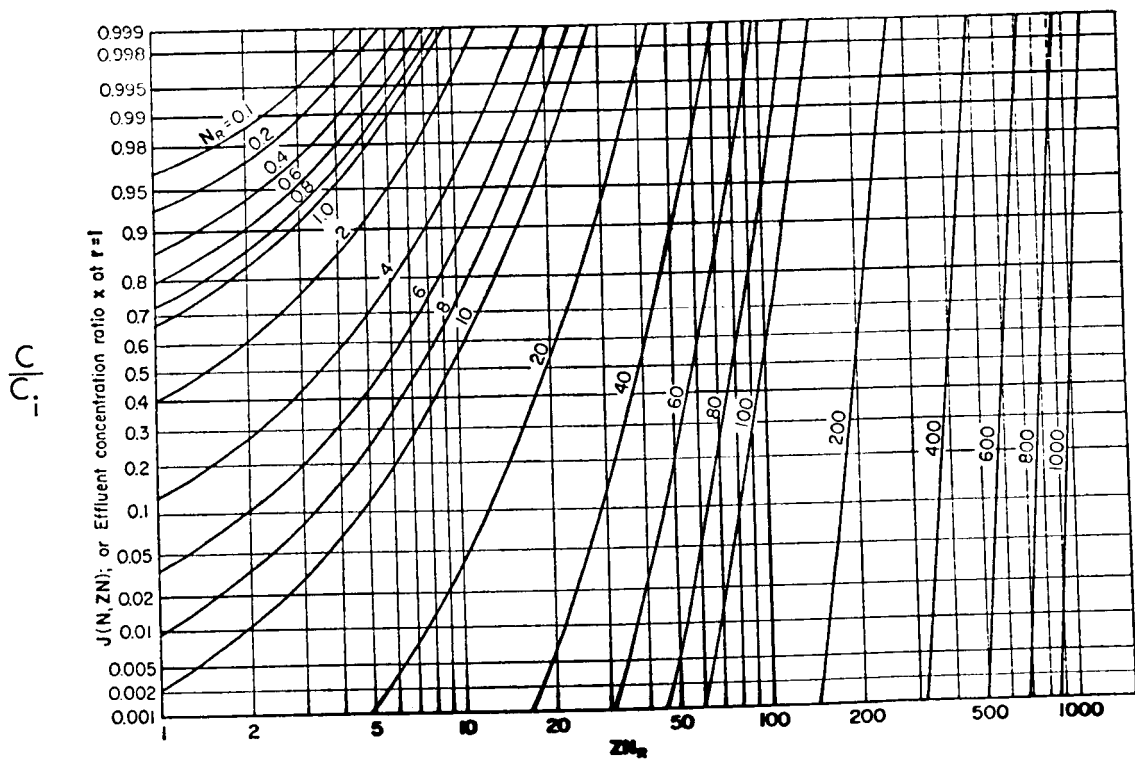


Fig. 3-16 C/C_i vs. Number of Plates and Dimensionless Time

diffusion and increase the effective number of theoretical plates. At very high flow rates (large Peclet numbers) the mass transfer rate due to gas phase velocity will be large compared to the rate of sorption, and further increases will lower the effective number of plates. As seen in Figure 3-14 the maximum effective number of plates occurs at Peclet numbers near unity.

At high Peclet numbers, Figure 3-14 has several branches depending on the ratio of gas phase diffusivity, D_f , to pore diffusivity, D_p , within the particle. This branching shows the most dramatic effect of the different possible mechanisms, i.e., the relative importance of gas phase and pore diffusion. A smaller effect of the rate controlling mechanism is depicted by the parameter b in the ordinate of Figure 3-15. The parameter b depends on the ratio, ζ , of fluid-phase and particle-phase mass transfer resistances, and the equilibrium parameter, r , which for Langmuir adsorption is given by

$$r = \frac{1}{1 + K_p P} \quad (3.12)$$

where

K_p = Langmuir adsorption constant
 P = Partial pressure of adsorbing species

The dependence of b on r and ζ is seen in Figure 3-15.

The most important feature of Figure 3-15, for the present work is that b is unity independent of ζ for an r value of unity.

It can be shown that

$$r = 1 - \theta \quad (3.13)$$

where

θ = Fraction of surface covered

For nearly all of the data reported herein, $\theta \ll 1$ and r is nearly unity.

Vermeulen gives the effluent concentration ratio, C/C_i , as a function of Z and N_p (or N_r) as shown in Figure 3-16. It is possible in theory, then, to predict the breakthrough curve as a function of injection-pulse or breakthrough-curve width, stoichiometric time, gas phase and pore diffusivities, bed geometry, particle size, and gas flow rates.

This is accomplished by the following steps:

- Determine N_p from experimental values of t_s and W
- Determine Pe from d_p , u , and D_f (D_f is calculated for the contaminant and conditions of interest)
- Determine the group $N_p d_p/b L$
- Locate the operating region corresponding to the above, on Figure 3-14.
- For other values of d_p and u , determine new value of Pe
- Find $N_p d_p/b L$ from Figure 3-14
- Knowing d_p , b , and L , determine N_p
- Using Figure 3-16, and knowing C_i , find C vs. Z

3.2.4 Demonstration of Breakthrough Curve Prediction

To determine the applicability of Vermeulen's calculated breakthrough curves for these adsorption studies, the number of theoretical plates, N_p , was estimated from the slope of a breakthrough curve, (see Fig. 3-13 and Eqs. 3.8 and 3.9) for Freon-12 on BD charcoal.

Using this value for N_p and Figure 3-16, the breakthrough curve was calculated; the results are seen in Figure 3-17 compared to the experimentally measured breakthrough curve. The agreement is almost within the experimental error of the measured points.

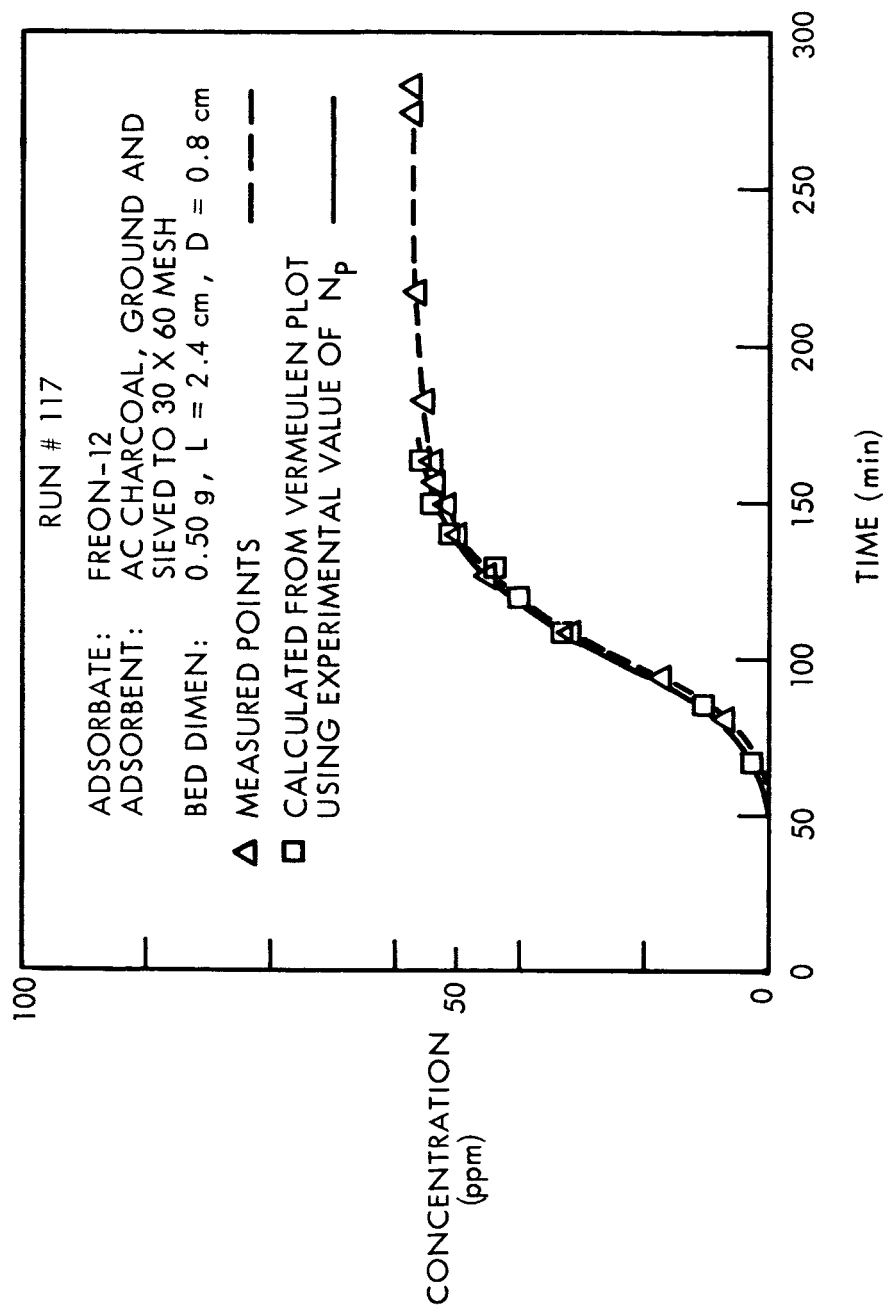


Fig. 3-17 Correlation of Experimental and Theoretical Breakthrough Curves Freon-12 on AC

To test the general validity of Vermeulen's calculations, three runs from Phase I of this work, on the adsorption of n-butane on BD charcoal were considered. The conditions of these experiments are summarized in Table 3-1.

Table 3-1
SUMMARY OF RUNS 50, 51 & 53

<u>Run No.</u>	<u>Wt. (g)</u>	<u>Flow Rate cc/min</u>	<u>D</u>	<u>L/D</u>	<u>Particle Size</u>	<u>C_i ppm</u>
50	0.334	5260	0.426 in	0.5	10 × 12 mesh	26.3
51	0.272	398	0.426 in	0.5	10 × 12 mesh	47.2
53	0.442	380	0.85 cm	3.2	28 × 60 mesh	34.5

The data from these runs are plotted in Figures 3-18, 3-19 & 3-20. Run 53 is a well defined "S"-shaped curve, run 51, a transition shape, is slightly "S"-shaped; and run 50 is definitely "C"-shaped.

Following the procedures outlined in the preceding section, values of N_p were determined for runs 50 and 51 to be 1.0 and 5.4 respectively, based on the experimental curve for run 53. Using these values of N_p and Figure 3-16, breakthrough curves represented by the square symbols were calculated. These are compared with the measured curves in Figures 3-19 and 3-20.

For these runs "best-fit" N_p values were also calculated. These are shown in Figures 3-19 and 3-20 with the resulting data depicted by the round symbols.

The predicted profiles are well within the variations expected from sample to sample of the charcoal as indicated by the measured deviations from the potential plot. Also changing the value of N_p by a factor of two has relatively little effect on the curves.

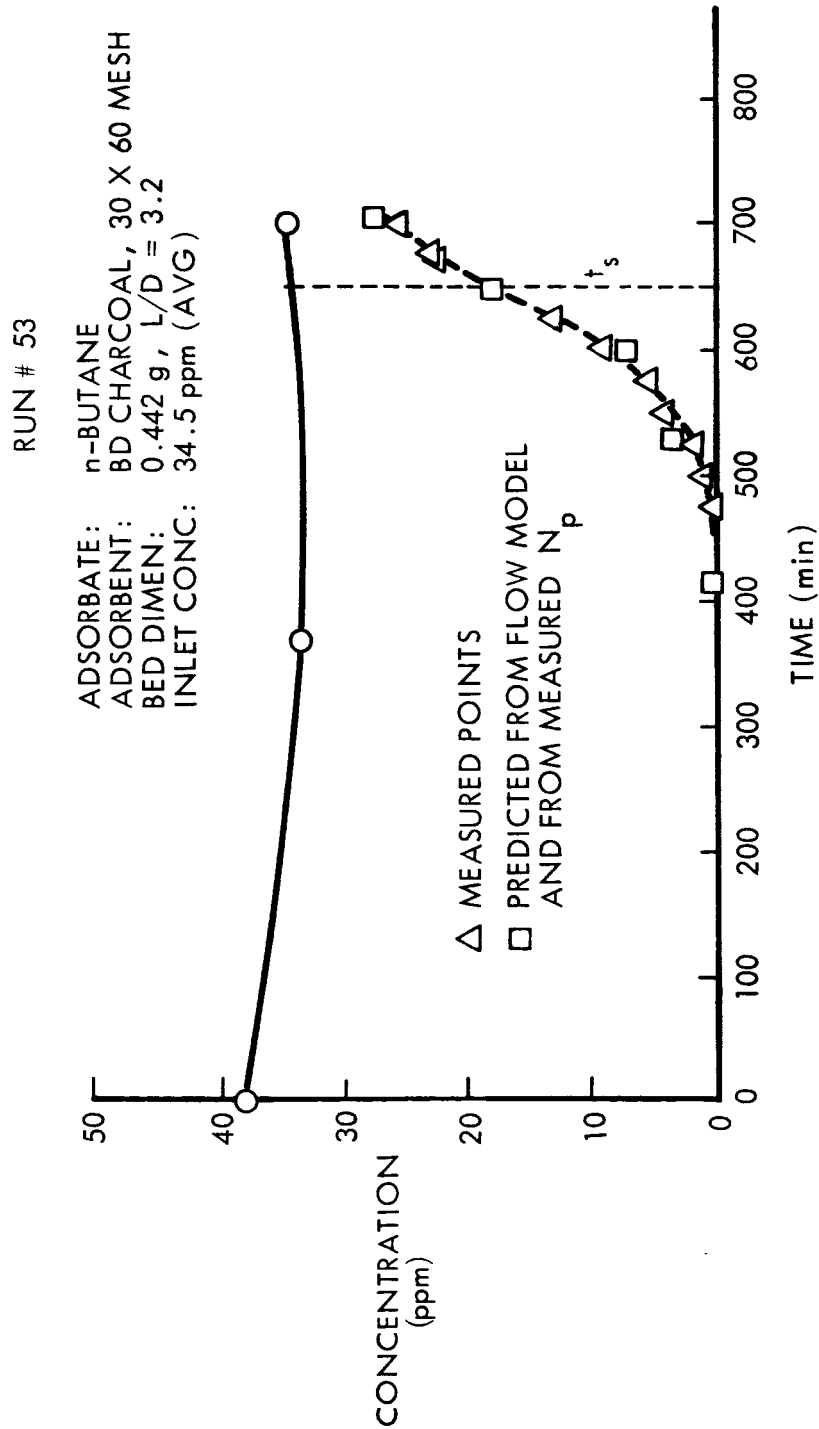


Fig. 3-18 Correlation of Experimental and Theoretical Breakthrough Curves n-Butane on BD

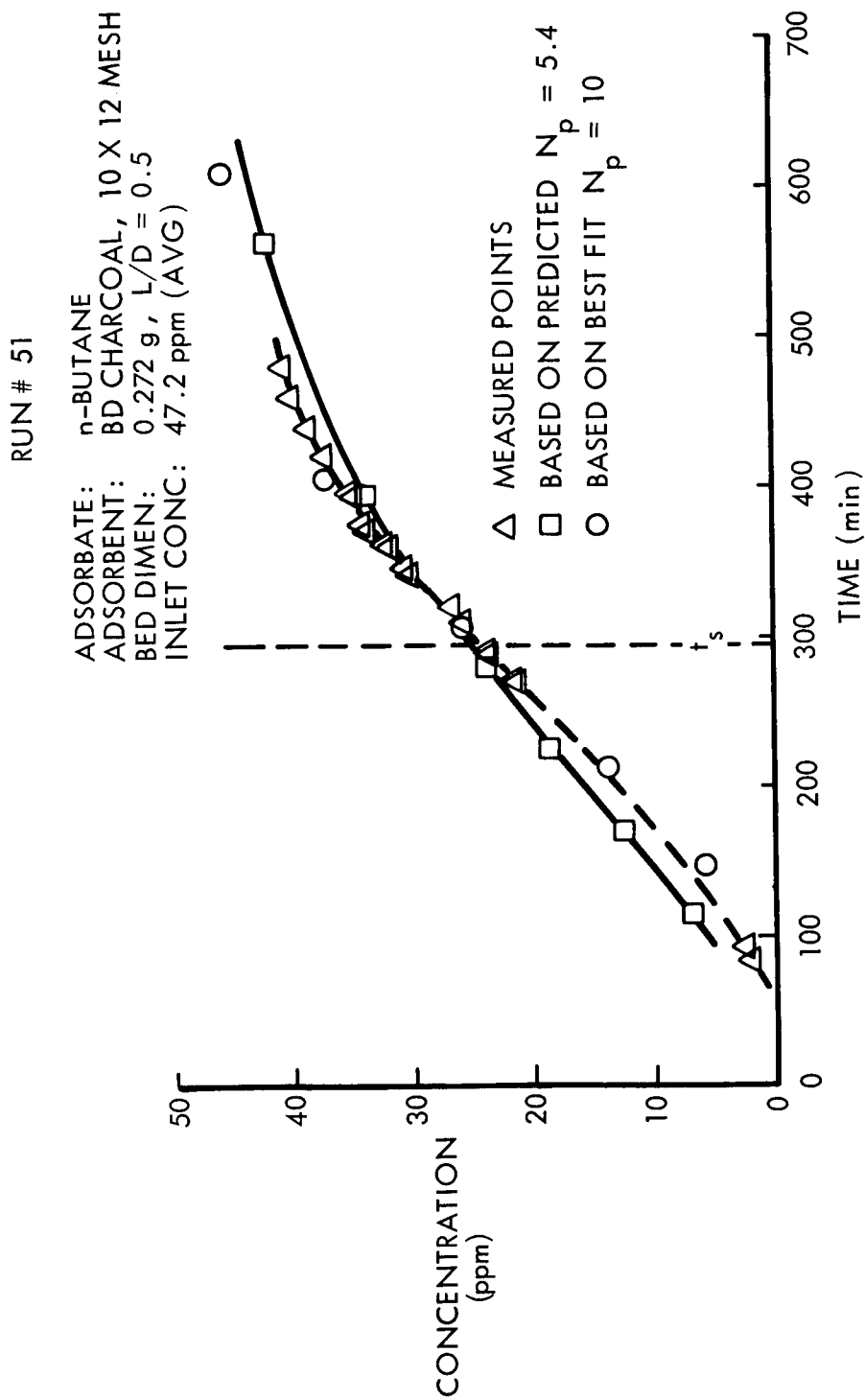


Fig. 3-19 Correlation of Experimental and Theoretical Breakthrough Curves n-Butane on BD

RUN # 50

ADSORBATE: n-BUTANE
 ADSORBENT: BD CHARCOAL, 10 X 12 MESH
 BED DIMEN: 0.339 g, L/D = 0.5
 INLET CONC: 36.3 ppm (AVG)

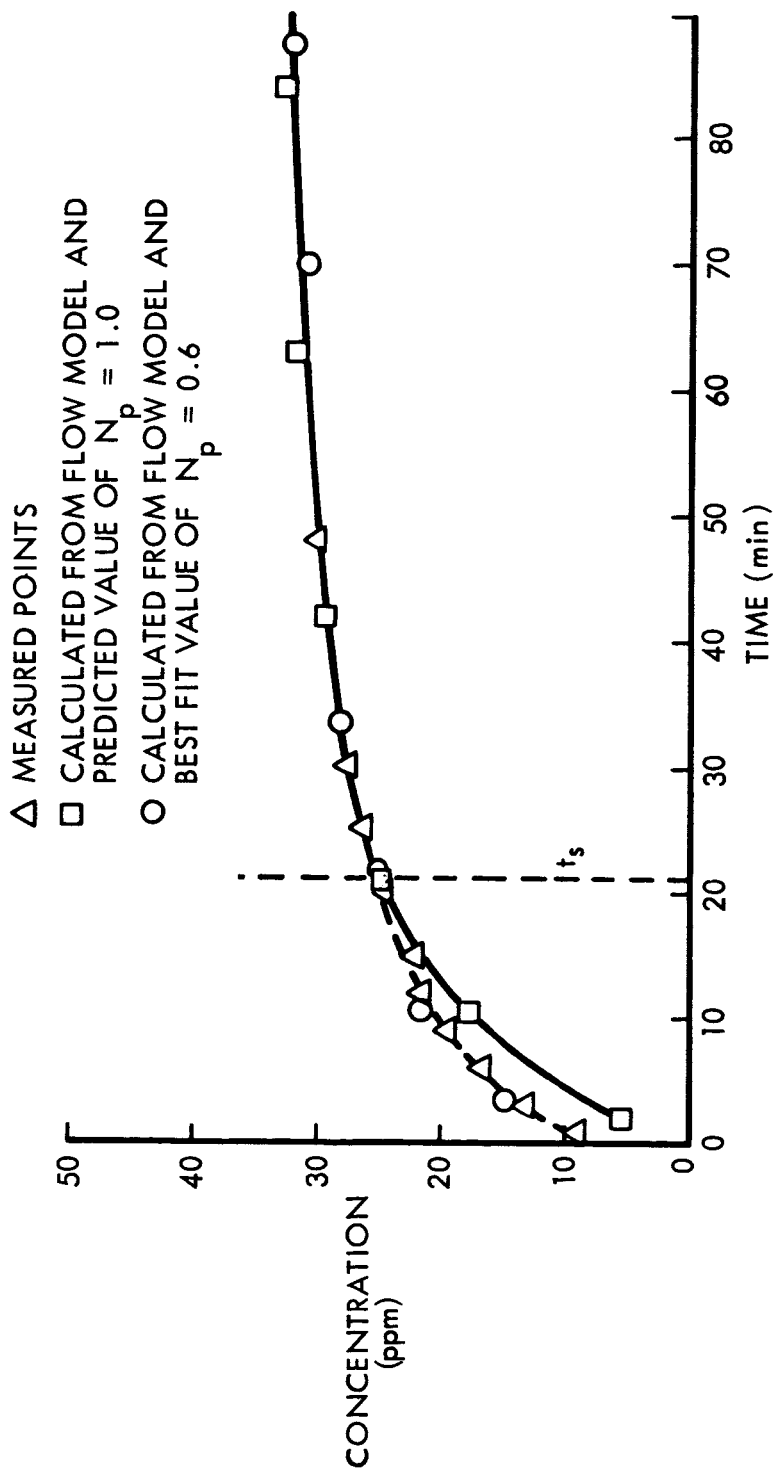


Fig. 3-20 Correlation of Experimental and Theoretical Breakthrough Curves n-Butane on BD

Thus, these calculations have predicted satisfactory profiles for a fourteen-fold change in flow rates, a six-fold change in L/D ratio, and particle sizes of 10×12 mesh and 28×60 mesh. Based on these results, it is expected that most changes in bed geometry, flow rates and particle size can be accounted for by these methods within the limits of the natural variations associated with different samples of charcoal and different packing techniques in the adsorbent beds.

Section 4

CATALYST TESTS - CO CONVERSION AND H₂S POISONING

4.1 OBJECTIVES

During the Phase I work it was observed that the 1% Pt - 1% Pd on Al₂O₃ catalyst (LI-4) was effective in oxidizing carbon monoxide at low temperature (75° F) and at low space velocities (2090 hr⁻¹). It was also observed that the ability of H₂S to poison this catalyst was more noticeable at lower temperature.

Work was, therefore, undertaken in Phase III to determine the poisoning effects of H₂S on LI-4 and on a commercially-prepared 0.5% Pd on Al₂O₃ catalyst.

The objectives of these tests were (1) to determine if the 0.5% Pd catalyst would oxidize CO effectively under low temperature and low space velocity conditions, and (2) to determine the effect of introduction of H₂S at or near SMAC on the CO conversion efficiencies of both the LI-4 and the 0.5% Pd catalysts.

4.2 APPARATUS

Tests were carried out in a flow system similar to the catalyst test apparatus used in Phase I (Fig. 4-1). The main stream of gas consisted of pre-mixed 95 mg/m³ CO in O₂. An H₂S stream was bled into this through a glass capillary.

The catalyst was contained in a stainless steel tube 3/8" in diameter and 5" long. Provisions were made to sample inlet and outlet CO concentrations using a small Sabatier reactor upstream of an F&M Model 700 gas chromatograph equipped with a flame ionization detector. The Sabatier reactor was provided with an upstream H₂S sorbent to prevent reactor poisoning. H₂S detections were made with the MSA Supersensitive Detector, Model 74664.

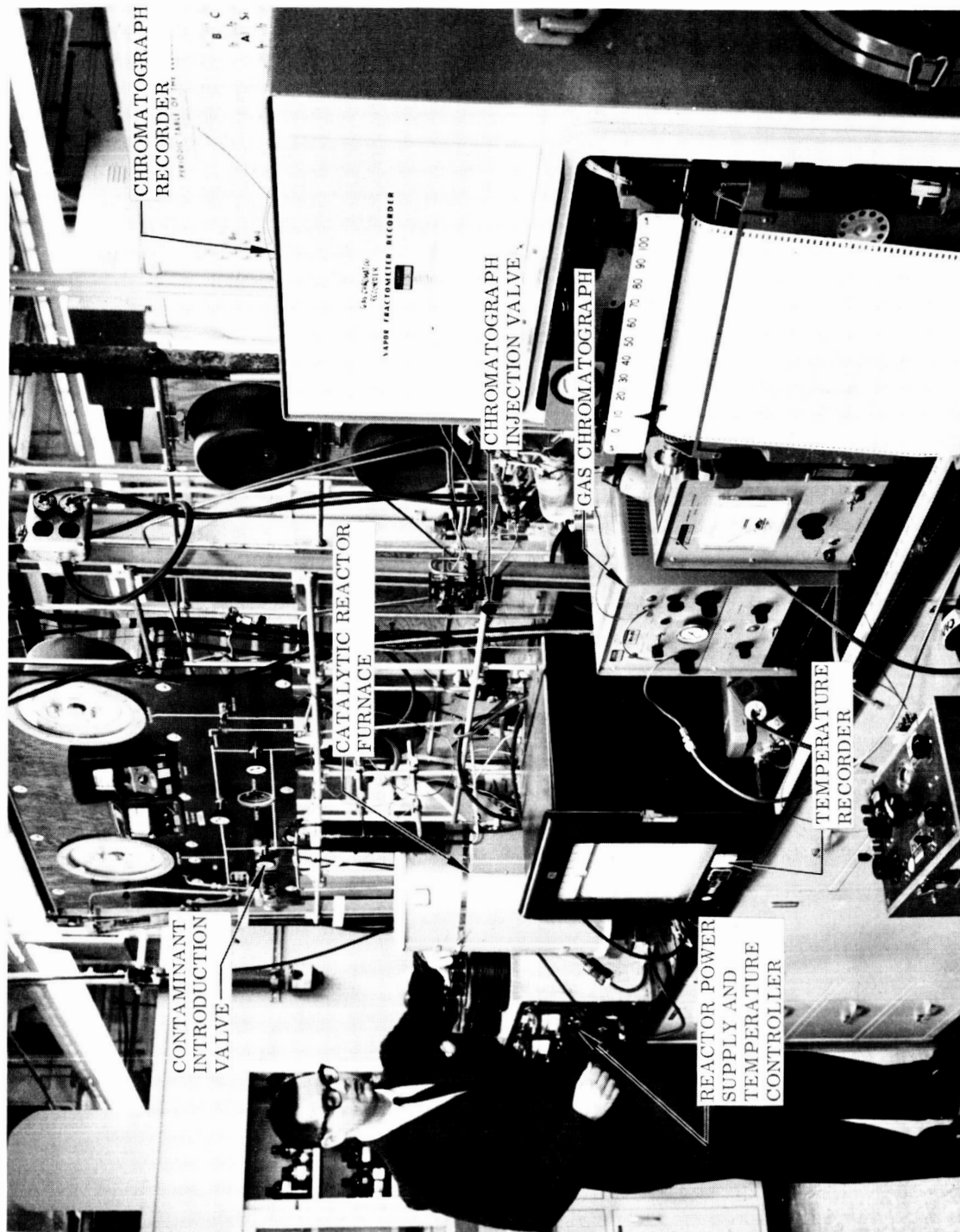


Fig. 4-1 Apparatus for Catalyst Studies

4.3 PROCEDURE

Oxygen gas at 5 psia, containing 95 mg/m³ CO, was bubbled through water at 18°C. Pure H₂S was mixed with the humidified gas to achieve an inlet H₂S concentration near SMAC (6 mg/m³). Inlet and outlet CO concentrations were measured vs. time in terms of the CH₄ output of the Sabatier reactor. Inlet H₂S concentrations were measured periodically using MSA adsorption tubes (noting the length of tube discoloration).

4.4 RESULTS

The conversion efficiency for CO over the two catalysts tested, vs. time, is shown in Figures 4-2 and 4-3. The inlet concentration of H₂S for each test is shown in Figures 4-4 and 4-5.

100% conversion of CO was noted at the beginning of the test for each catalyst, and for several days thereafter. A drop in concentration was noted after about six days of testing with LI-4 and after about ten days with the 0.5% Pd catalyst. Conversion had dropped to 10% or less on the ninth day for LI-4 and on the twelfth day for the 0.5% Pd.

4.5 DISCUSSION

The average H₂S inlet concentrations were slightly higher than SMAC (6 mg/m³) in each case; for the LI-4 tests inlet H₂S averaged 6.1 mg/m³, while for the 0.5% Pd, inlet concentration averaged 7.2 mg/m³. This was due to H₂S inflow variations through the glass capillary.

On the assumption that the poisoning is cumulative, new time scales were calculated, based on inlet concentrations equal to SMAC. These are shown on Figures 4-2, 4-3, 4-4 and 4-5.

At a temperature of 77°F and actual space velocity of 2090 hr⁻¹, both the LI-4 and 0.5% Pd catalysts oxidized CO at 100% per pass prior to H₂S introduction. The 0.5% Pd catalyst continued to perform CO oxidation for a longer period than the same quantity of LI-4.

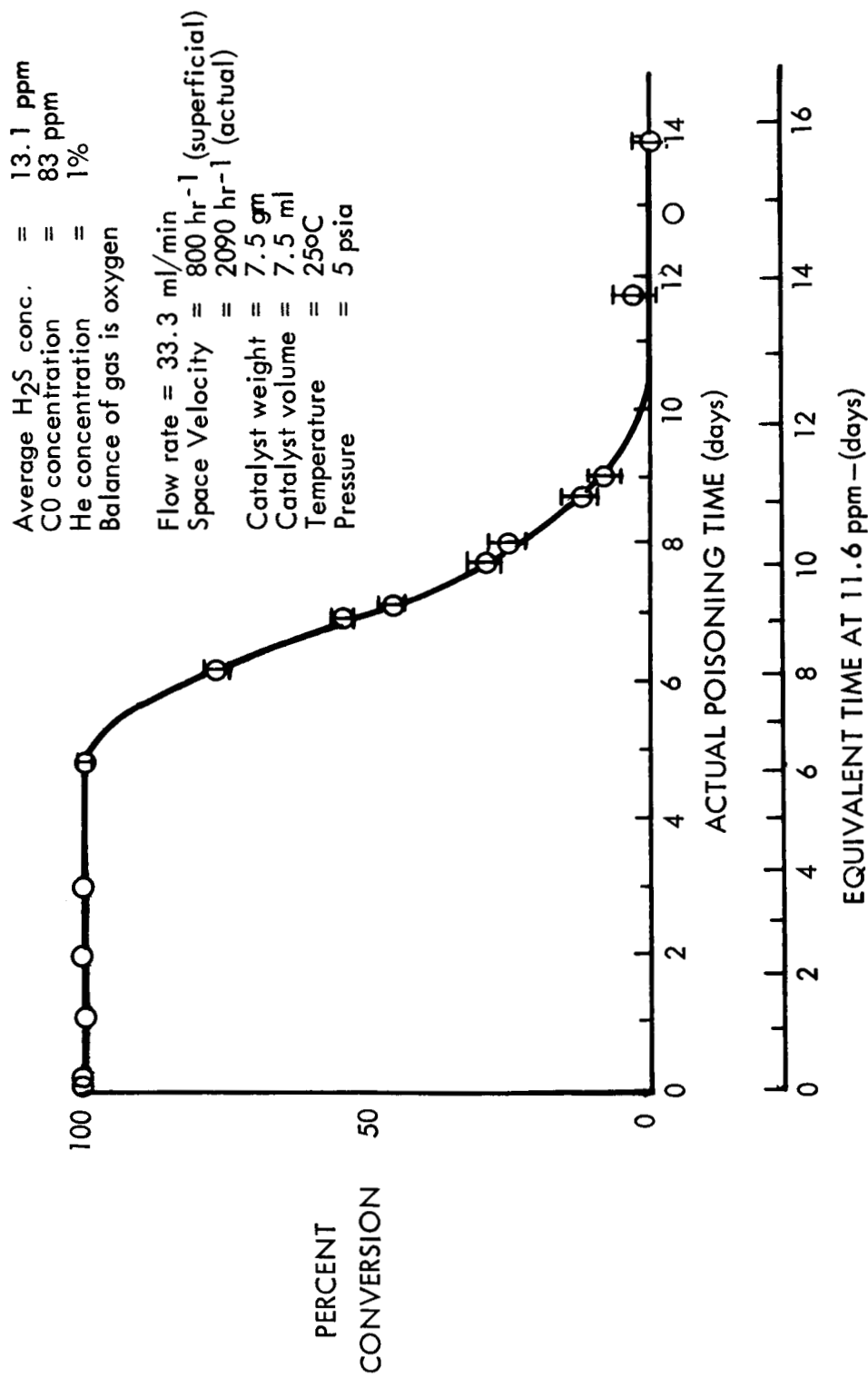


Fig. 4-2 CO Conversion vs. Time - 1% Pt, 1% Pd Catalyst

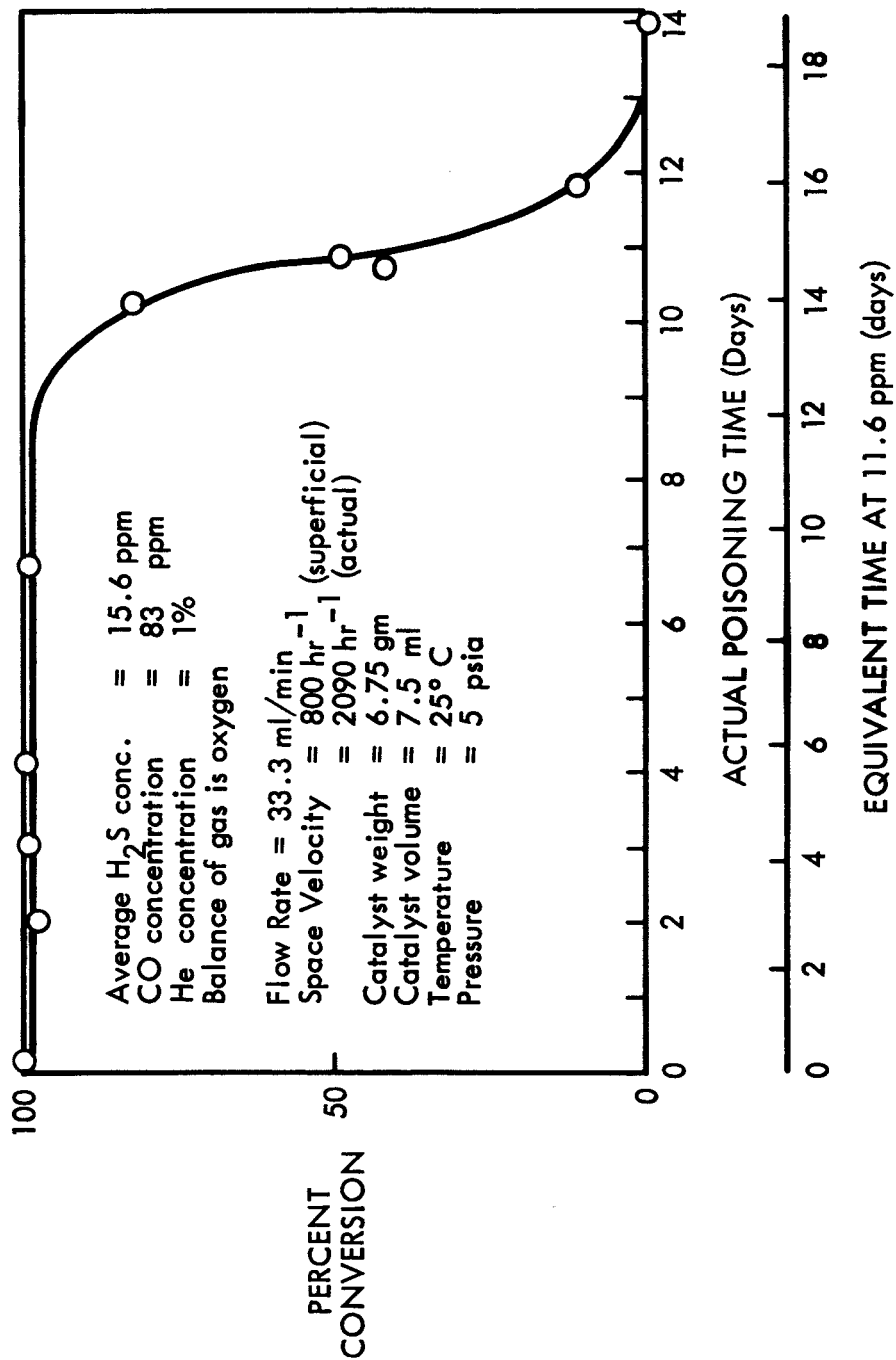


Fig. 4-3 CO Conversion vs Time, 0.5% Pd Catalyst

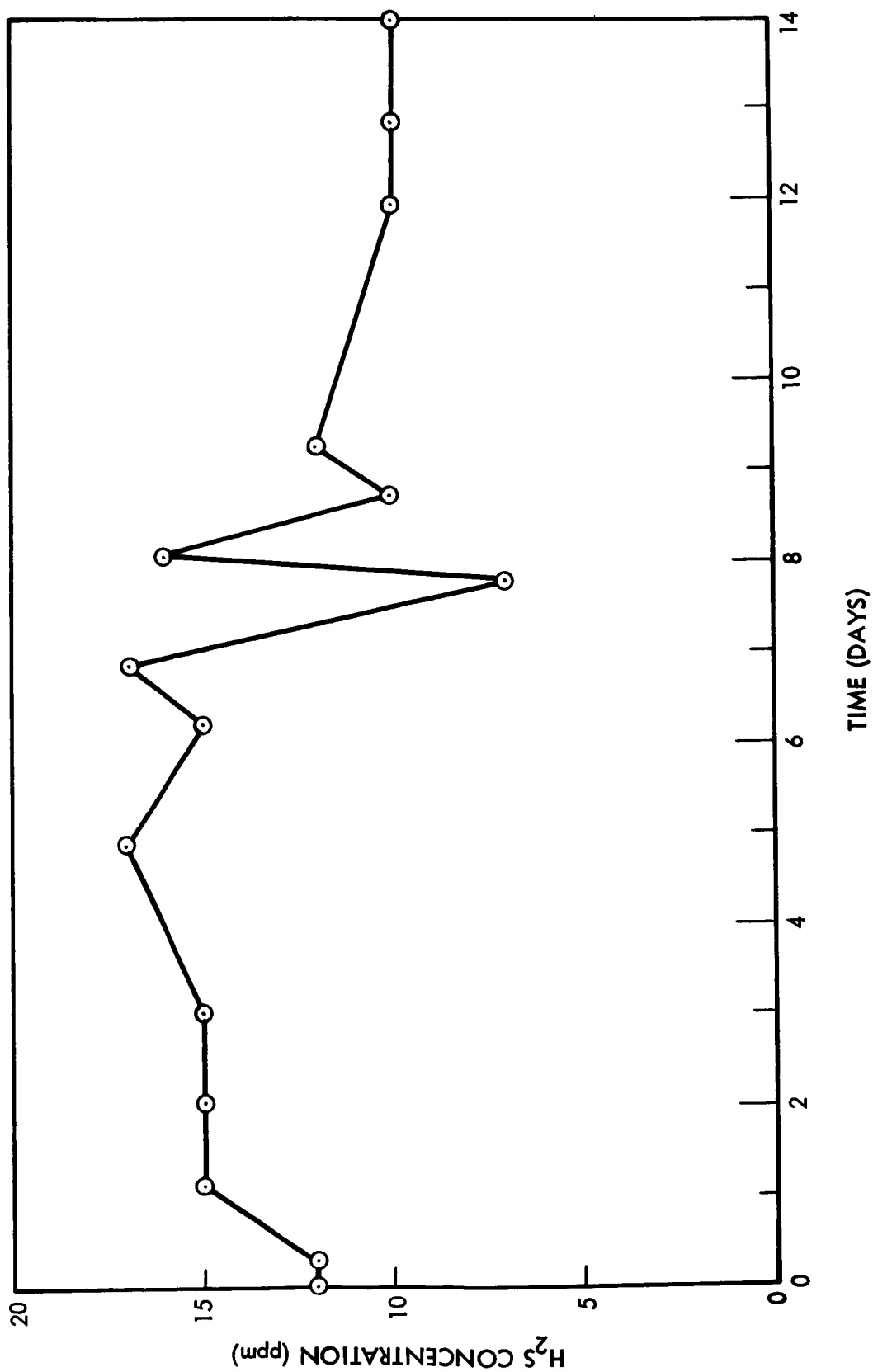


Fig. 4-4 H_2S Concentration vs. Time Over 0.5% Pd Catalyst

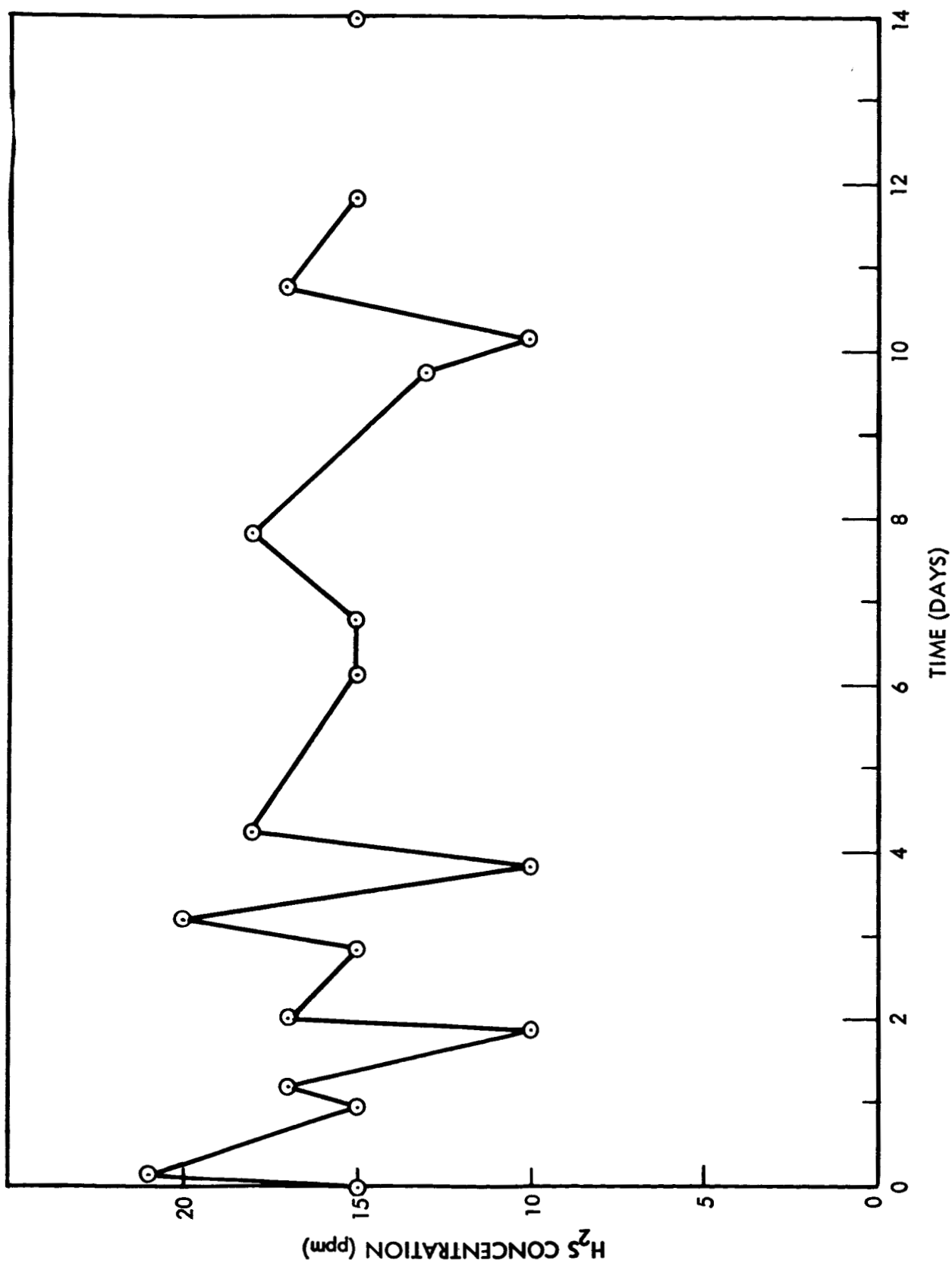


Fig. 4-5 H₂S Concentration vs. Time Over 0.5% Pd Catalyst

Assuming the same dispersed metal thickness, the LI-4 should have approximately 2.5 times the metal surface area as the 0.5% Pd. The time to deactivate equal volumes of catalyst under equivalent conditions of flow and inlet "poison" concentration should be proportional to catalyst surface area. On the basis of the test data it appears that the LI-4 may have metal incompletely dispersed or incompletely reduced.

It should be noted that by increasing the volume of catalyst, poisoning time will be increased proportionally. The fact that the amount of catalyst used in these tests poisoned in less than 14 days does not mean that it is impossible to provide a room temperature, 14-day, CO conversion unit. The data obtained from these tests provides sufficient data to allow design of such a unit based on H_2S as the "typical" poison.

Section 5

CATALYST TESTS - OXIDATION EFFICIENCY OF 0.5% PD CATALYST *

The oxidation efficiency tests on the 0.5% palladium catalyst were performed from 20 December 1965 through 20 January 1966. This section presents the objectives of the test, apparatus and procedures followed, the results obtained, and a discussion of the results.

5.1 OBJECTIVES

The objectives of the test were to:

- Determine the ability of the 0.5% Pd catalyst to oxidize a mixture of compounds while being operated at a space velocity of approximately $15,000 \text{ hr}^{-1}$ and at three temperatures, high enough to obtain approximately 25%, 50%, and 100% methane conversion.
- Determine the effect of Freon 12 on the oxidation efficiency of the 0.5% Pd catalyst.

5.2 APPARATUS

The apparatus utilized in performing the partial oxidation tests on the 0.5% Pd catalyst are shown in Figures 5-1 and 5-2. The major test equipment included the following items:

- Cylinders for gaseous contaminants, oxygen, and carbon dioxide supply
- Flow meters to monitor contaminant and total flow rates
- Motorized syringe unit for liquid contaminant introduction
- Total pressure gage to measure system pressure
- LMSC catalytic oxidizer unit and temperature controller

*0.5% Palladium on 1/8-inch aluminum pellets (Englehard, Newark, N. J.)

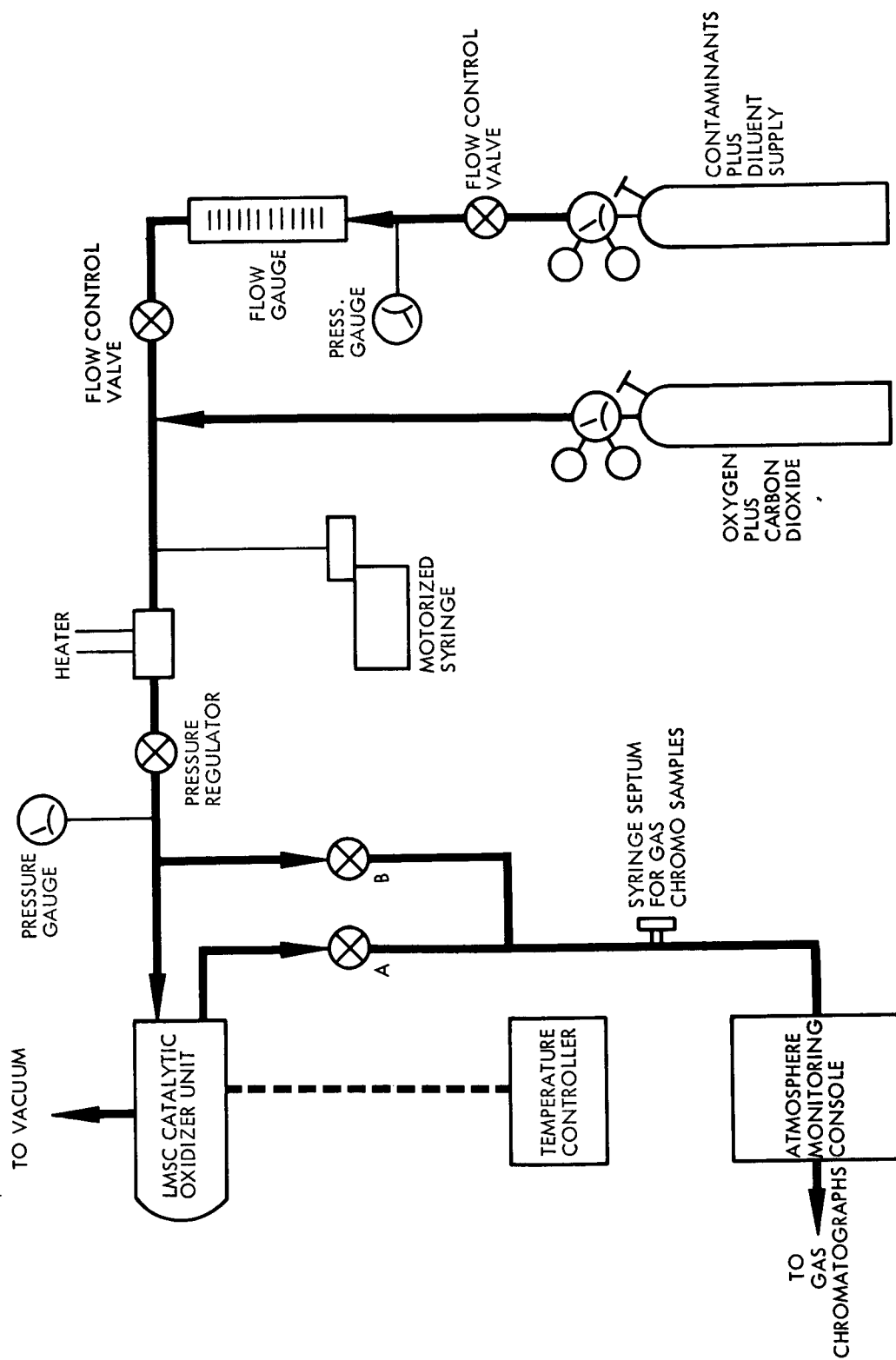


Fig. 5-1 Apparatus For Oxidation Efficiency Tests Schematic Diagram

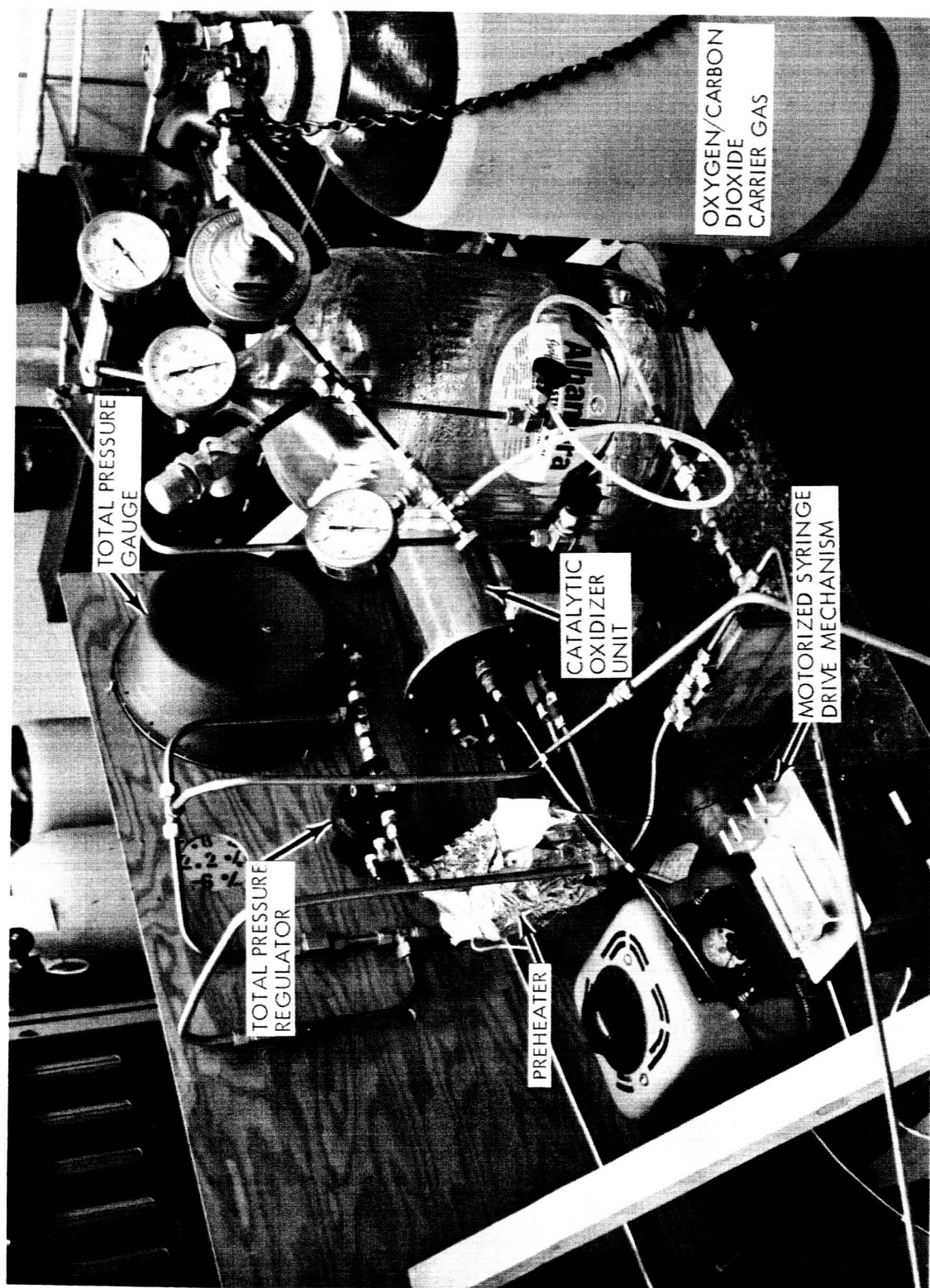


Fig. 5-2 Test Apparatus for Oxidation Efficiency Tests

5.3 PROCEDURE

The partial oxidation tests on the 0.5% Pd catalyst were initiated in the following manner. With the system operating at a space velocity of $15,000 \text{ hr}^{-1}$, a total pressure of 5 psia, and in an oxygen atmosphere with a carbon dioxide concentration of 7.6 mm Hg, the contaminants listed in Table 5-1 were introduced at the system inlet. The system was allowed to stabilize and contaminant inlet concentrations were measured. The desired catalyst bed temperatures were then established and contaminant outlet concentration measured at each temperature condition. At the conclusion of each test, contaminant inlet concentrations were verified.

As a result of catalyst poisoning during the first series of tests, it was determined that the contaminants to be introduced should be revised. The revised contaminant list appears in Table 5-2. The revised procedure consisted of performing the oxidation efficiency tests outlined above, first without Freon-12 and then with Freon-12 to observe poisoning effects due to this contaminant. A fresh catalyst charge was used for these tests.

Table 5-1
CONTAMINANTS USED IN INITIAL OXIDATION
EFFICIENCY TESTS

Acetaldehyde
Acetylene
Carbon Monoxide
Formaldehyde
Freon-12
Hydrogen
Methane
Methyl Alcohol
Methyl Mercaptan
Propylene
Propyl Mercaptan
Vinyl Chloride

Table 5-2
CONTAMINANTS USED IN FINAL OXIDATION
EFFICIENCY TESTS

Acetylene
Butene-1
Carbon Monoxide
Freon-12
Hydrogen
Methane
Methyl Alcohol
n-Butane
Propane
Propylene
Propyl Mercaptan
trans-Butene-2

Three test series were conducted: (1) initial tests using the contaminants listed in Table 5-1, (2) final tests using the contaminants listed in Table 5-2, and (3) final tests using the contaminants listed in Table 5-2, except Freon-12.

5.4 RESULTS

Results of the initial test series are shown in Figure 5-3. Results of the final oxidation efficiency test without Freon-12 are shown graphically in Figure 5-4 and in tabular form in Table 5-3. Results of the final oxidation tests with Freon-12 are shown graphically in Figure 5-5 and in tabular form in Table 5-4.

5.5 DISCUSSION

5.5.1 Contaminant Revision

During the system checkout prior to the initial tests, data were obtained on methane conversion efficiency versus temperature. This checkout was performed with the

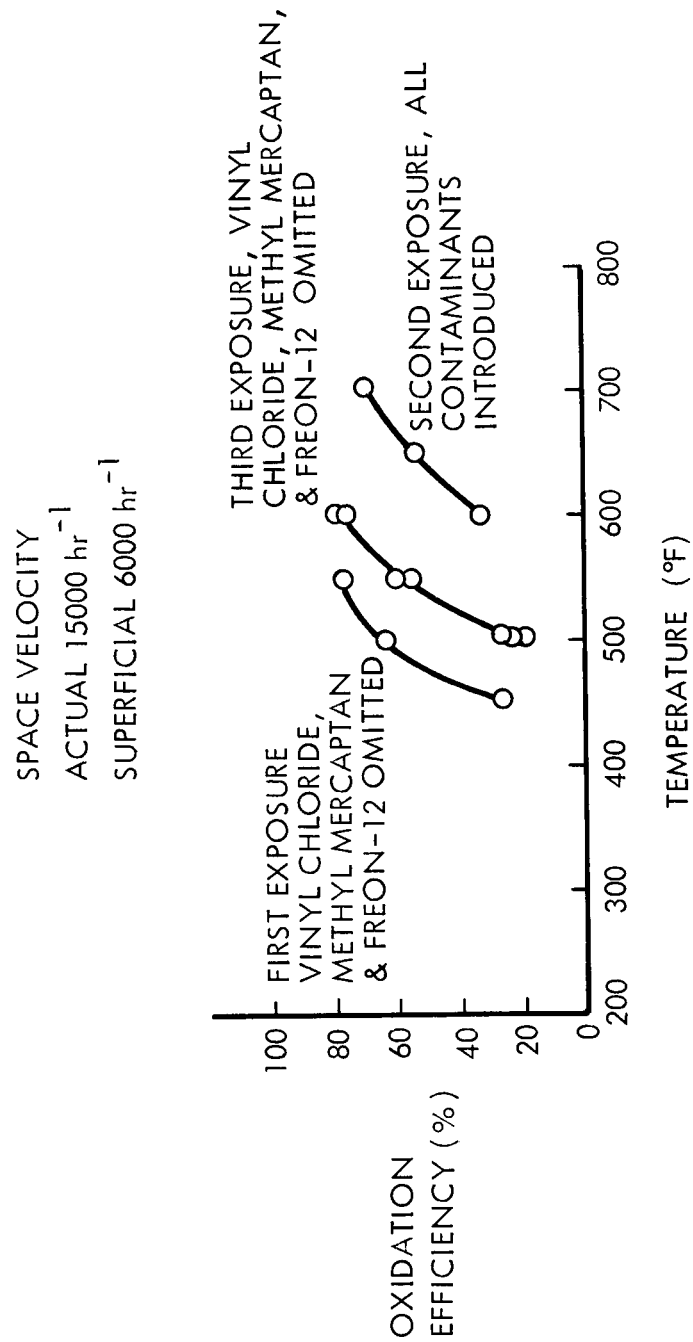


Fig. 5-3 Methane Oxidation Efficiency in Presence of Contaminants Listed in Table 5-1

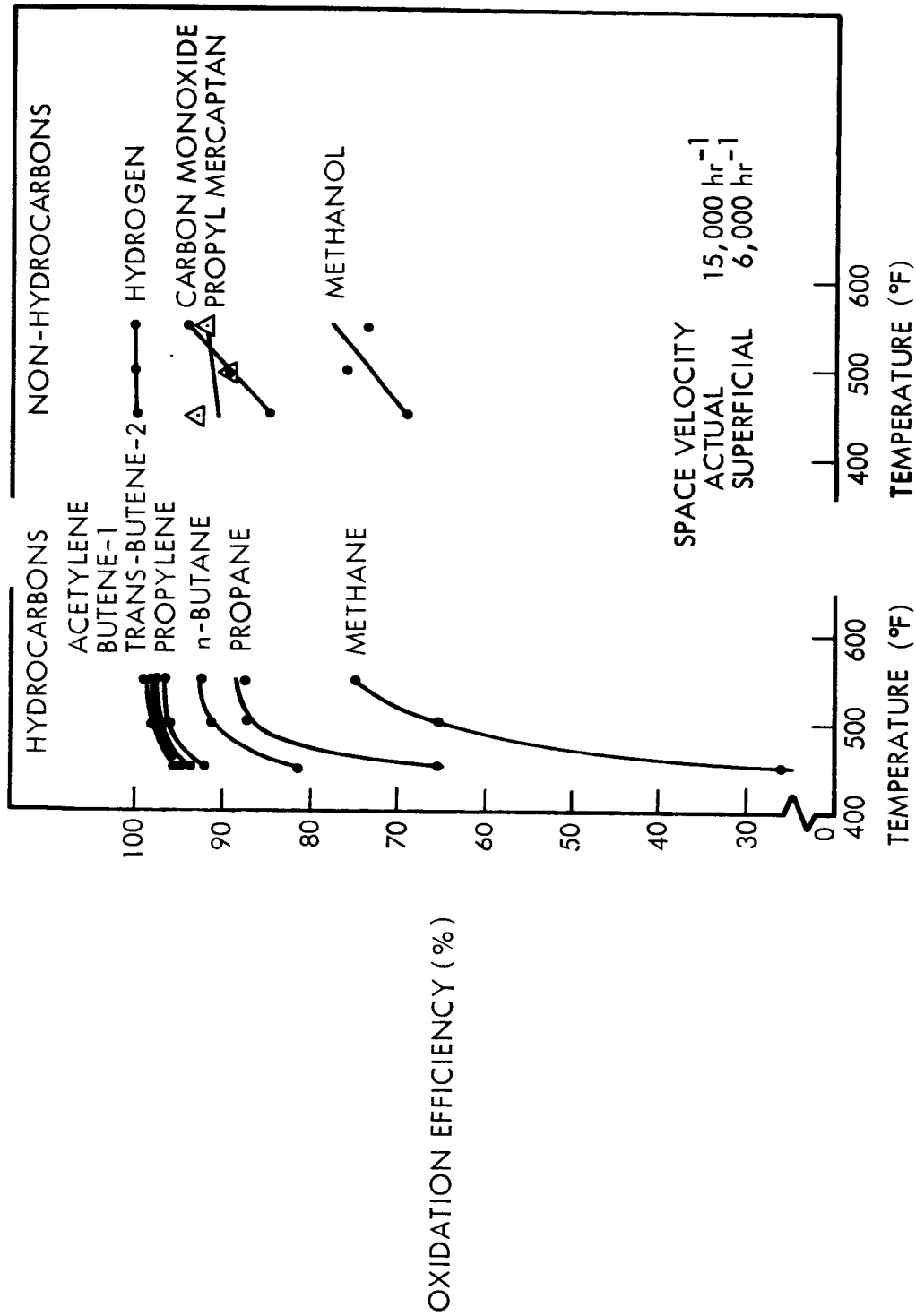


Fig. 5-4 Final Oxidation Efficiency Test Results Without Freon-12

Table 5-3

FINAL OXIDATION EFFICIENCY TEST RESULTS - WITHOUT FREON-12

Contaminant	MAC mg/m ³	Estimated Instrument Sensitivity mg/m ³	Inlet Concentration mg/m ³	Oxidation Efficiency (%)		
				450° F	500° F	550° F
Acetylene	28.0	0.9	42.0 ± 0.5	94.6 ± 0.0	98.0 ± 0.4	98.5 ± 0.1
Butene-1	60.4	0.3	47.7 ± 0.5	95.3 ± 0.8	97.3 ± 0.2	97.7 ± 0.2
Carbon Monoxide	22.0	3.5	9.3 ± 0.0	84.0 ± 1.3	92.0 ± 1.4	94.0 ± 0.0
Hydrogen	215.0	3.6	191.0 ± 6.5	100.0 ± 0.0	100.0 ± 0.0	100.0 ± 0.0
Methane	1720.0	17.0	2930.0 ± 44.0	25.6 ± 6.4	64.1 ± 4.3	75.0 ± 6.6
Methyl Alcohol	34.4	1.0	45.5 ± 4.6	69.0 ± 1.9	76.1 ± 5.2	73.5 ± 2.6
n-Butane	26.5	0.3	22.6 ± 0.3	81.7 ± 1.2	91.4 ± 0.0	92.0 ± 0.4
Propane	47.4	0.3	24.5 ± 0.3	64.7 ± 3.3	87.4 ± 0.4	87.7 ± 0.0
Propylene	45.2	0.2	63.6 ± 0.7	92.2 ± 1.2	96.3 ± 0.4	96.2 ± 0.1
Propyl Mercaptan	82.0	0.5	94.6 ± 4.7	93.8 ± 0.8	89.0 ± 1.1	91.9 ± 1.7
t-Butene-2	60.4	0.3	40.1 ± 0.4	93.5 ± 1.0	97.0 ± 0.1	97.4 ± 0.3

Table 5-4
FINAL OXIDATION EFFICIENCY TEST RESULTS - WITH FREON-12

Contaminant	SMAC mg/m ³	Estimated Instrument Sensitivity mg/m ³	Inlet Concentration mg/m ³	Oxidation Efficiency (%)		
				450° F	500° F	550° F
Acetylene	28.0	0.9	44.2 ± 0.4	96.4 ± 0.3	98.3 ± 0.0	98.8 ± 0.6
Butene-1	60.4	0.3	42.8 ± 0.1	93.1 ± 0.4	95.3 ± 0.3	97.2 ± 0.3
Carbon Monoxide	22.0	3.5	9.3 ± 0.0	68.0 ± 0.0	75.0 ± 0.0	84.0 ± 0.0
Freon-12	120.0	0.3	101.0 ± 5.6	57.5 ± 2.5	75.1 ± 1.4	83.9 ± 0.0
Hydrogen	215.0	3.6	199.0 ± 7.0	96.5 ± 0.0	100.0 ± 0.0	100.0 ± 0.0
Methane	1720.0	17.0	3060.0 ± 46.0	10.5 ± 1.0	14.1 ± 1.7	47.3 ± 16.3
Methyl Alcohol	34.4	1.0	46.2 ± 3.0	81.5 ± 2.5	86.8 ± 1.9	86.0 ± 1.5
n-Butane	26.5	0.3	20.7 ± 0.5	54.9 ± 0.0	74.0 ± 2.3	85.9 ± 3.3
Propane	47.4	0.3	18.8 ± 0.2	51.1 ± 10.0	72.5 ± 2.7	85.1 ± 5.5
Propylene	45.2	0.2	62.4 ± 1.6	90.6 ± 2.3	92.5 ± 0.5	95.5 ± 0.3
Propyl Mercaptan	82.0	0.5	65.5 ± 3.1	97.0 ± 0.3	97.7 ± 0.4	97.9 ± 0.4
t-Butene-2	60.4	0.3	35.7 ± 0.1	92.0 ± 0.3	93.3 ± 0.6	96.3 ± 0.3

contaminants listed in Table 5-1, excluding Freon-12, methyl mercaptan and vinyl chloride. After it was determined that the apparatus was operating satisfactorily, a test was performed using all of the contaminants listed in Table 5-1. The purpose of this test was to establish methane conversion efficiency versus temperature in order to select the operating temperatures for the final runs. It was observed during this test that the methane removal efficiency at a given temperature was considerably less than that observed during the checkout. To verify that this was caused by the addition of Freon-12, methyl mercaptan and vinyl chloride, a third test was performed in which these three contaminants were not present. This test indicated partial recovery of the catalyst efficiency for methane conversion, as shown in Figure 5-3.

The poisoning effect caused by one or more of these three contaminants was extreme; consequently, a new group of contaminants was selected as shown in Table 5-2. In this new list, methyl mercaptan, vinyl chloride, formaldehyde, and acetaldehyde were replaced with butene-1, trans-butene-2, n-butane, and propane. Freon-12 was retained and the final evaluations were performed with and without Freon-12. Acetaldehyde and formaldehyde were replaced due to difficulties in obtaining a reliable chemical analysis.

5.5.2 Selection of Operating Temperatures

Methane oxidation efficiency vs. temperature was determined using the contaminants listed in Table 5-2, except Freon-12. It was found that for a space velocity of $15,000 \text{ hr}^{-1}$, that (1) the threshold for methane oxidation occurred slightly below 450°F , and (2) above 550°F , oxidation efficiency increased very slowly with increasing temperature.

The temperature range of 450°F to 550°F provided a range of methane oxidation from approximately 25% to 80%, which was considered to be the range of primary interest. Runs were also made at an intermediate temperature of 500°F to further define curves of oxidation efficiency vs. temperature.

5.5.3 Inlet Concentration

At each operating condition during the test, three or more gas samples were analyzed. The inlet concentration data reported in Tables 5-3 and 5-4 represent the average value of these multiple analyses. The experimental error indicated with each inlet concentration is the average deviation of the individual measurements from the reported value.

The inlet concentrations were desired to approximate SMAC values. Due to differences between the delivered and requested concentrations of the purchased pre-mixed contaminants, the introduction rates were arranged so that some contaminants were below SMAC and some greater than SMAC.

5.5.4 Oxidation Efficiency Data

The contaminant oxidation efficiencies were based on the relationship

$$\eta_r = \frac{C_i - C_o}{C_i} \quad (5.1)$$

where

- C_i = Contaminant inlet concentration
- C_o = Contaminant outlet concentration
- η_r = Removal efficiency

The removal efficiency was calculated from equation 5.1 using the data from each of the three or more analyses performed at each operating condition. The average value of these removal efficiencies was then reported in Tables 5-3 and 5-4 for each operating condition. The experimental error indicated with each removal efficiency is the average deviation of the individual efficiencies from the reported value.

5.5.5 Comparison With Predicted Performance

As shown in Table 5-5 from Ref. 1, it was predicted that methane would be the most difficult contaminant to oxidize and that carbon monoxide would be the easiest. Inspection of the oxidation efficiency data, and their accuracies, shown in Tables 5-3 and 5-4 reveals that all but three of the contaminants – acetylene, carbon monoxide, and methyl alcohol – followed the predicted order.

With only one exception (550° F test without Freon-12, Table 5-4) methane was the most difficult contaminant to oxidize. This one anomaly, however, is attributed to the accuracy of the data.

Carbon monoxide, however, was not the easiest to oxidize. Depending on the run examined, as many as six of the twelve contaminants tested were oxidized with greater efficiency. In all cases but one (450° F with Freon-12, Table 5-4) hydrogen was the easiest to oxidize, although the differences between oxidation efficiencies are quite small.

It should be noted that the classification according to ease of oxidation described in the Phase I report was primarily theoretical and based on single rather than multiple contaminant oxidation. The multiple contaminant oxidation experiments reported herein were conducted to obtain more data on oxidation efficiencies for the simultaneous oxidation of a number of contaminants. Variations between the Phase I theoretical classification and the Phase III experimental results are attributed primarily to interference among the contaminants being oxidized. In the case of CO, however, the apparent reduction in oxidation efficiency could well be due to the production, in the reactor, of CO from the many organic compounds undergoing reaction.

5.5.6 Effect of Freon-12

It was determined (Figure 5-3) that the presence of Freon-12, methyl mercaptan and vinyl chloride caused significant degradation in the performance of the 0.5% palladium catalyst. However, it was not determined which of these contaminants caused the poisoning.

Table 5-5
PREDICTED ORDER OF OXIDATION EFFICIENCY
FOR SINGLE CONTAMINANTS
(From Highest to Lowest)

Carbon Monoxide
Hydrogen
Methyl Alcohol
Butene-1
trans-Butene-2
Propylene
Acetylene
n-Butane
Propane
Methane

Tests performed with the revised group of contaminants were carried out both with and without Freon-12 to observe if poisoning occurred. These results can be observed by comparing the data shown in Figure 5-4 with that shown in Figure 5-5. It can be seen from this comparison that the presence of Freon-12 did cause a reduction in catalyst performance. The extent of this effect varied among contaminants but in general, the presence of Freon-12 caused the temperature required for a given oxidation efficiency to increase about 50° F.

The poisoning encountered with Freon-12 is not as significant as with the Freon-12/methyl mercaptan/vinyl chloride mix, where the shift in temperature required to maintain a given oxidation efficiency was as great as 180° F. It appears from this that methyl mercaptan and/or vinyl chloride are more significant potential poisons, for the 0.5% palladium catalyst, than Freon-12.

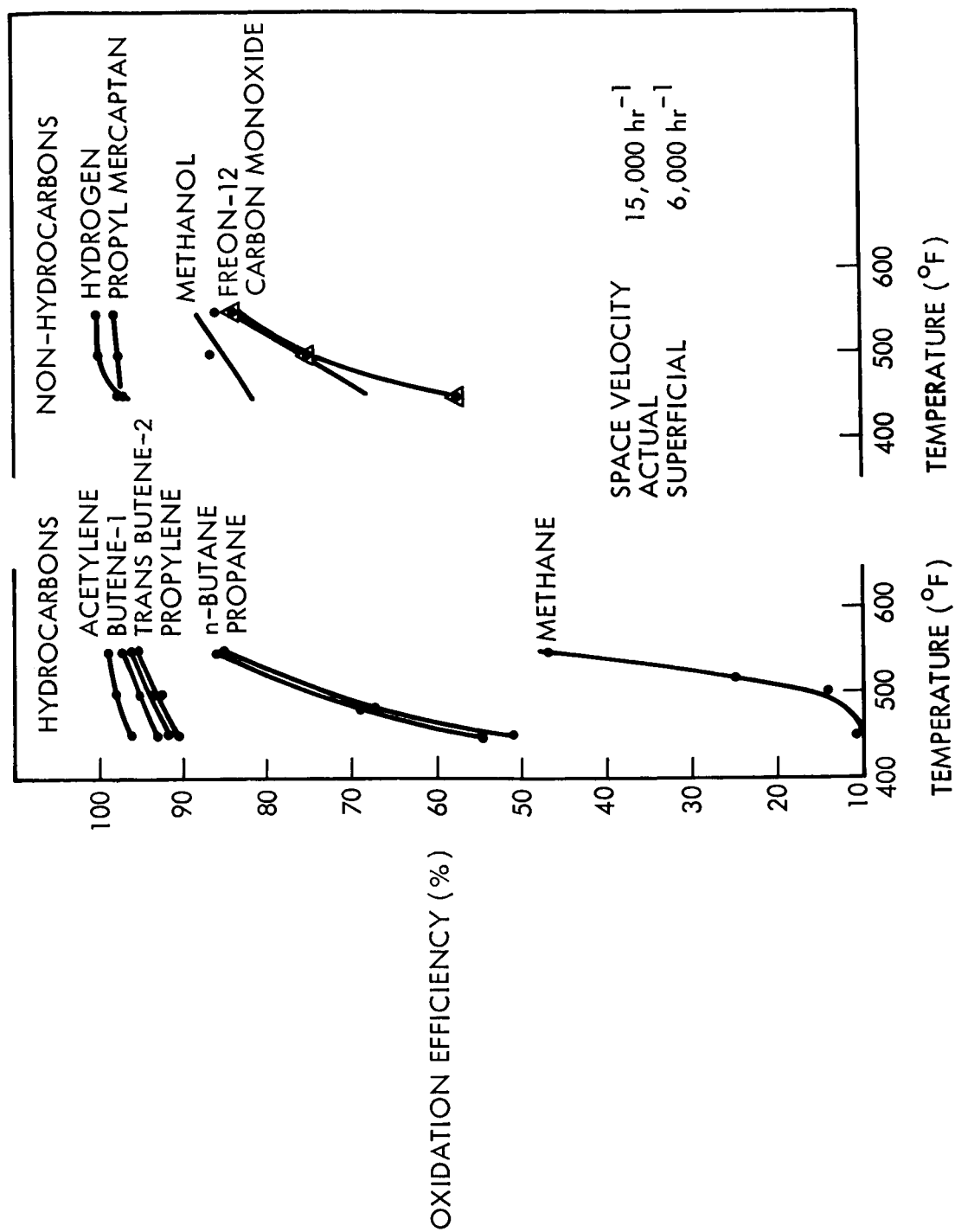


Fig. 5-5 Final Oxidation Efficiency Test Results with Freon-12

Section 6

CONCLUSIONS AND RECOMMENDATIONS

6.1 CONCLUSIONS

6.1.1 Potential-Plot Verification

Based on the results shown in Figure 2-3 there appear to be two correlating lines, one for the Freons and one for the hydrocarbons. The results of the mercaptan runs were scattered. The point for propyl mercaptan lies closest to the Freon line while the point for methyl mercaptan lies above the hydrocarbon line. The point for vinyl chloride lies slightly above the hydrocarbon line.

The nonconvergence of inlet and outlet concentrations for Freon-23, the mercaptans, ethylene, and acetylene is attributed to a slow oxidation or possibly polymerization. A poisoning of the surface for this process may occur after a sufficient time interval. Nonconvergence is therefore a process which provides removal capability greater than that attributed only to adsorption. However, points on the potential plots represent only the adsorption contribution.

6.1.2 Sorbent Comparison

As depicted in Figure 2-7, of the four sorbents tested, BD has the highest capacity for A less than 32. AC has the highest capacity for A greater than 32. The acid-impregnated BD (C1) has a consistently lower capacity than AC, however, C1 has an appreciable capacity for ammonia. The capacity is quoted as cc contaminant per gram of sorbent. In the case of C1, one gram of sorbent contains only 0.80 grams of BD charcoal; consequently, it would be expected to have a lower capacity than unimpregnated BD. The capacity of the MSA sorbent was significantly lower than the other sorbents tested for A values of major interest.

6.1.3 Retention-Time Correlation With Saturation Capacity

Figures 3-1, 3-2, and 3-3 show the correlation between retention time and saturation capacity based on high temperature injection experiments in a helium background. It appears that this correlation is a rough estimating tool; the most accurate method for determining capacities is still the flow-type or low-temperature injection experiment approach.

6.1.4 Prediction of Breakthrough Curve Characteristics

Use of either an injection-type or continuous flow experiment allows one to establish the rate controlling step for a given contaminant and sorbent by means of Figure 3-14. Predictions of breakthrough-curve shapes can then be made for a wide range of particle diameter, velocity, and bed-length conditions. This bears out, and places on a better quantitative basis, the general conclusion in the Phase I work that particle diameter and space velocity are the primary determinants of breakthrough-curve shape for a given contaminant and a given sorbent.

6.1.5 Catalyst Tests - CO Oxidation and H₂S Poisoning

Both the 1% Pt - 1% Pd and the 0.5% Pd catalysts will oxidize CO at 100% per pass at room temperature and an actual space velocity of 2090 hr⁻¹ (superficial space velocity of 800 hr⁻¹). After continued exposure to average H₂S concentrations in the range of 6.1 to 7.2 mg/m³, both catalysts are eventually rendered inoperative. For 6.75 grams of the 0.5% catalyst, total deactivation occurs after approximately 18 days. For 7.5 grams of the 1% Pt - 1% catalyst, total deactivation occurs after approximately 13 days.

The difference in behavior of the two catalysts is attributed to different noble-metal surface areas resulting from different dispersion procedures. It is expected that greater surface areas of noble metal require a longer period for coverage by contaminants which could deactivate the catalyst.

If a room-temperature CO converter is to be constructed for a 14 day mission, it should (1) probably contain a catalyst with a high metal-surface area, (2) be provided with a pre-sorbent to maintain potential poison concentration at very low levels, and (3) be tested to ensure it contains a sufficient quantity of catalyst to survive the entire mission including pre-launch checkout.

6.1.6 Catalyst Tests - Oxidation Efficiency For Multiple Contaminants

These tests verified the capability of the 0.5% Pd catalyst to provide 25% methane conversion at an actual space velocity of $15,000 \text{ hr}^{-1}$ (superficial space velocity of 6000 hr^{-1}) and a temperature of 450°F . A temperature of 520°F was required for 25% methane conversion in the presence of Freon-12 at 101 mg/m^3 .

In the presence of Freon-12, vinyl chloride, and methyl mercaptan, temperatures as high as 590°F were required to achieve the 25% methane conversion.

Inspection of the oxidation efficiency data, and associated accuracies, shown in Tables 5-3 and 5-4 reveals that all but three contaminants - acetylene, carbon monoxide, and methyl alcohol - followed the predicted order of ease of oxidation.

With only one exception (550°F tests without Freon-12, Table 5-4) methane was the most difficult contaminant to oxidize. This one anomaly, however, can be attributed to the accuracy of the data.

Carbon monoxide, however, was not the easiest to oxidize. Depending on the run examined, as many as six of the twelve contaminants tested were oxidized with greater efficiency. In all cases but one (450°F with Freon-12, Table 5-4), hydrogen was the easiest to oxidize. In this case, propyl mercaptan was oxidized with slightly greater efficiency than was hydrogen.

It should be noted that the classification according to ease of oxidation described in the Phase I report was primarily theoretical and based on single rather than multiple

contaminant oxidation. The multiple contaminant oxidation experiments reported herein were conducted to obtain more data on the efficiency of simultaneous oxidation of a number of contaminants. Variations between the Phase I theoretical classification and the Phase III experimental results are attributed primarily to interference among the contaminants being oxidized. In the case of CO, however, the apparent reduction in oxidation efficiency could well be due to production, in the reactor, of CO from the many organic compounds undergoing reaction.

Comparison of Tables 5-3 and 5-4, or Figures 5-4 and 5-5, show that the presence of Freon-12 causes a reduction in catalyst performance. The extent of this effect varied among contaminants, but in general the presence of Freon-12 caused the temperature required for a given oxidation efficiency to increase about 50° F.

The poisoning encountered with Freon-12 is not as significant as with the Freon-12/methyl mercaptan/vinyl chloride mix, where the shift in temperature required to maintain a given oxidation efficiency was as great as 180° F. It appears from this that methyl mercaptan and/or vinyl chloride are more significant potential poisons, for the 0.5% palladium catalyst, than Freon-12.

6.2 RECOMMENDATIONS

6.2.1 Potential-Plot Verification

Based on the work presented herein, it is recommended that (1) the lower potential plot lines be used for estimating sorbent capacities for Freons, (2) the upper potential plot lines be used for estimating sorbent capacities for hydrocarbons, and (3) the lower lines be used as a conservative estimate of sorbent capacities for other compounds until further experimental work is done to justify another approach.

6.2.2 Sorbent Comparison

It is recommended that further consideration be given to the effect of replacing the present Apollo charcoal (AC) with the acid-impregnated BD (C1). The question to be

resolved in whether the significant NH_3 removal capability of the C1 is worth the reduction in adsorption capacity for other contaminants. Another possibility to consider is use of the unimpregnated BD, if removal of contaminants below an A of 32 is of primary interest. Analytical studies along these lines should be undertaken.

6.2.3 Retention-Time Correlation with Saturation Capacity

At the present time the use of high temperature injection experiments in a helium background is not recommended as the preferred method for determining saturation capacities.

Additional studies are recommended to try and relate the low-temperature injection experiments in an oxygen background with the simpler and shorter high temperature helium tests. The low temperature injection experiments in oxygen appear to be a satisfactory substitute for continuous flow experiments as a means of determining saturation capacities.

6.2.4 Prediction of Breakthrough Curve Characteristics

The method described in this report for predicting breakthrough curve characteristics appears to be sound but has had limited experimental verification. It is recommended that further experimentation be conducted to provide additional verification. This is, potentially, a very powerful tool for the prediction of sorbent bed performance over a wide variety of operating conditions.

6.2.5 Catalyst Tests - CO Oxidation and H_2S Poisoning

These tests clearly showed the effects of H_2S at SMAC in reducing the performance of low temperature CO oxidation catalysts. Since low-temperature CO conversion is of significant interest for spacecabin contaminant removal, the effectiveness of a pre-sorber and increased catalyst noble-metal surface area should be determined.

6.2.6 Catalyst Tests — Oxidation Efficiency for Multiple Contaminants

During the experiments conducted, the 0.5% Pd catalyst was more efficient than the 1% Pt — 1% Pd catalyst tested under previous phases of the contract. The 0.5% Pd catalyst can be recommended as a potential replacement for the 1% Pt — 1% Pd, however, until 14-day elevated-temperature tests are conducted with representative multiple contaminants the satisfactory performance of either catalyst for the full Apollo mission cannot be guaranteed. It is recommended that such an extended-duration test be conducted on either the 0.5% Pd or a higher surface area noble-metal catalyst.

Appendix A
DATA FROM DYNAMIC ADSORPTION TESTS

Table A-1

SUMMARY OF DYNAMIC ADSORPTION EXPERIMENTS*

Run No.	Adsorbent (28 x 60 mesh)	Wt. (g) (initial)	Adsorbate	Flow Rate (cc/min) @ 5 psia	t (min) @ C = 1/2 C _i (eff)	L/D	Bed Vol. (cc)	(mg/m ³)	C (effective) (ppm)	q cc (liq)/g	A
103	BD	15.000	Methane	230	5	9.38	30.1	167.5	765	2.33×10^{-5}	52.0
104 (e)	BD	1.000	Propane	230	179.5	7.48	1.5	47.7	79	3.54×10^{-3}	24.3
105 (a)	BD	5.001	Ethylene	230	19.8	3.12	10.05	31.0	80.8	4.96×10^{-5}	42.0
106 (a)	AC	5.000	Ethylene	198	16.7	3.12	10.05	30.0	78	3.81×10^{-5}	42.2
107	C1	5.000	Ethylene	230	13.1	3.12	10.05	34.6	90.3	4.0×10^{-5}	42.2
108 (a)	MSA-Fiber	3.636	Ethylene	230	5	9.38	30.1	28.4	74.2	2.1×10^{-5}	42.2
109 (a)	BD	15.000	Acetylene	230	24.2	9.38	30.1	21.4	60	1.34×10^{-5}	49.2
110 (a)	AC	15.000	Acetylene	230	21.8	9.38	30.1	21.8	61.2	1.21×10^{-5}	49.2
111	C1	15.000	Acetylene	230	22.1	9.38	30.1	24.4	68.4	1.4×10^{-5}	48.8
112	BD	2.000	Propylene	230	295	15.0	3.2	45.7	79.4	2.54×10^{-3}	27.6
113 (a)	MSA-Fiber	8.173	Acetylene	77.4	17.7	2.1	76	21.7	61	6.77×10^{-6}	49.2
114 (a)	MSA-Fiber	6.011	Ethylene	77.4	12.3	1.98	66.3	28.0	73	7.9×10^{-6}	42.1
115	BD	5.000	Ethylene	43.2	79	3.12	10.05	23.4	61	2.66×10^{-5}	42.6
116 (c)	AC	0.500	n-Butane	295	—	5.17	—	57.3	72	—	—
117	AC	0.500	Freon-12	223	105	3.0	1.2	94	56.7	3.03×10^{-3}	22.5
118	C1	0.500	Freon-12	230	64	3.0	1.2	88.8	53.5	1.52×10^{-3}	22.6
119	AC	0.500	n-Butane	223	788	3.0	1.2	53.3	66.8	3.07×10^{-2}	17.2
120	BD	0.500	Freon-12	230	115	3.0	1.2	94.5	56.5	3.06×10^{-3}	22.5
121 P	AC	0.500	Freon-12	238	122	3.0	1.2	—	75 μ l inj.	—	—
122 (b)	C1	0.500	n-Butane	238	465	3.0	1.2	—	65.5	1.96×10^{-2}	17.35
123 P	BD	0.500	Freon-12	223	71	3.0	1.2	—	700 μ l inj.	—	—
124	MSA-Fiber	0.302	n-Butane	198	50	5.5	2.2	53.7	67.5	3.12×10^{-3}	17.2
125 (b)	MSA-Fiber	0.708	Freon-12	198	22	11.7	4.7	88.5	53.4	3.93×10^{-4}	22.5
126	BD	1.000	Vinyl Chloride	198	320	4.6	1.86	61.7	72	4.04×10^{-3}	27.3
127 P	BD	45.0	Methane	175	6	2.4	77	—	3000 μ l inj.	—	—
128 P(d)	BD	45.0	Methane	223	7	2.4	77	—	300 μ l inj.	—	—
129 (d)	BD	45.0	Methane	211	9	2.4	77	—	8.55×10^3	1.48×10^{-4}	44.3
130 P(d)	BD	45.0	Methane	223	7	2.4	77	—	30 μ l inj.	—	—
131	BD	2.0	Freon-23	211	4	8.75	3.5	68.3	71	2.56×10^{-5}	40.4
132 (c)	BD	0.500	Freon-21	198	410	3	1.2	82.8	50	8.13×10^{-3}	23.7
133	BD	1.000	Freon-22	180	68	5	2.0	63.2	53.3	5.74×10^{-4}	30.8
134 P(d)	BD	1.000	Freon-22	185	58	5	2.0	—	15 μ l inj.	—	—
135 P(d)	BD	1.000	Freon-22	173	57	5	2.0	—	30 μ l inj.	—	—
136 P(d)	BD	1.000	Freon-22	170	55	5	2.0	—	5 μ l inj.	—	—
137 (b)	C1	1.000	Freon-22	180	31	5	2.2	61.6	52	2.52×10^{-4}	30.9
138	AC	1.000	Freon-22	157	63	5	2.0	62.2	52.5	4.38×10^{-4}	30.8
139 (b)	MSA-Fiber	1.006	Freon-22	157	16	15	5.9	61.6	52	1.14×10^{-4}	30.9
140 (a)(b)	BD	10.000	Freon-23	190	12	5.5	17.7	53.3	55.5	9.22×10^{-6}	41
141	BD	313	Methane	225	40	0.9	720	1.37×10^3	6.25×10^3	1.16×10^{-4}	44.3
142 (d)	BD	46.9	Freon-23	211	69	2.4	77	63.2	66	1.44×10^{-5}	40.6
143 (d)	BD	46.9	Freon-23	211	69	2.4	77	63.2	66	1.44×10^{-5}	40.6
144	BD	0.500	Freon-21	203	410	3	1.2	84.7	50.2	7.75×10^{-3}	23.7
145 P	BD	1.000	Freon-22	203	45	5	2.0	—	50 μ l inj.	—	—
146 (d)	BD	1.000	Freon-22	203	52	5	2.0	66.4	56	5.03×10^{-4}	30.8
147 P(d)	BD	1.000	Freon-22	203	45	5	2.0	—	50 μ l inj.	—	—
150	BD	0.476	Propyl Mercaptan	3000	150	1.5	0.73	48.5	46.5	3.5×10^{-2}	14.8
151	BD	1.002	Methyl Mercaptan	3000	34	2.6	1.26	81.5	124.0	2.45×10^{-3}	32.0

*For all runs: RH = 23%, carrier gas = 0.8%, CO₂ in O₂. Pressure = 10.2" Hg. Temp = 43.8°C.

NOTES:

P Denotes pulse run.

a Effluent concentration did not reach inlet conc.

b Initial part of breakthrough not obtained

c Final bed wt. > initial wt., indicating leakage of fluid from constant temp. bath into bed

d Same bed used as in preceding run

e Final part of breakthrough not obtained

f MSA fiber is easily compressible and bed volume is not reproducible

Table A-2
INJECTION EXPERIMENTS^(a)

Adsorbate T°c	Adsorbent (30 x 60 mesh)										
	BD				C1				AC		
	t _r (min)	h (in.)	w @ 1/2h (in.)	Attn	t _r	h	w @ 1/2h	Attn	t _r	h	w @ 1/2h
n-Butane 250	6.1	9.5	— ^(b)	10 ² x 4	3.4	4.8	1.3	10 ² x 16	5.5	6.9	—
250	6.2	9.7	—	10 ² x 4	3.3	6.2	1.26	10 ² x 16	5.5	6.9	—
n-Butane 200	20	8.6	—	10 x 16	15.7	8.3	—	10 ² x 2	21.8	7.6	—
200	20	9.4	—	10 x 16	15.7	8.8	—	10 ² x 2	22	7.2	—
Freon-12 200	3.4	5.35	—	10 x 8	3.0	8.3	1.12	10 ² x 1	3.85	7.4	—
200	3.4	5.95	1.5	10 x 8	3.0	8.2	1.12	10 ² x 1	3.9	8.2	—
Methanol 200	1.65	6.75	—	10 ² x 64	2.05	2.0	—	10 x 16	1.33	8.1	—
200	1.63	7.22	—	10 ² x 64	1.98	4.4	—	10 x 8	1.18	5.9	—
200	1.59	7.95	—	10 ² x 64	1.9	5.7	—	10 x 8	1.2	6.1	—
Ethylene 200	0.52	5.0	0.16	10 ² x 64	0.53	5.3	1.3	10 ² x 64	0.62	8.7	0.15
200	0.52	5.06	0.16	10 ² x 64	0.52	6.2	1.3	10 ² x 64	0.62	9.0	0.15
200	0.52	5.1	0.16	10 ² x 64	0.55	4.8	1.3	10 ² x 64	0.62	9.1	0.15
Ethylene 100	3.65	3.7	1.28	10 ² x 8	2.42	3.45	0.87	10 ² x 16	3.22	5.8	1.01
100	3.55	6.65	1.24	10 ² x 4	2.43	6.9	0.87	10 ² x 8	3.23	6.0	1.01
100									3.23	6.0	1.01
Acetylene 100	2.58	7.75	0.84	10 ² x 8	1.6	5.7	0.63	10 ² x 16	2.3	4.2	0.72
					1.6	5.9	0.63	10 ² x 16	2.35	4.3	0.74
					1.6	5.5	0.63	10 ² x 16	2.32	4.3	0.74

(a) Helium carrier gas @ F ≈ 30 cc/min, Volume of contaminant used; gases 0.015 cc, liq 0.001 cc (Flame Ionization Detector),
1.00 g Adsorbent 1 = 10 cm d = 0.483 cm.
(b) "Half width" not given for tailing peaks.

Table A-3

INJECTION EXPERIMENTS – FLOW RATE EFFECTS^(a)

Adsorbate	Fcc/min	t_r (min)	h (in.)	w @ 1/2 h	Attn
Ethylene	40	2.85	7.0	0.98	$10^2 \times 8$
	40	2.85	6.95	0.98	$10^2 \times 8$
Acetylene	40	2.23	4.35	0.8	$10^2 \times 8$
Ethylene	80	1.2	4.35	0.46	$10^2 \times 32$
	80	1.15	8.5	0.46	$10^2 \times 16$
Acetylene	80	0.94	5.76	0.35	$10^2 \times 32$

^(a)He carrier gas, T = 100°C, Adsorbent: 1.00 g DB (30 × 60 mesh),
Volume of contaminant = 0.015 cc

Table A-4

INJECTION EXPERIMENTS – VOLUME EFFECTS^(a)

Vol (cc)	t_r (min)	h (in.)	w @ 1/2 h (in.)	Attn
0.015	4.0	6.45	1.8	10 × 8
	4.0	6.35	1.8	10 × 8
0.050	3.9	5.3	1.45	10 × 32
	3.9	5.1	1.45	10 × 32
0.10	3.8	8.1	1.4	$10^2 \times 4$
	3.8	8.2	1.4	$10^2 \times 4$
0.20	3.65	8.4	1.32	$10^2 \times 8$
	3.65	8.5	1.35	$10^2 \times 8$
0.50	3.2	5.7	— ^(b)	$10^2 \times 32$
1.0	2.8	3.6	—	$10^3 \times 8$

^(a)Contaminant – Freon-12, Adsorbent – BC type "AC" (30 × 60),
T = 200°C, Flow He = 30 cc/min Adsorbent Bed, wt – 1.00 g,
l = 10 cm, id = 0.485 cm.

^(b)Tailing Peaks

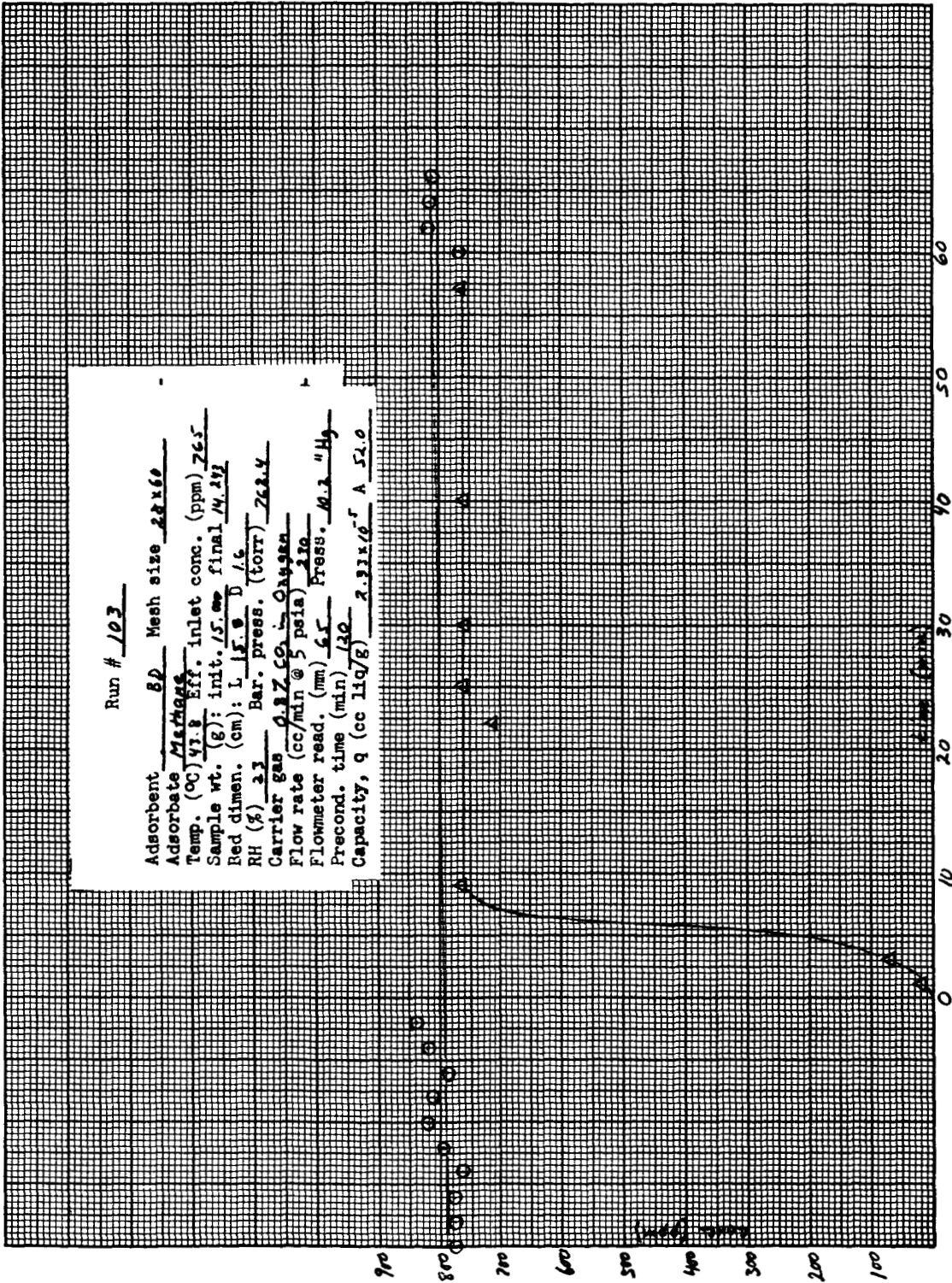


Fig. A-1 Run Number 103

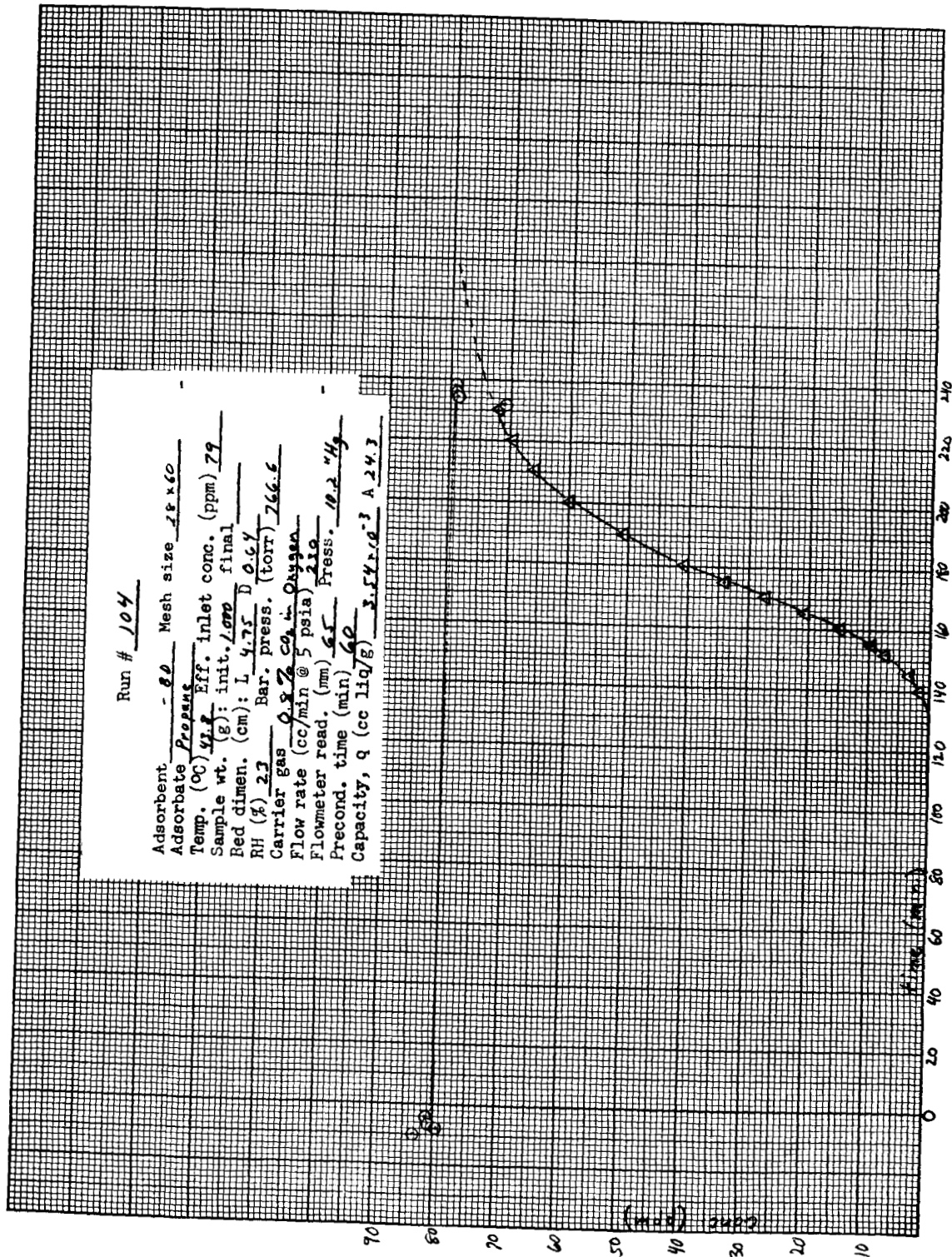


Fig. A-2 Run Number 104

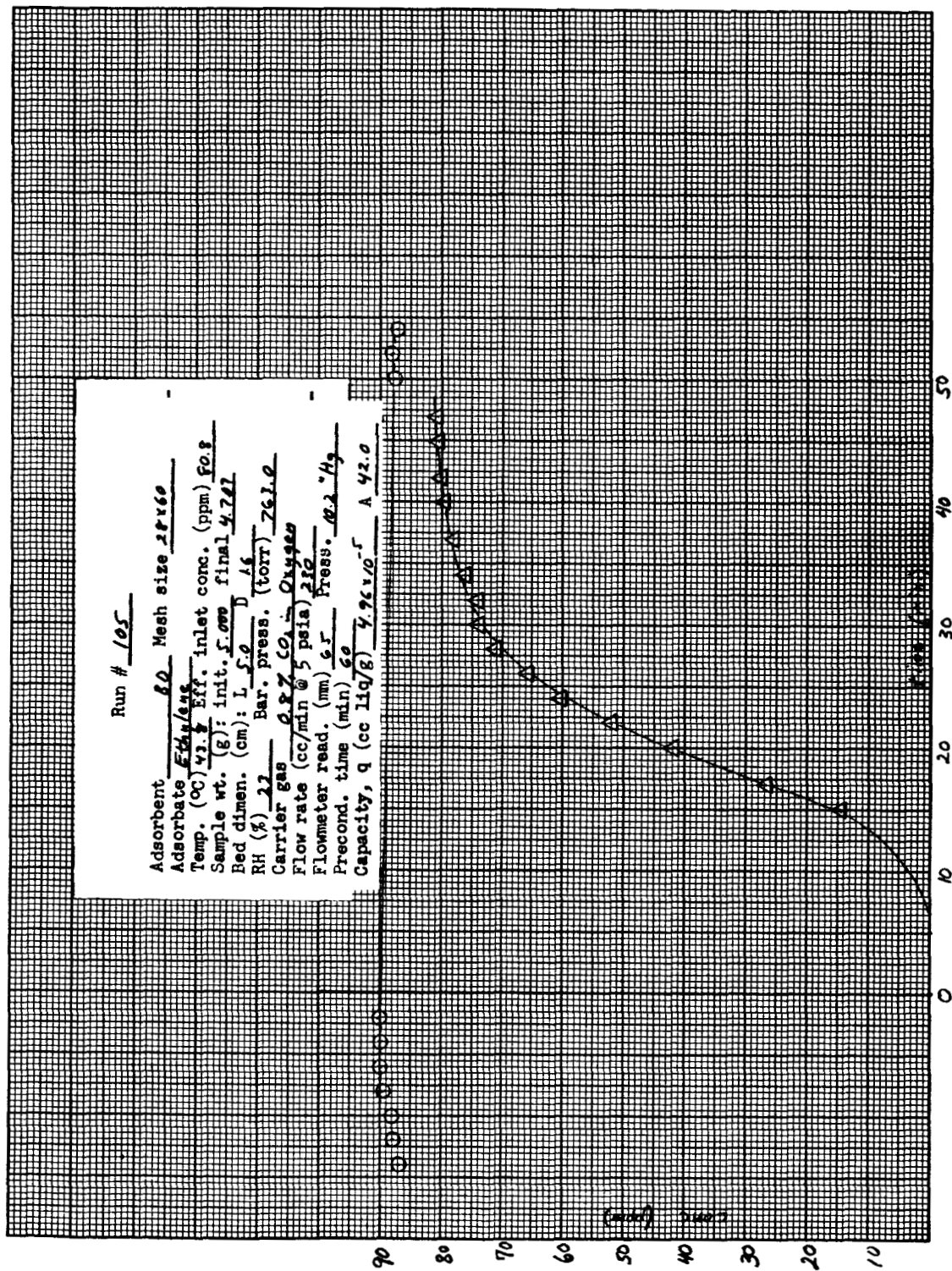


Fig. A-3 Run Number 105

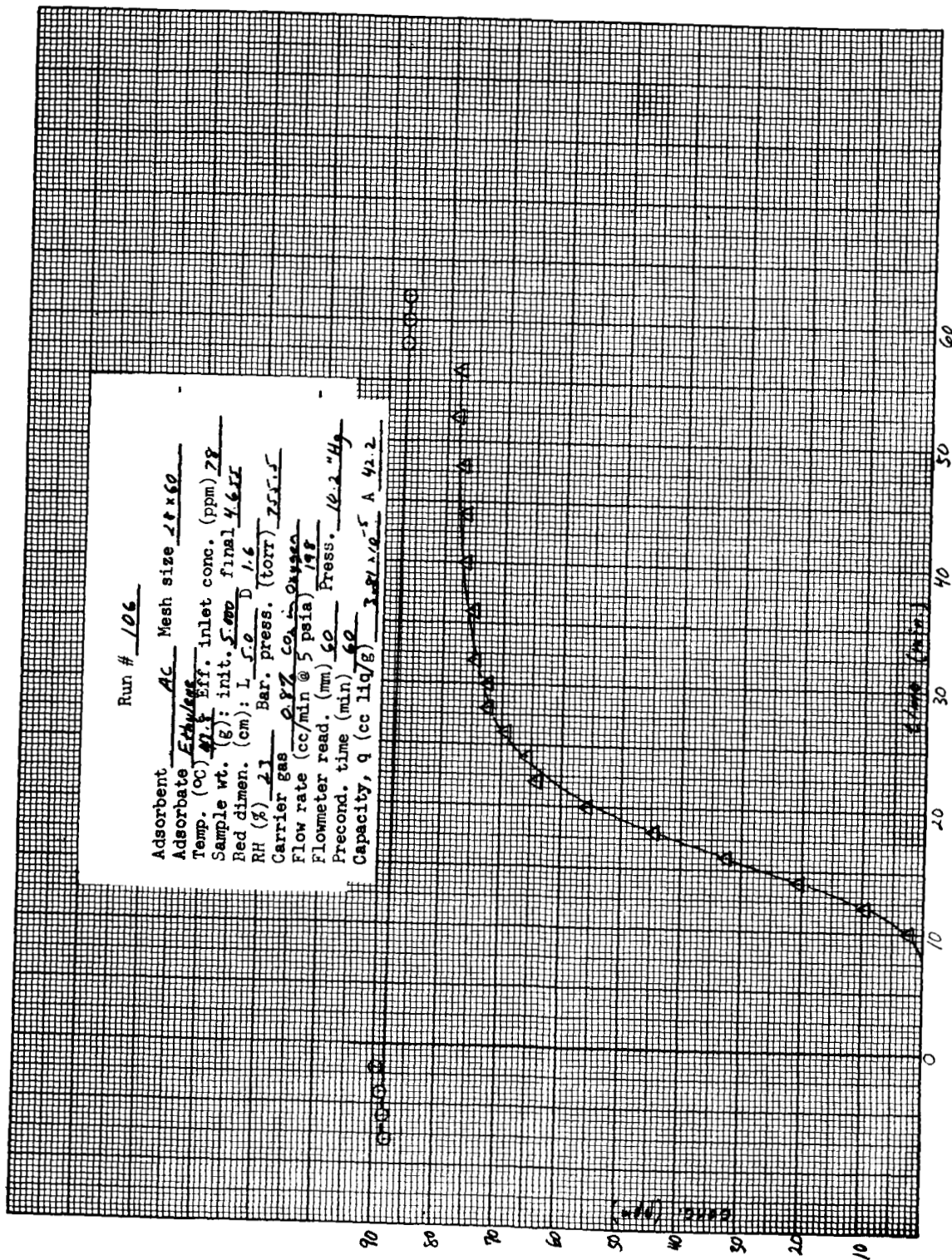


Fig. A-4 Run Number 106

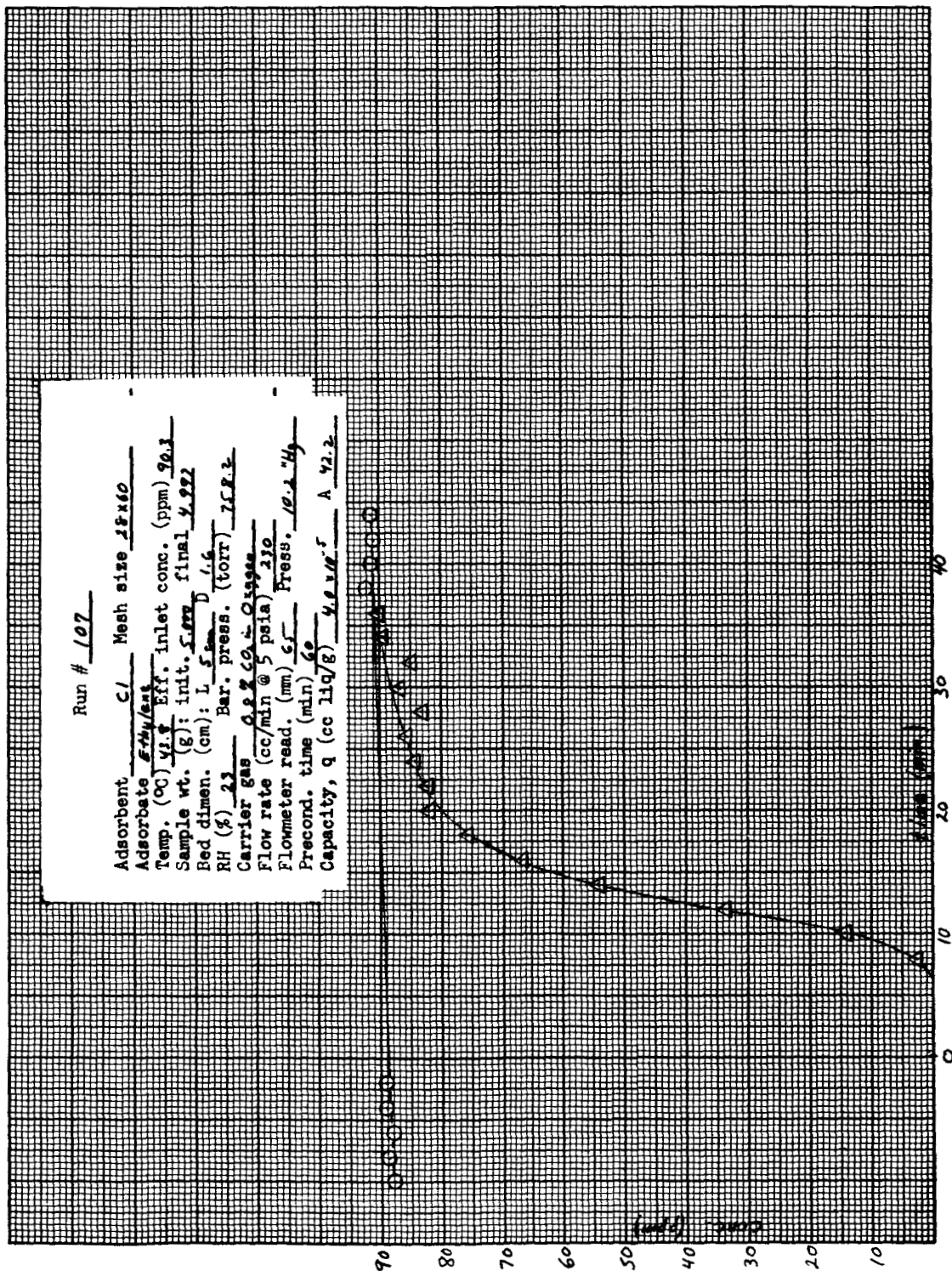


Fig. A-5 Run Number 107

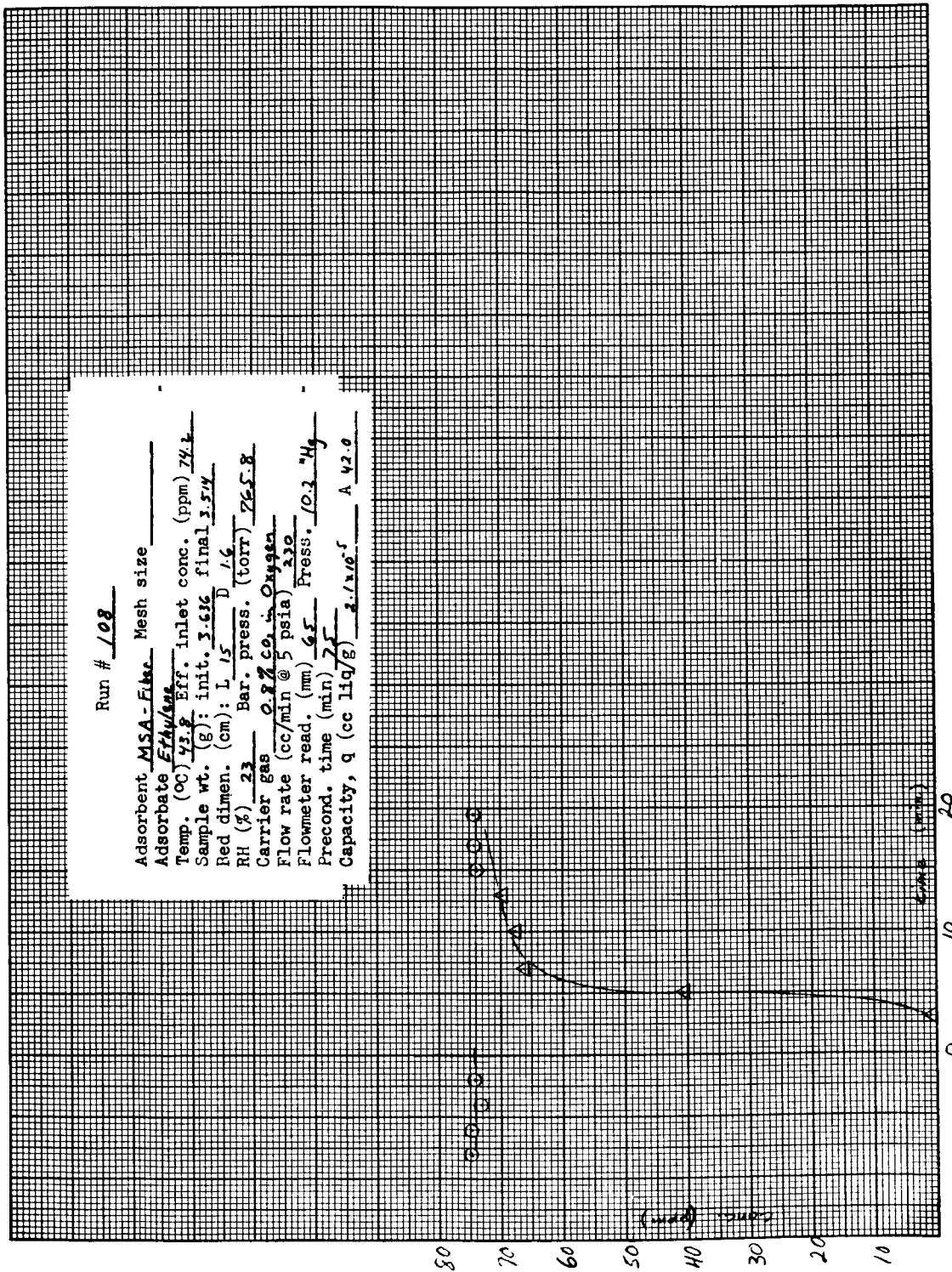


Fig. A-6 Run Number 108

Adsorbent 80 Mesh size 10x10
 Adsorbate Acetylene
 Temp. (°C) 47.2 Eff. inlet conc. (ppm) 60
 Sample wt. (g) : init. 15.00 final 14.462
 Bed dimen. (cm) : L 15.0 D 6.6
 RH (%) 21 Bar. press. (torr) 761.9
 Carrier gas O.2% CO₂ in Oxygen
 Flow rate (cc/min @ 5 psia) 120.0
 Flowmeter read. (mm) 65 Press. 10.2 °Hg
 Precond. time (min) 20
 Capacity, q (cc liq/g) 1.34 x 10⁻⁵ A 49.2

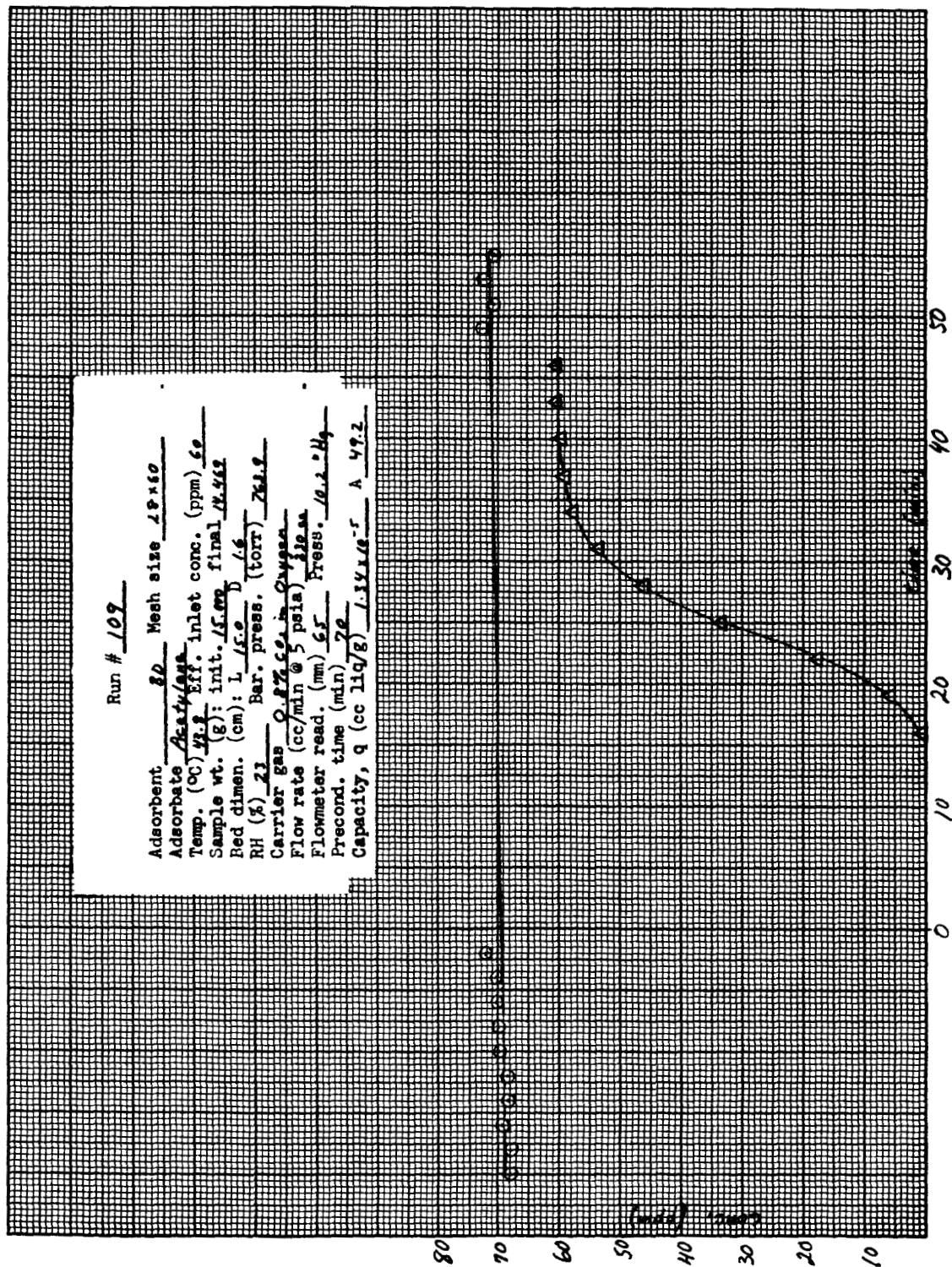


Fig. A-7 Run Number 109

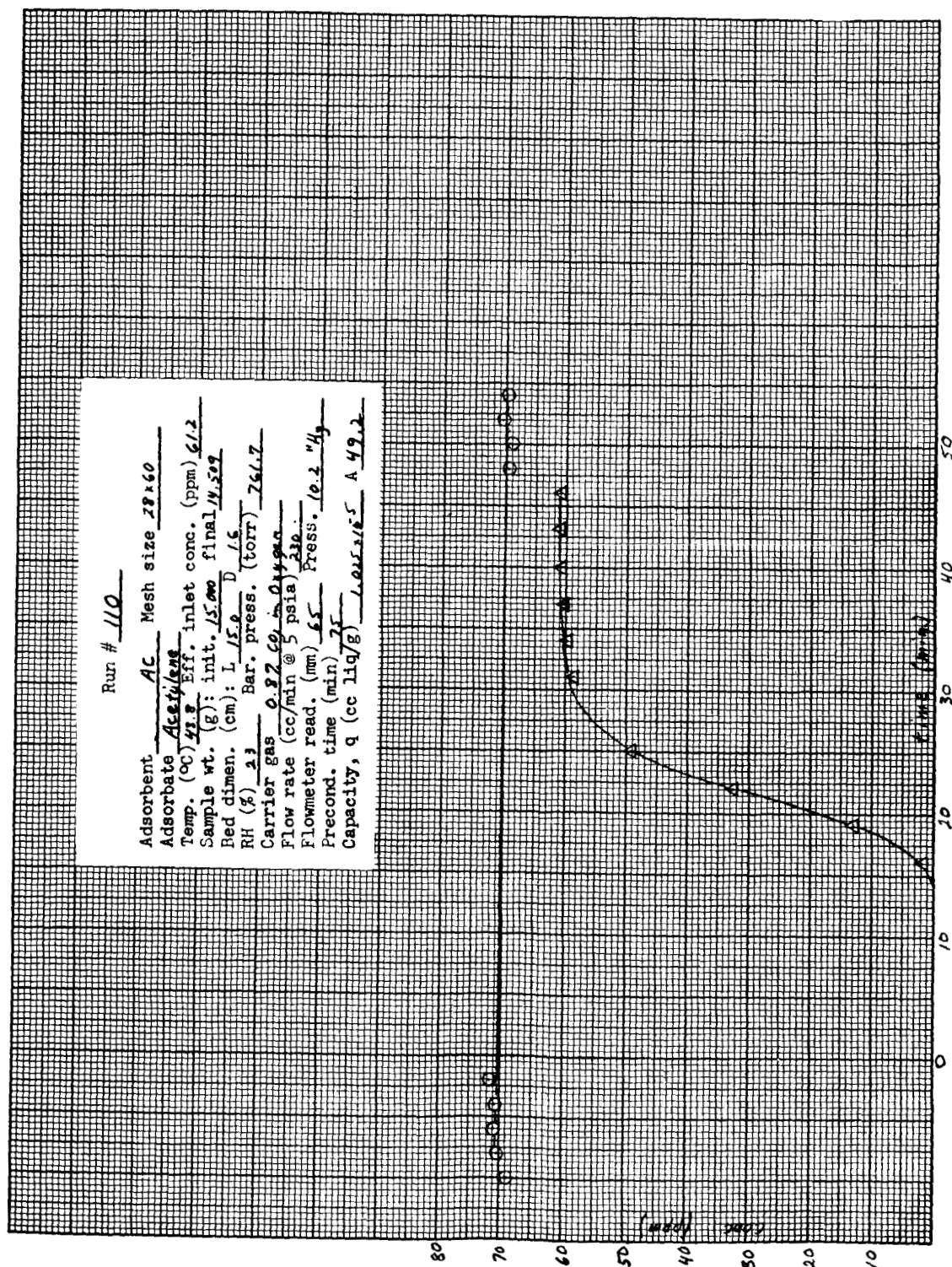


Fig. A-8 Run Number 110

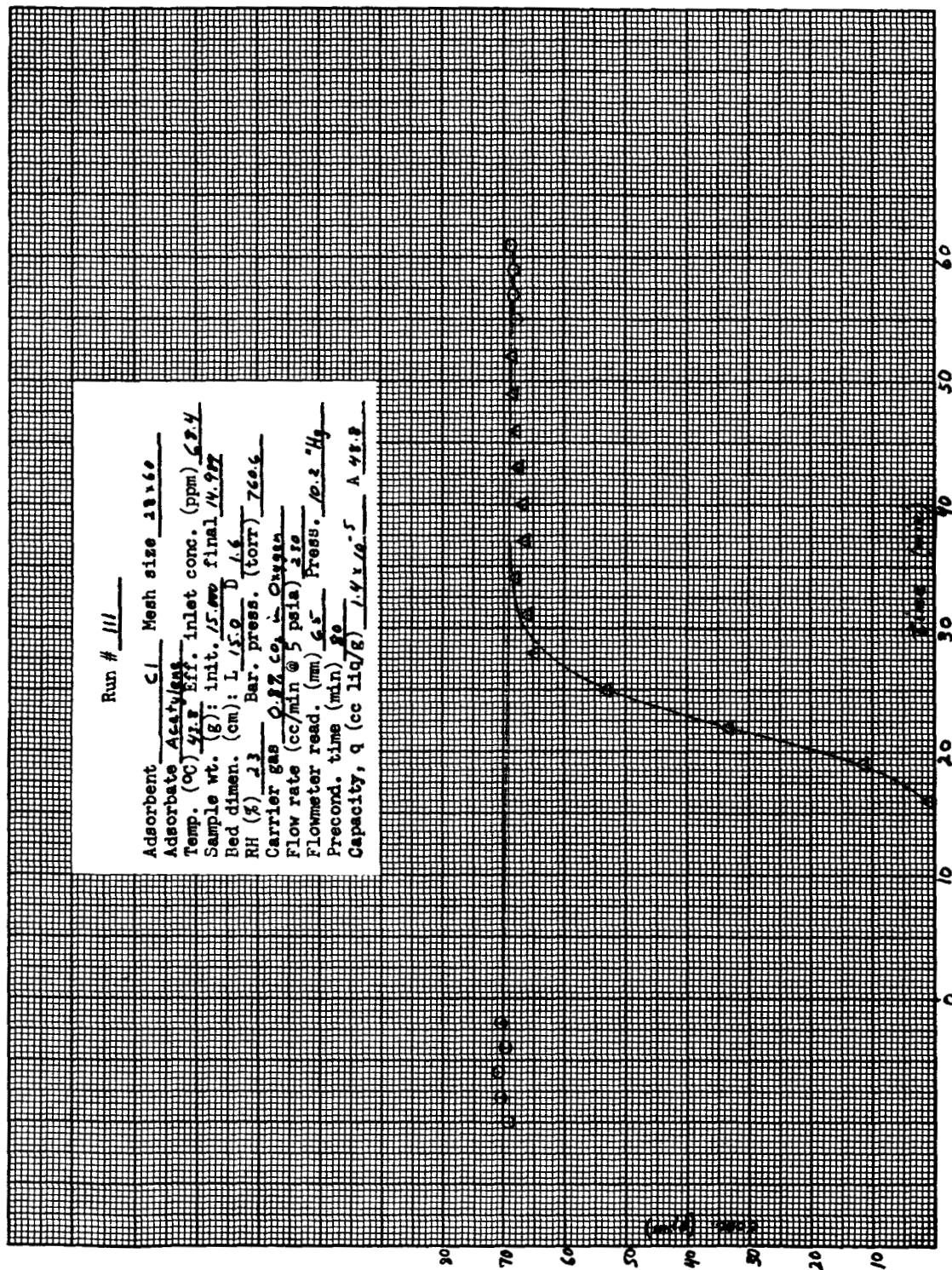


Fig. A-9 Run Number 111

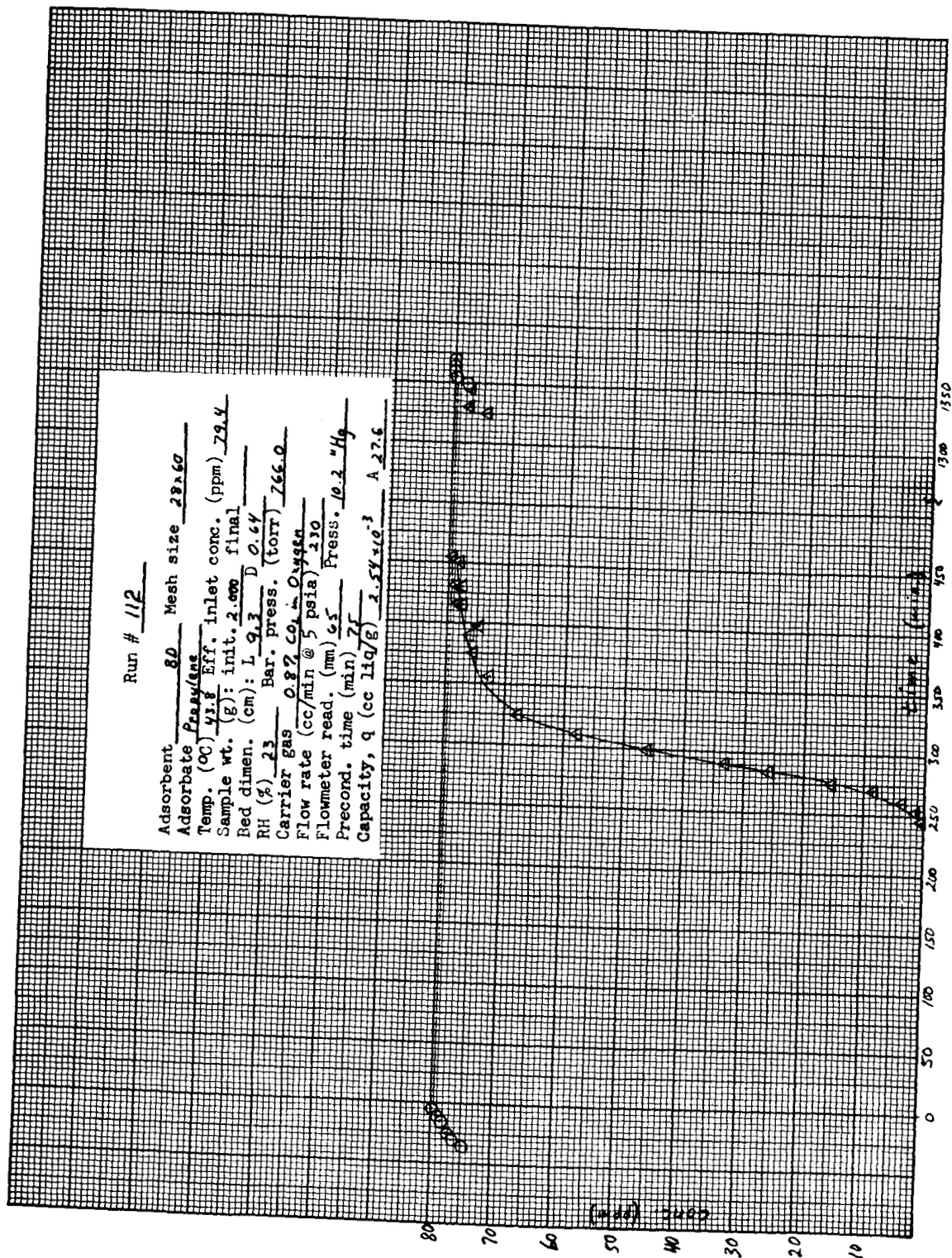


Fig. A-10 Run Number 112

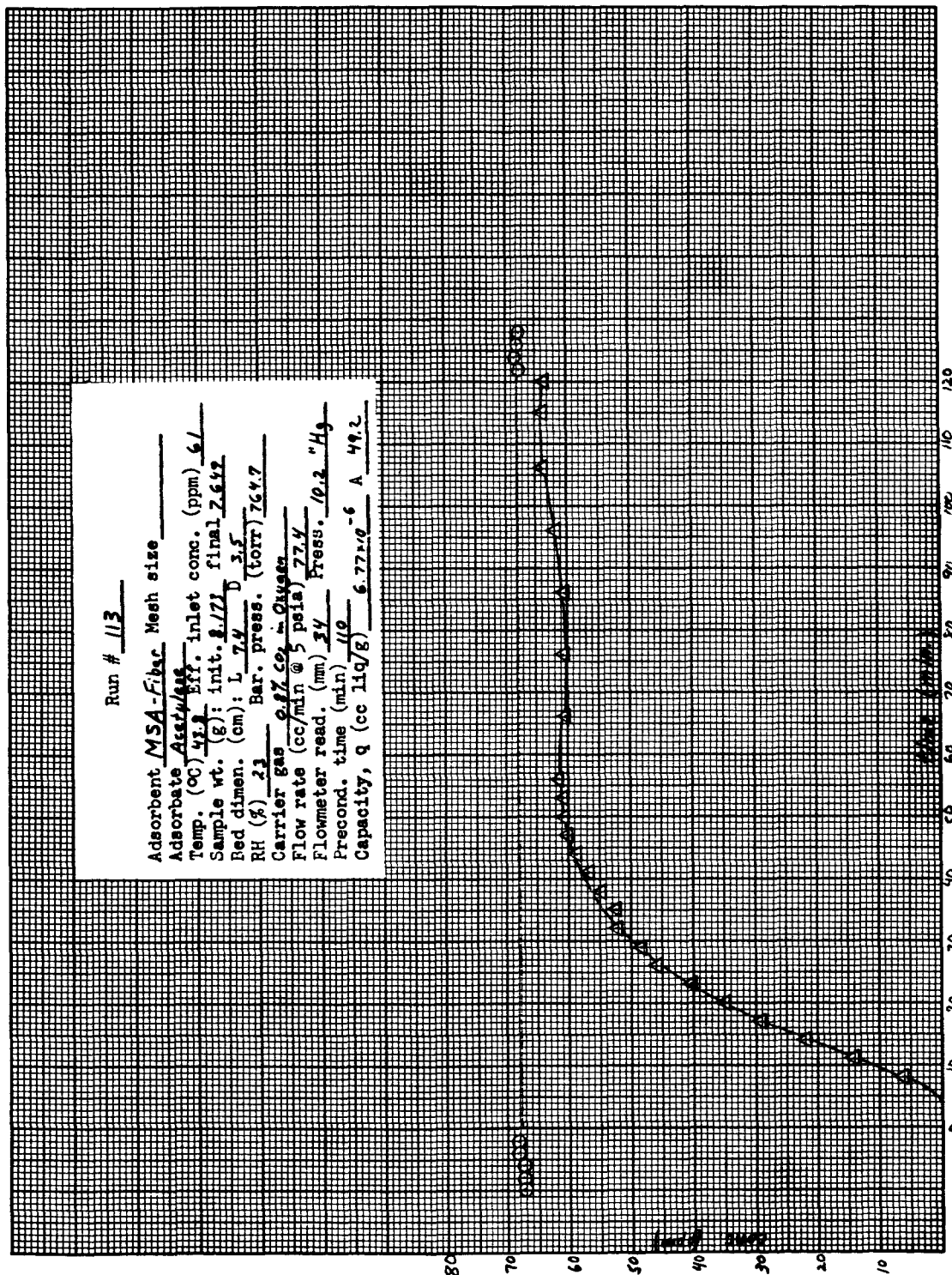


Fig. A-11 Run Number 113

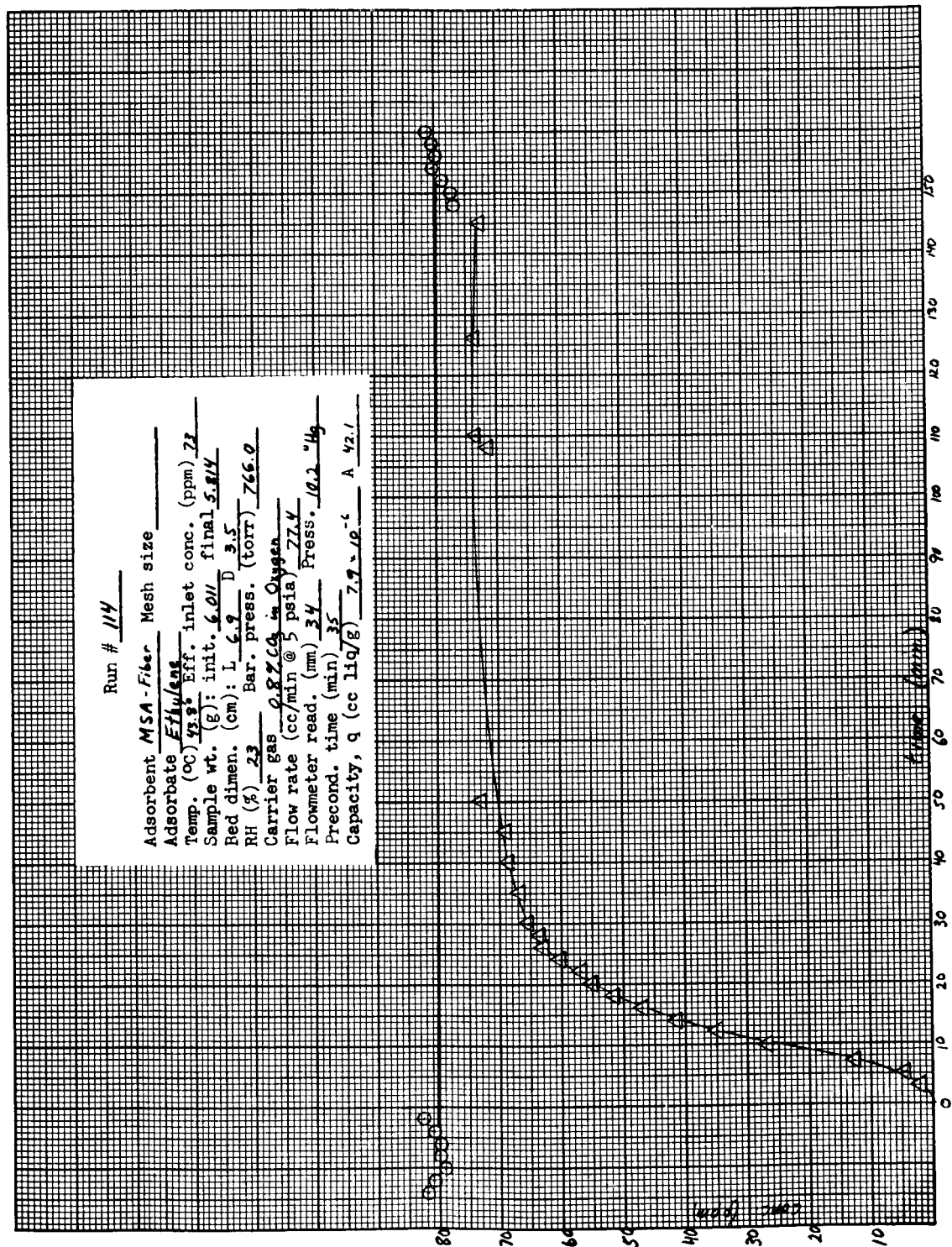


Fig. A-12 Run Number 114

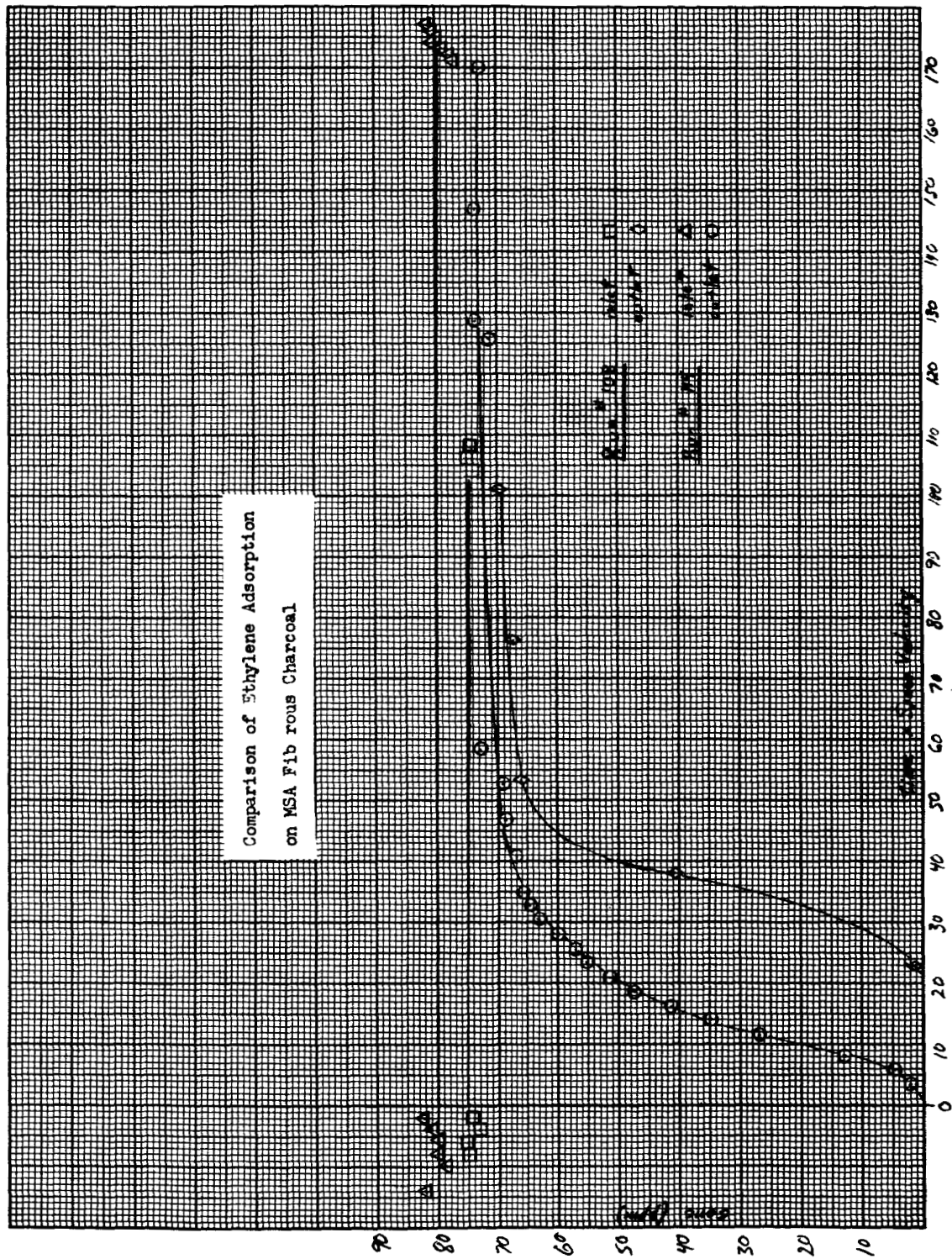


Fig. A-13 Comparison of Run Numbers 108 and 114

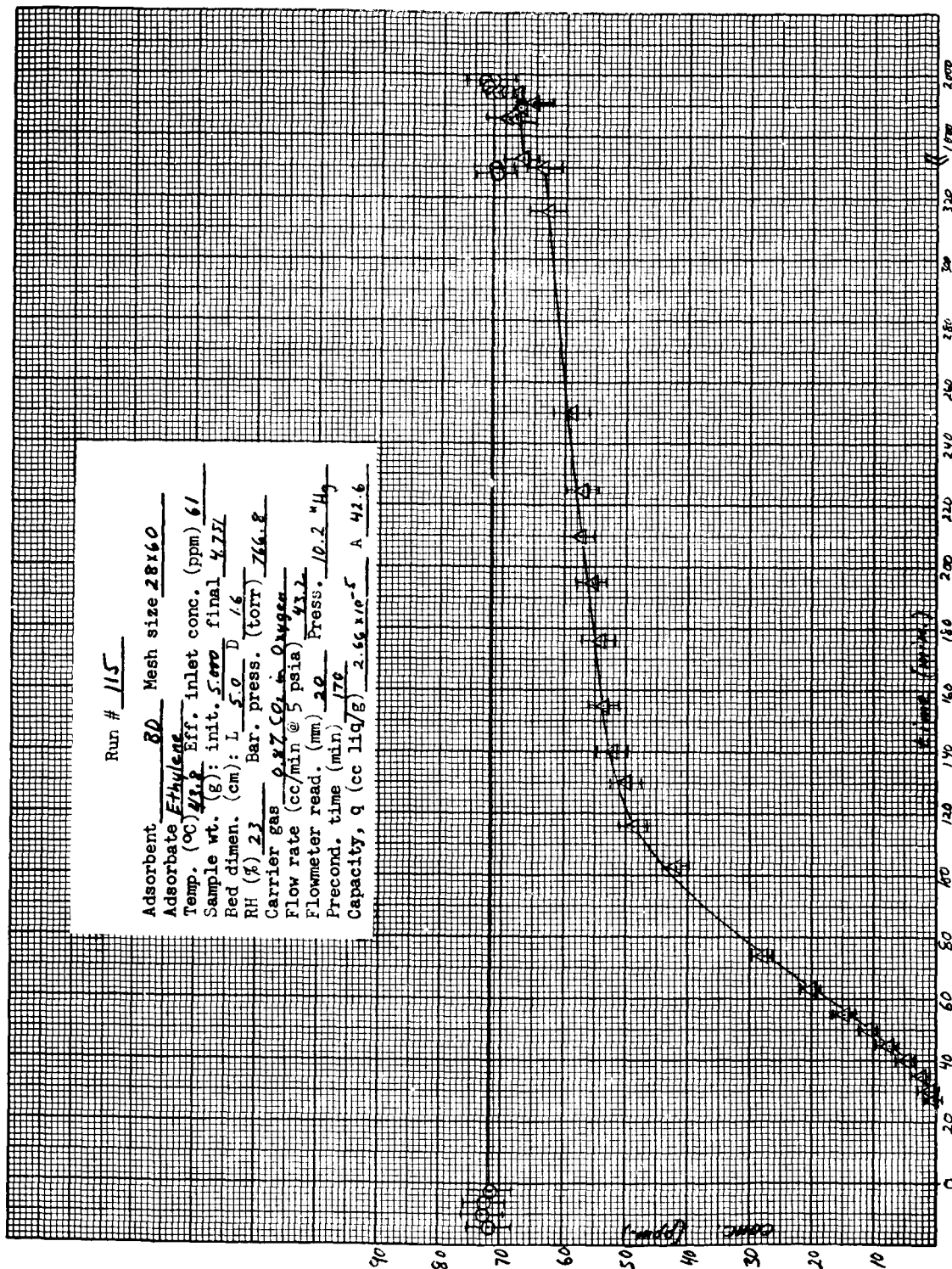


Fig. A-14 Run Number 115

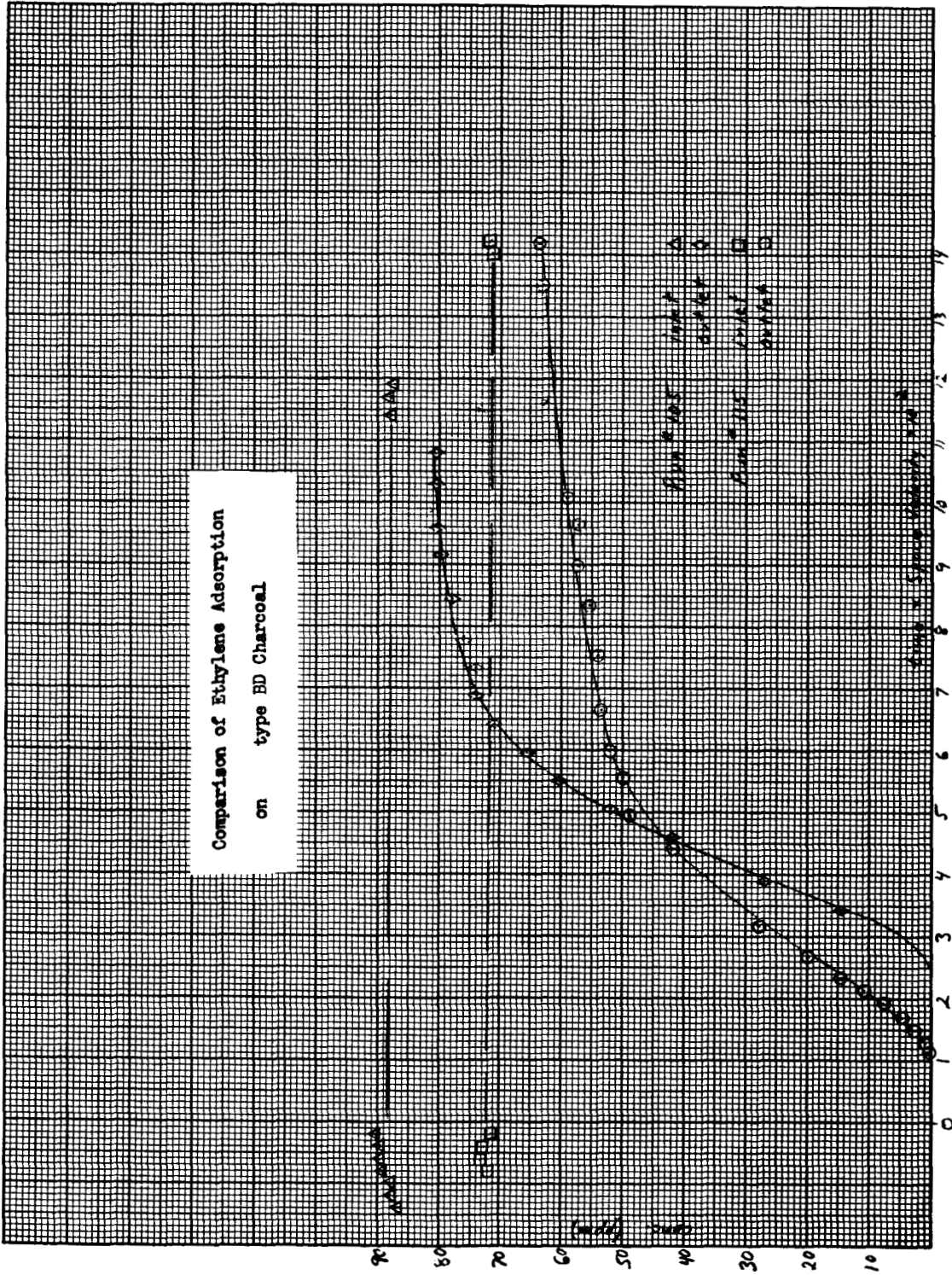


Fig. A-15 Comparison of Run Numbers 105 and 115

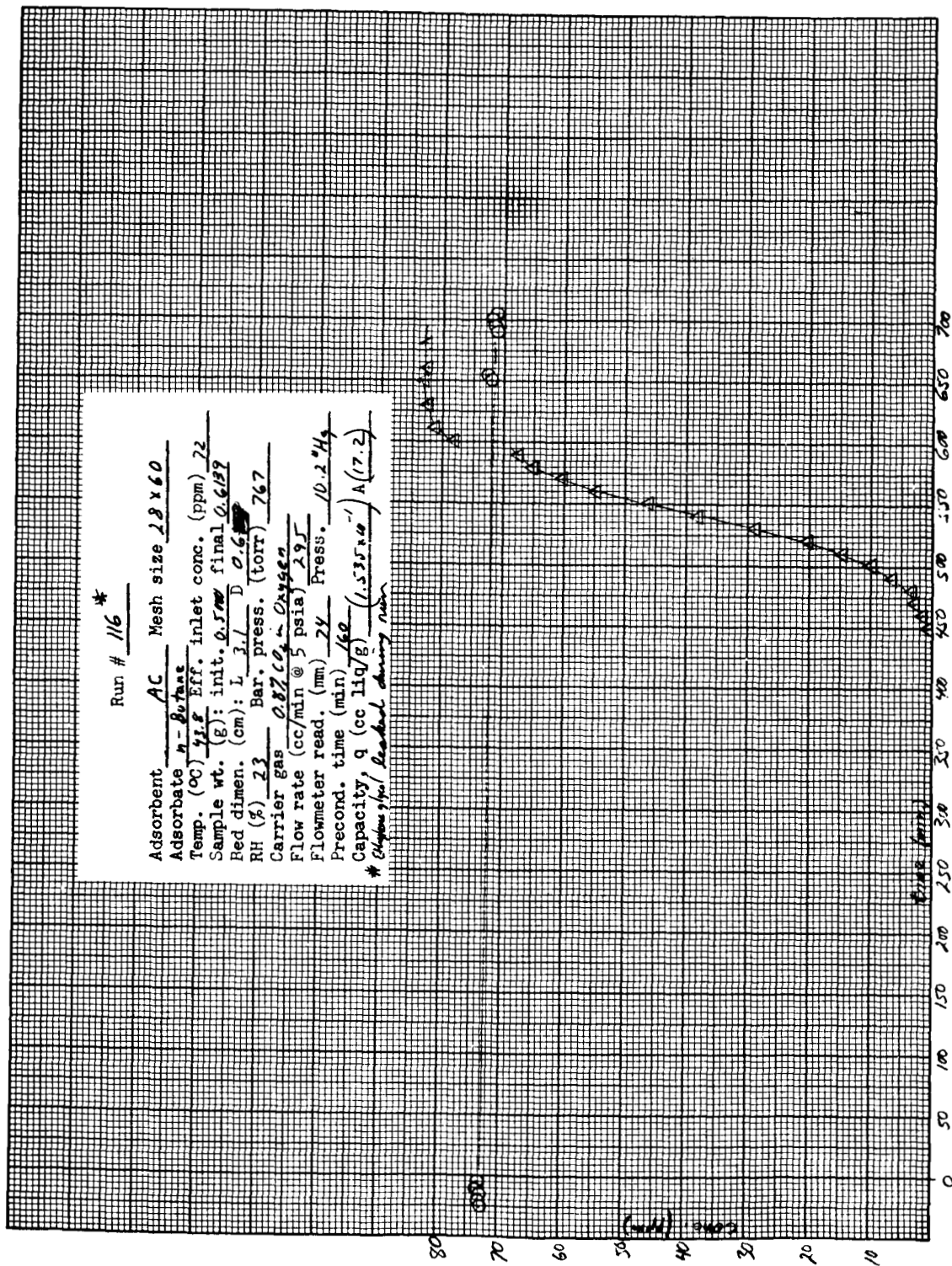


Fig. A-16 Run Number 116

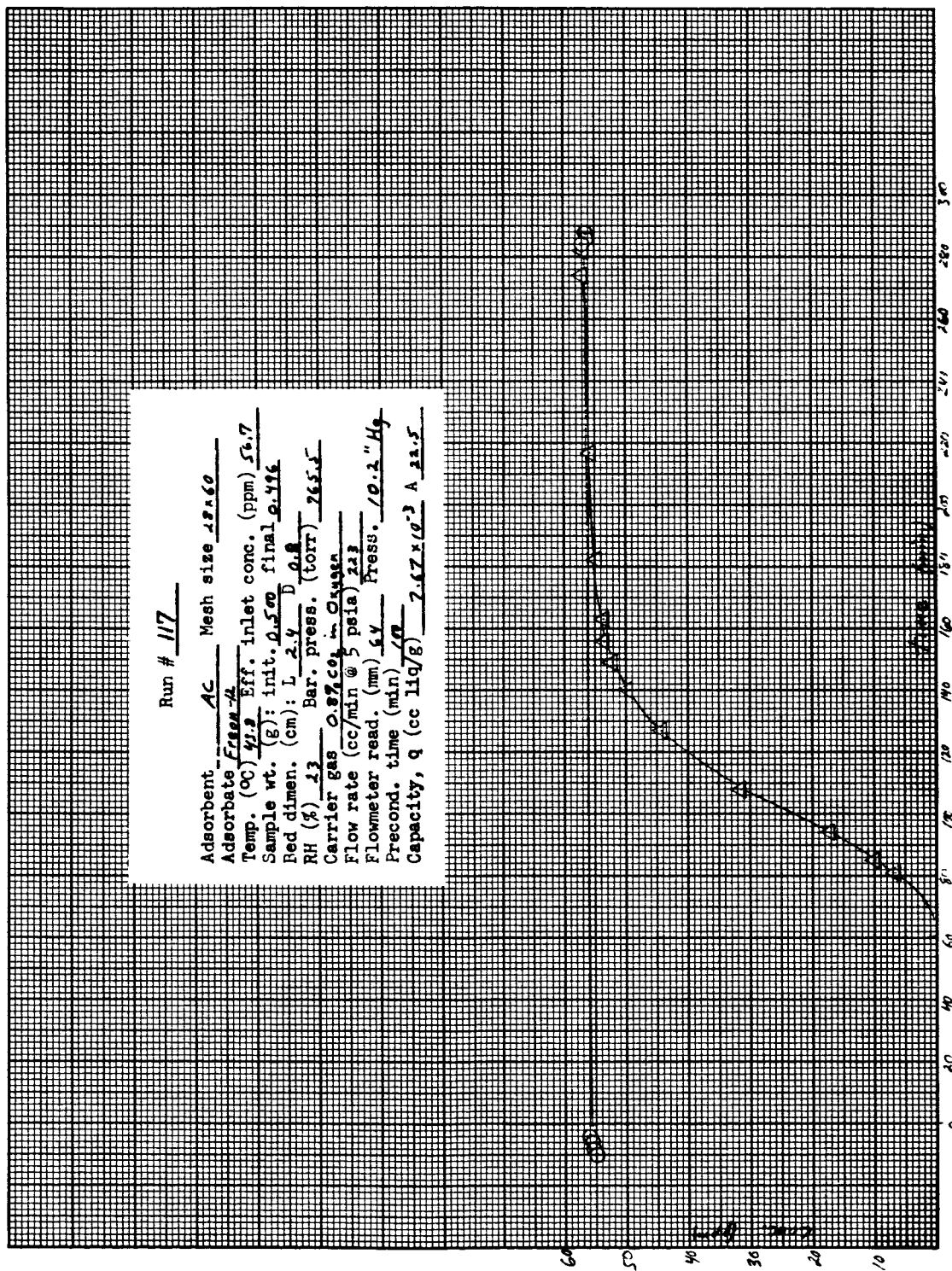


Fig. A-17 Run Number 117

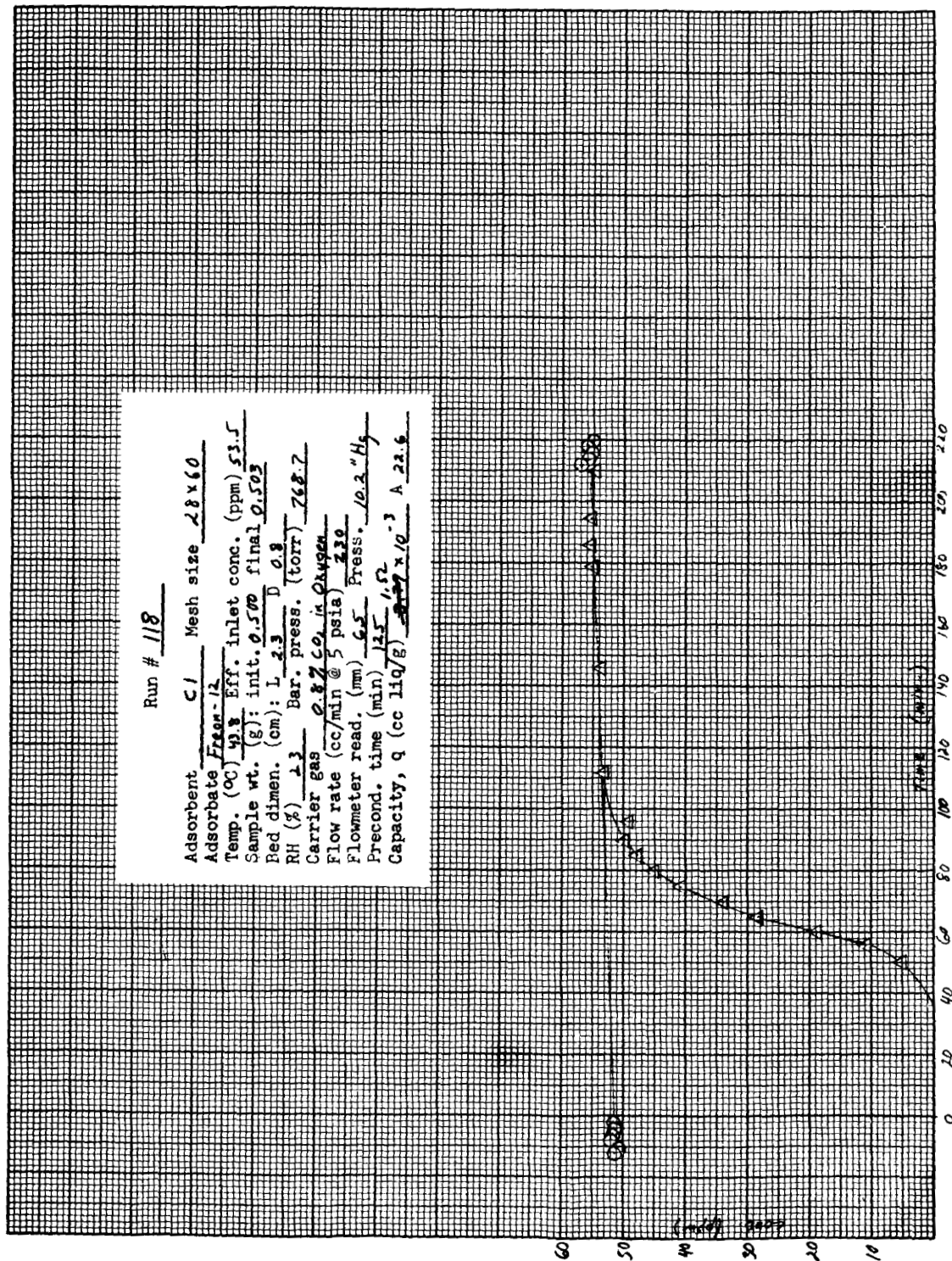


Fig. A-18 Run Number 118

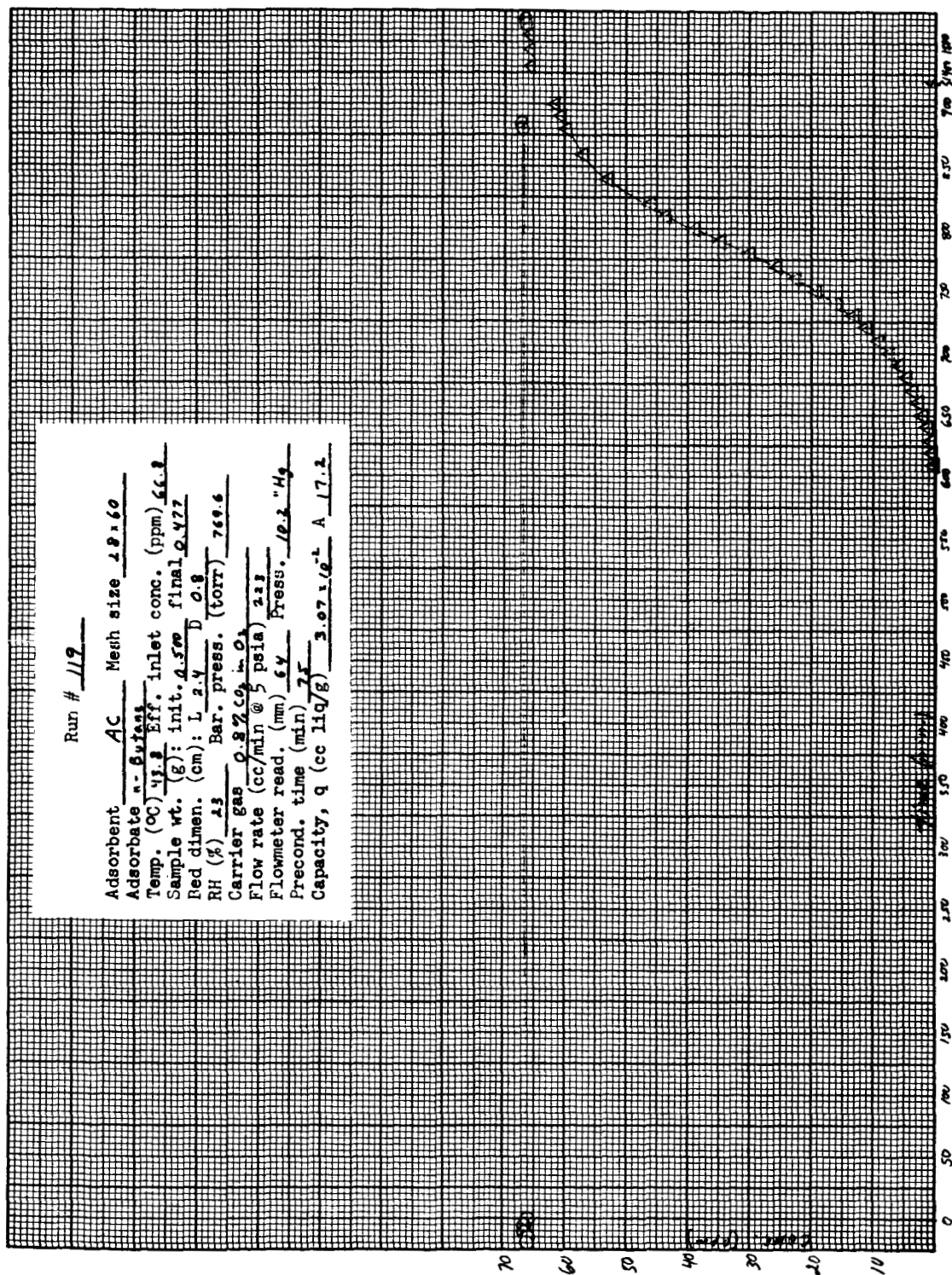


Fig. A-19 Run Number 119

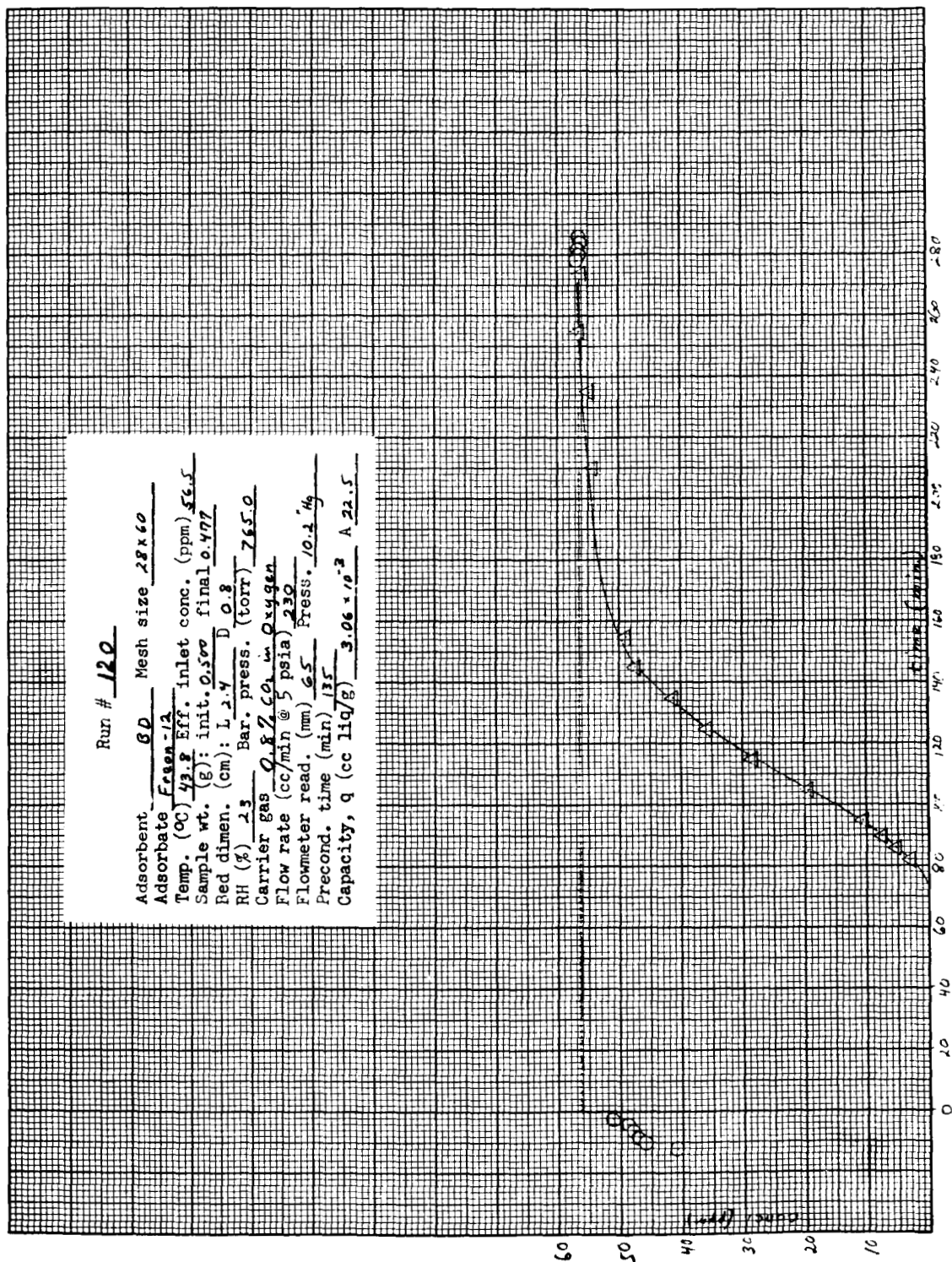


Fig. A-20 Run Number 120

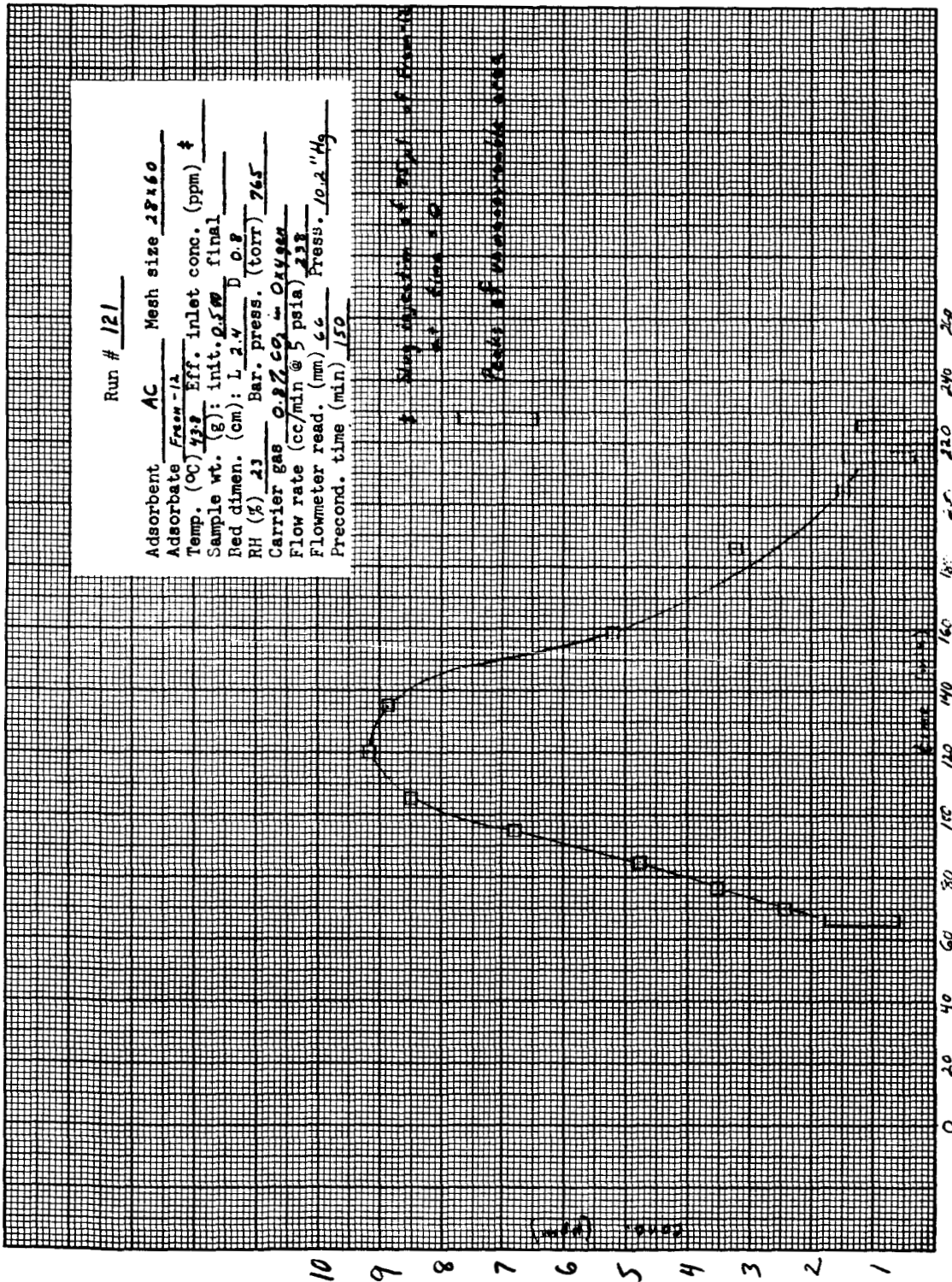


Fig. A-21 Run Number 121

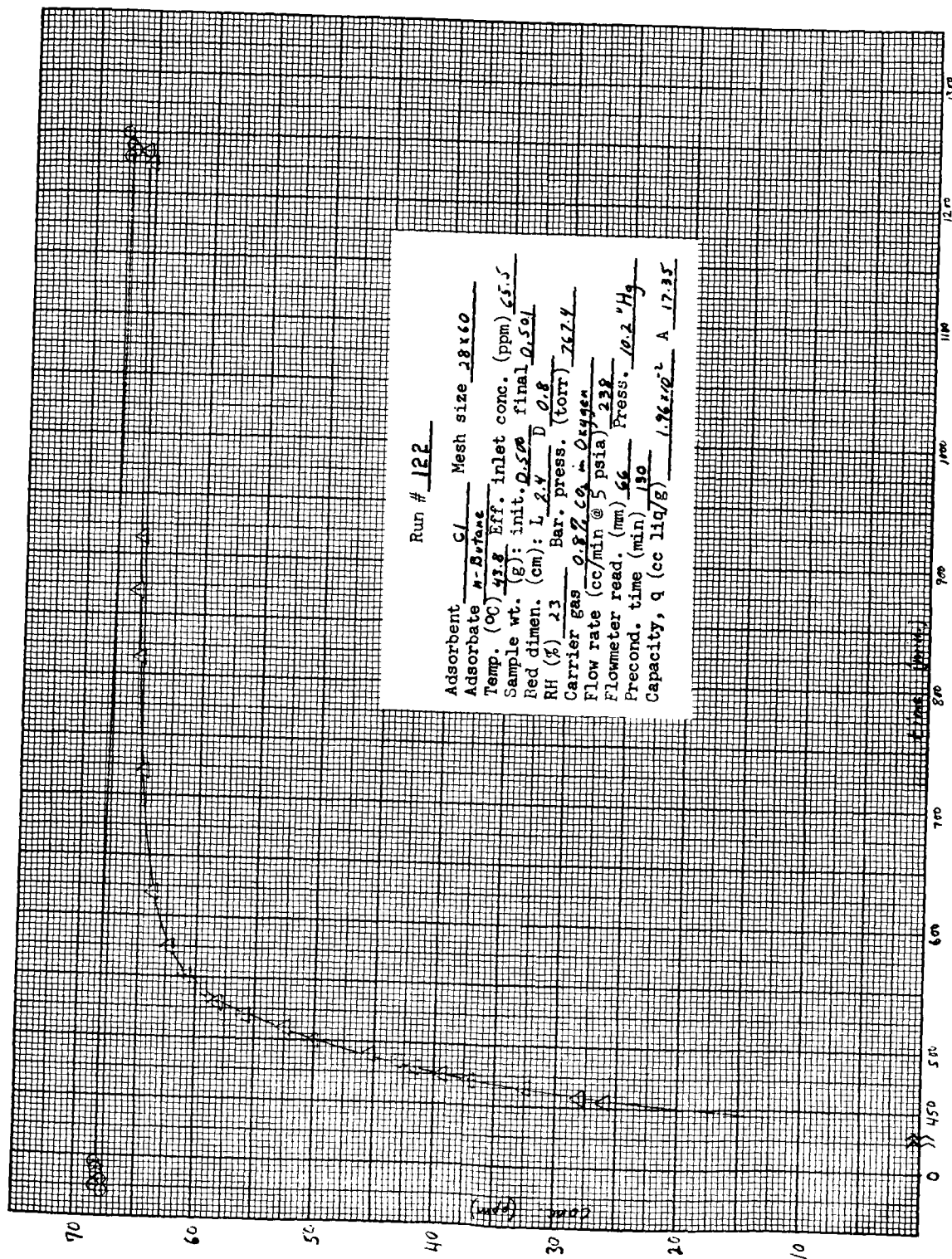


Fig. A-22 Run Number 122

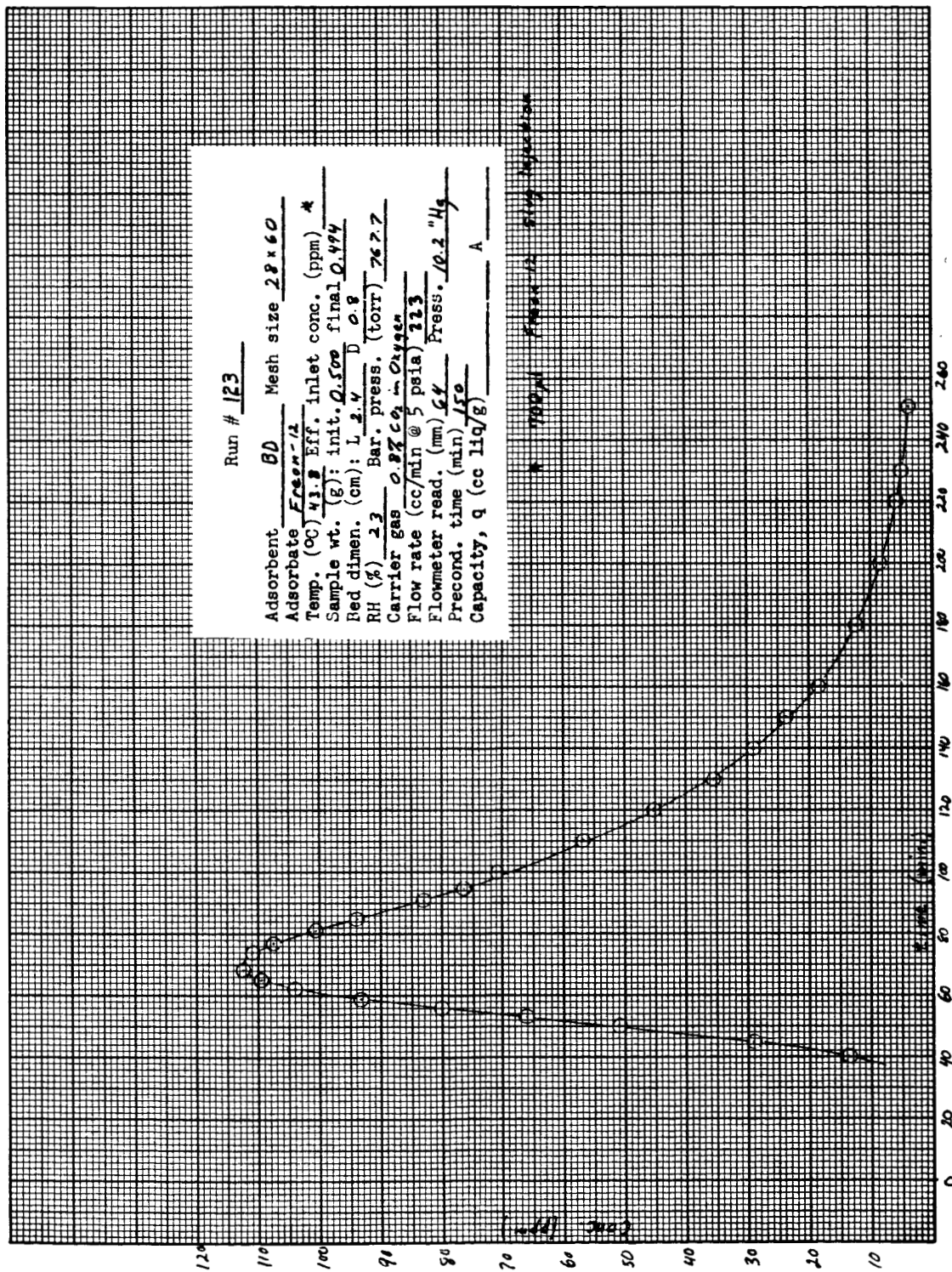


Fig. A-23 Run Number 123

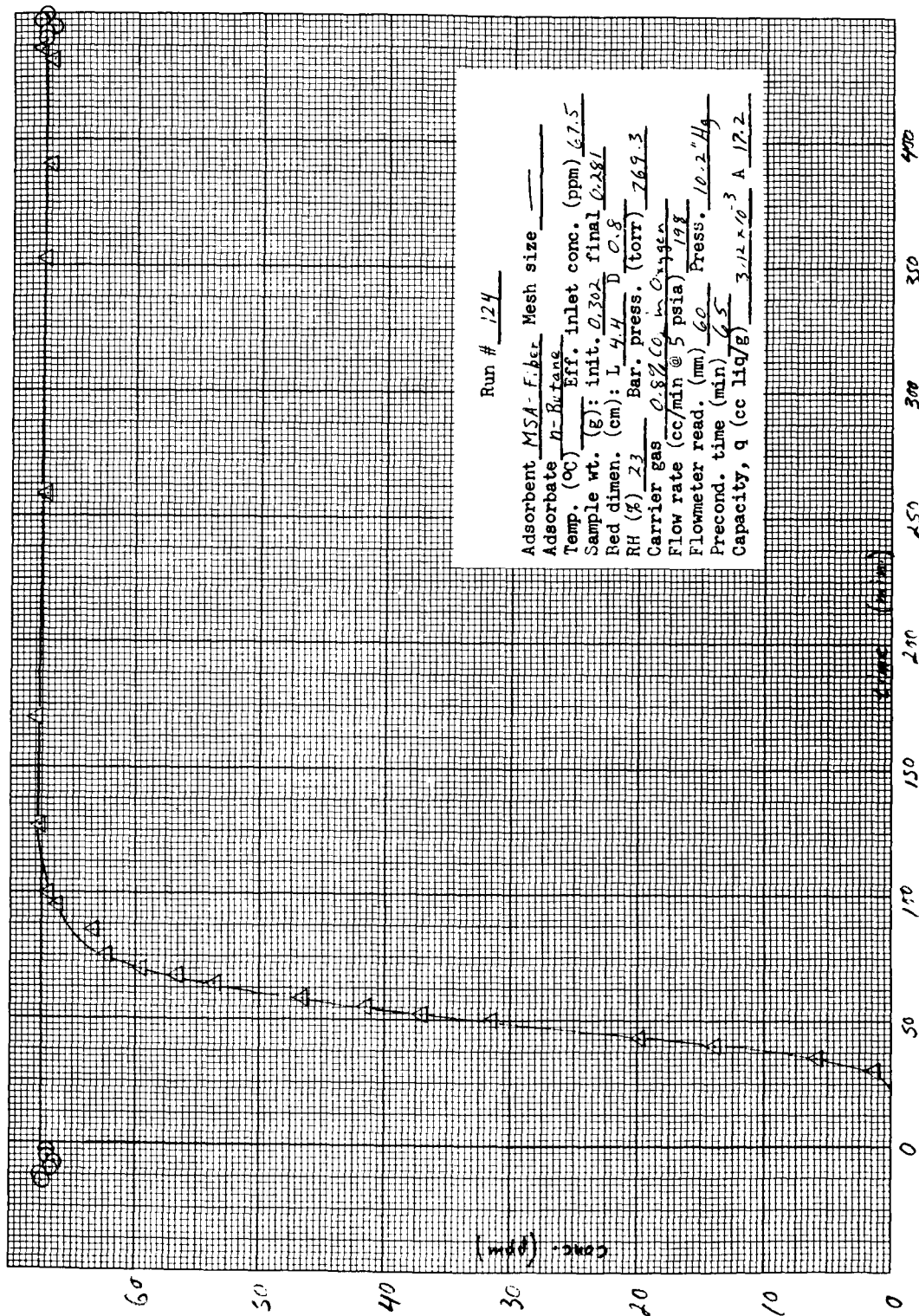


Fig. A-24 Run Number 124

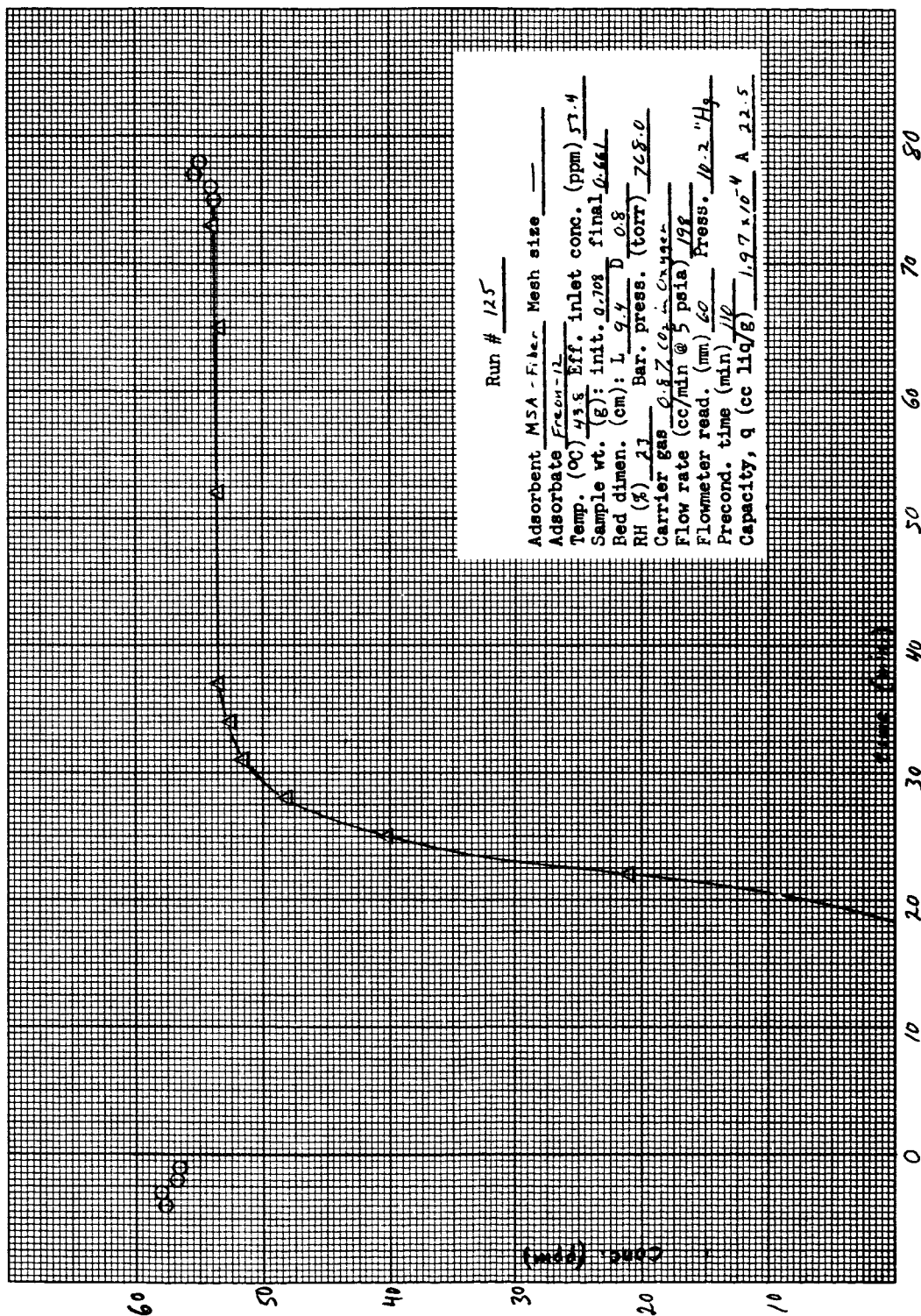


Fig. A-25 Run Number 125

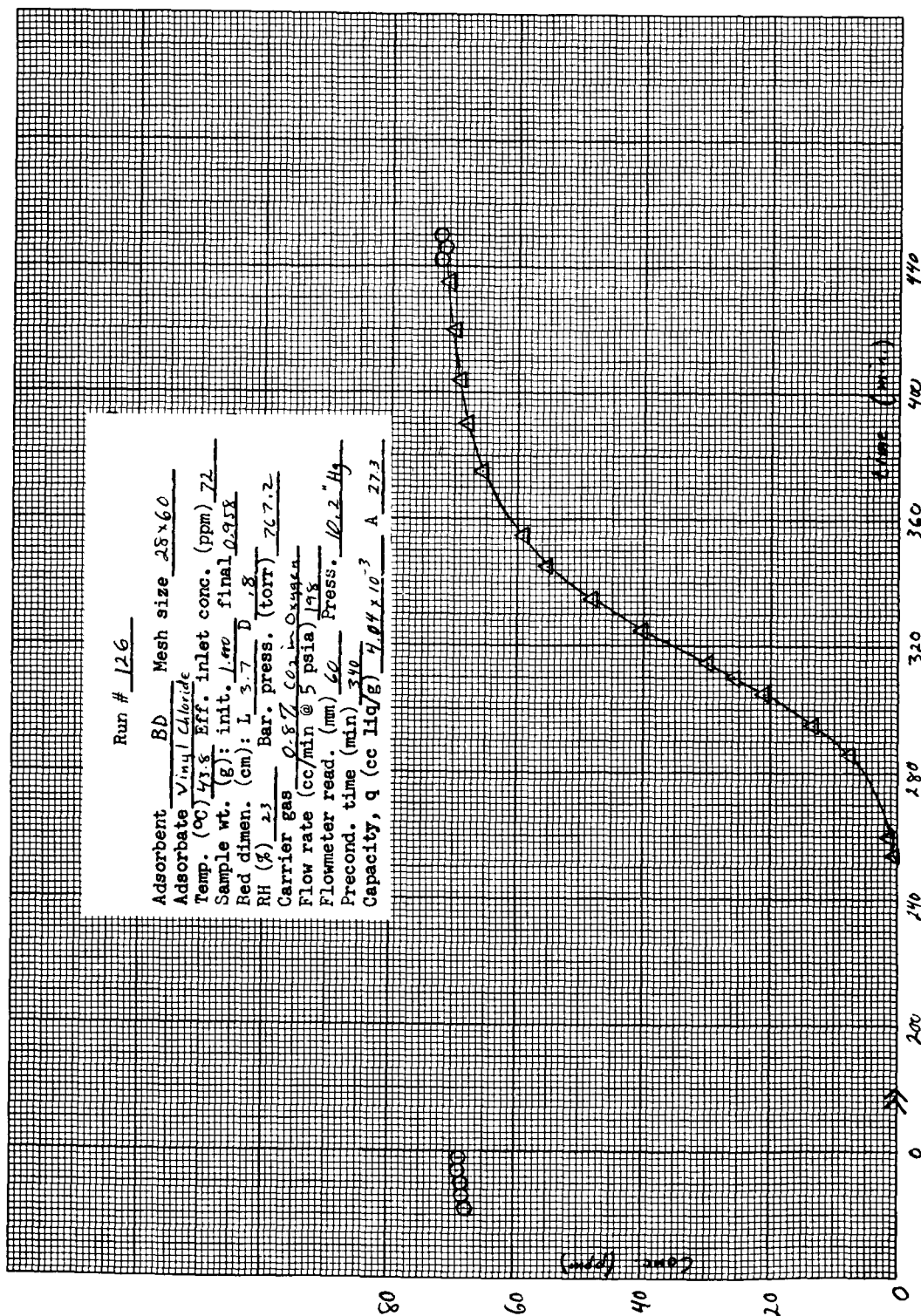


Fig. A-26 Run Number 126

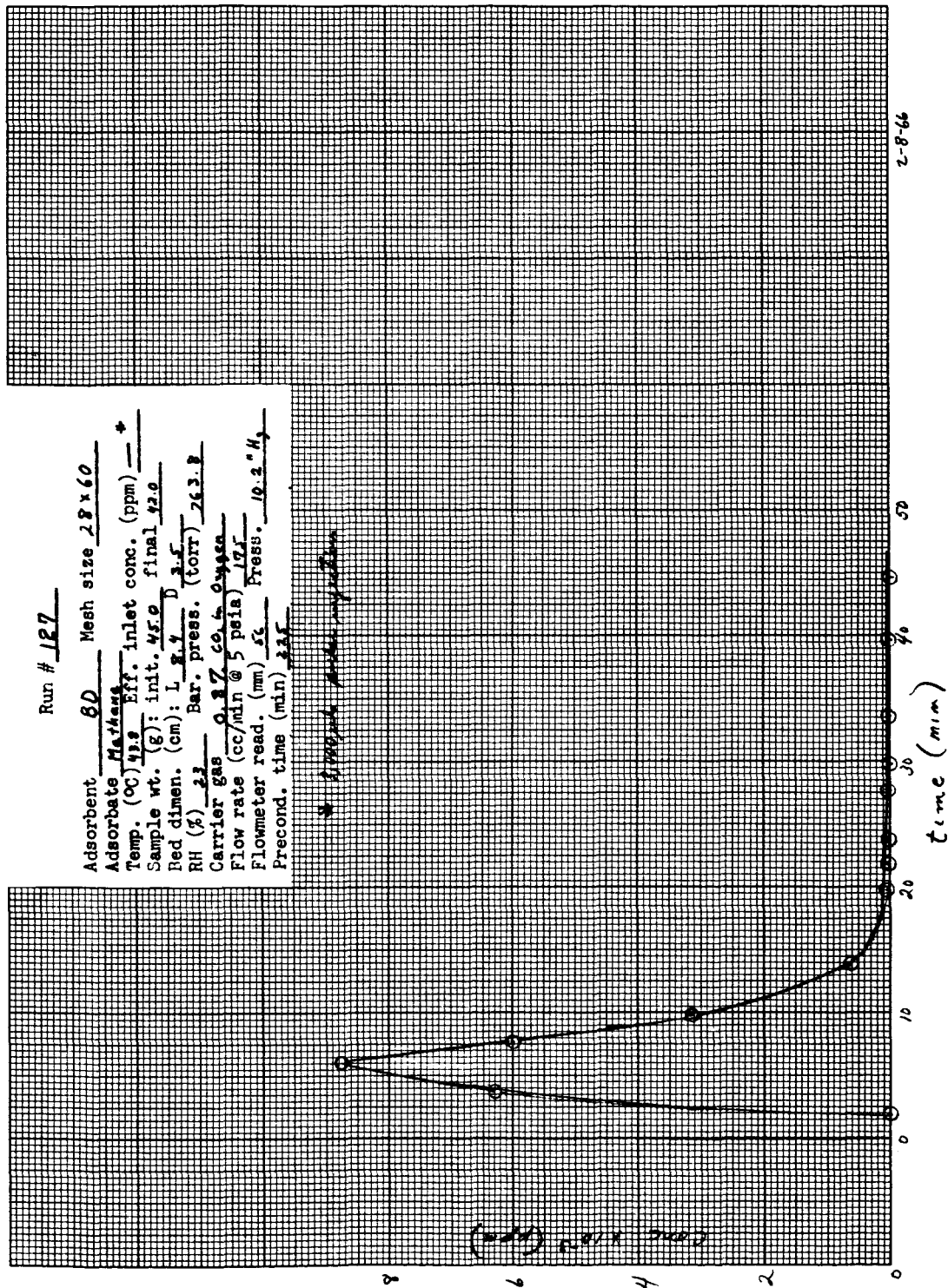


Fig. A-27 Run Number 127

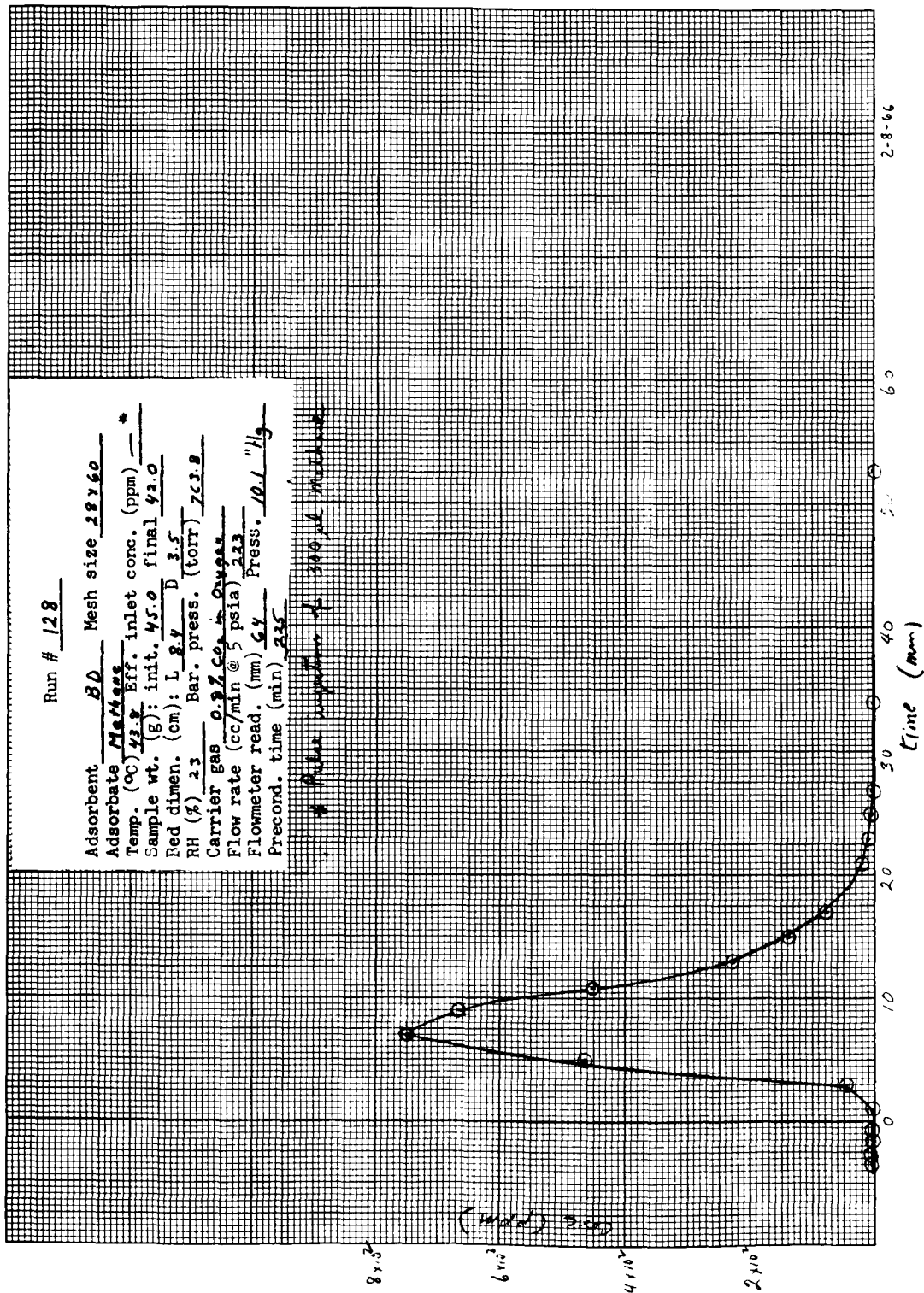


Fig. A-28 Run Number 128

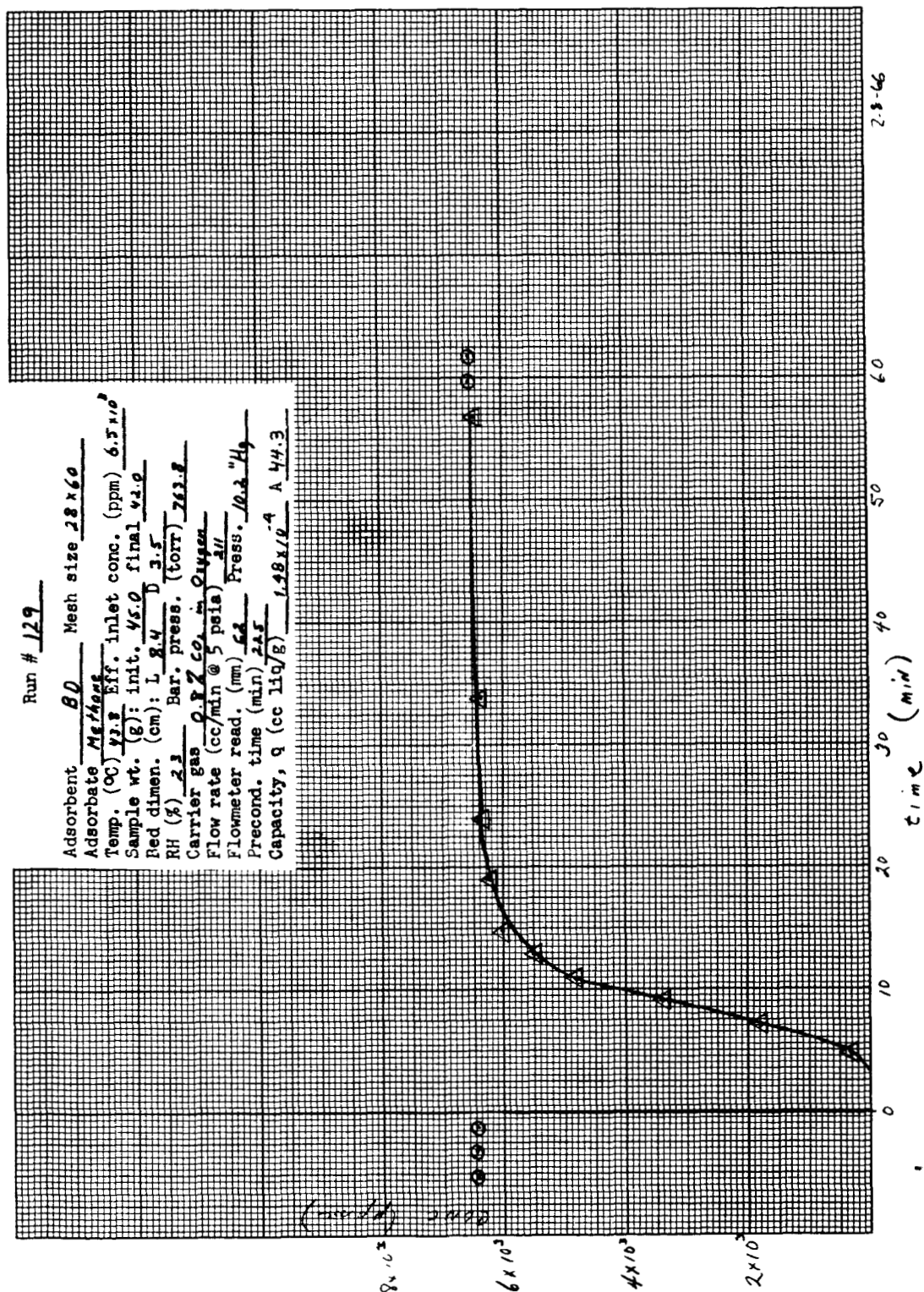


Fig. A29 Run Number 129

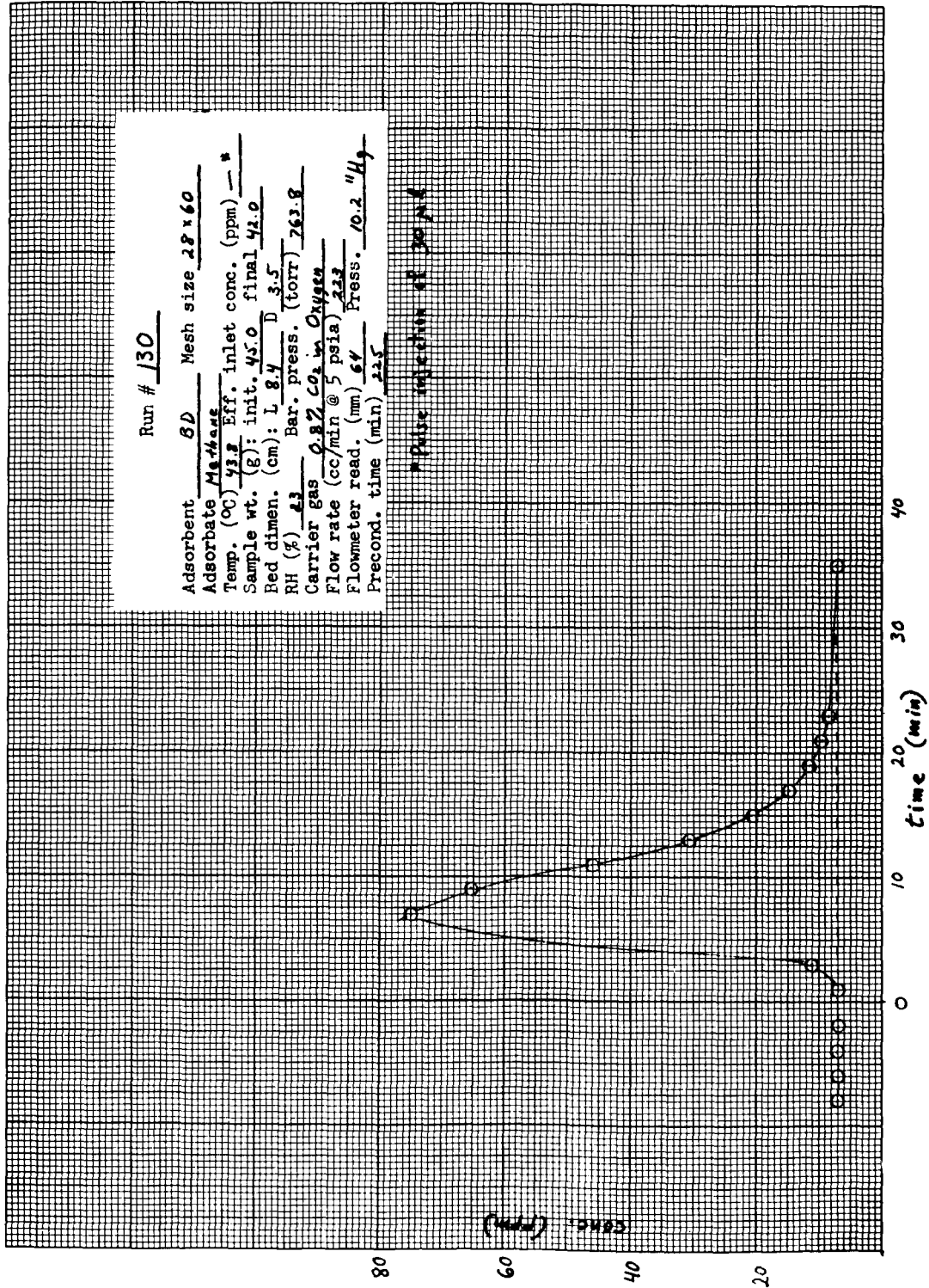


Fig. A-30 Run Number 130

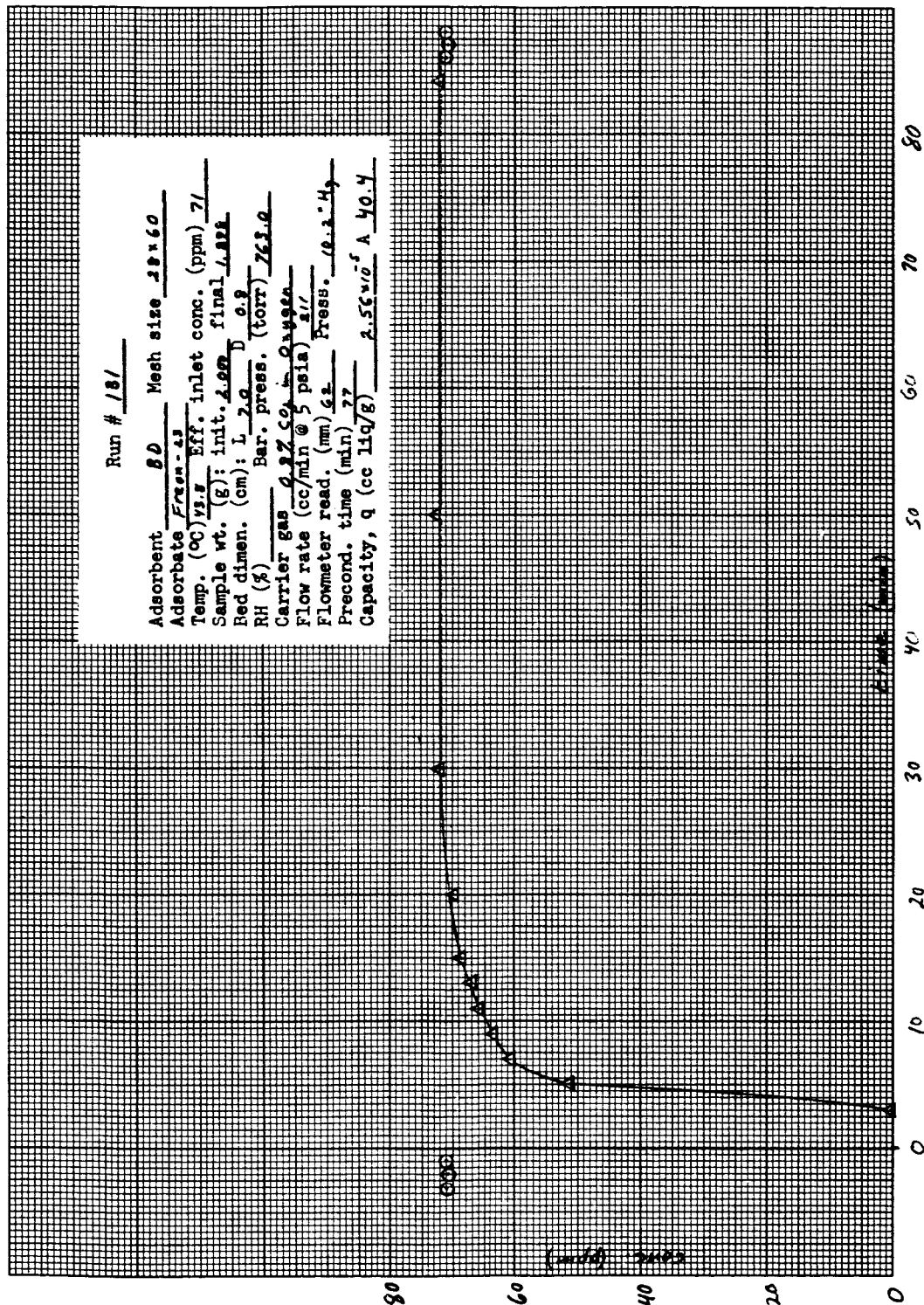


Fig. A-31 Run Number 131

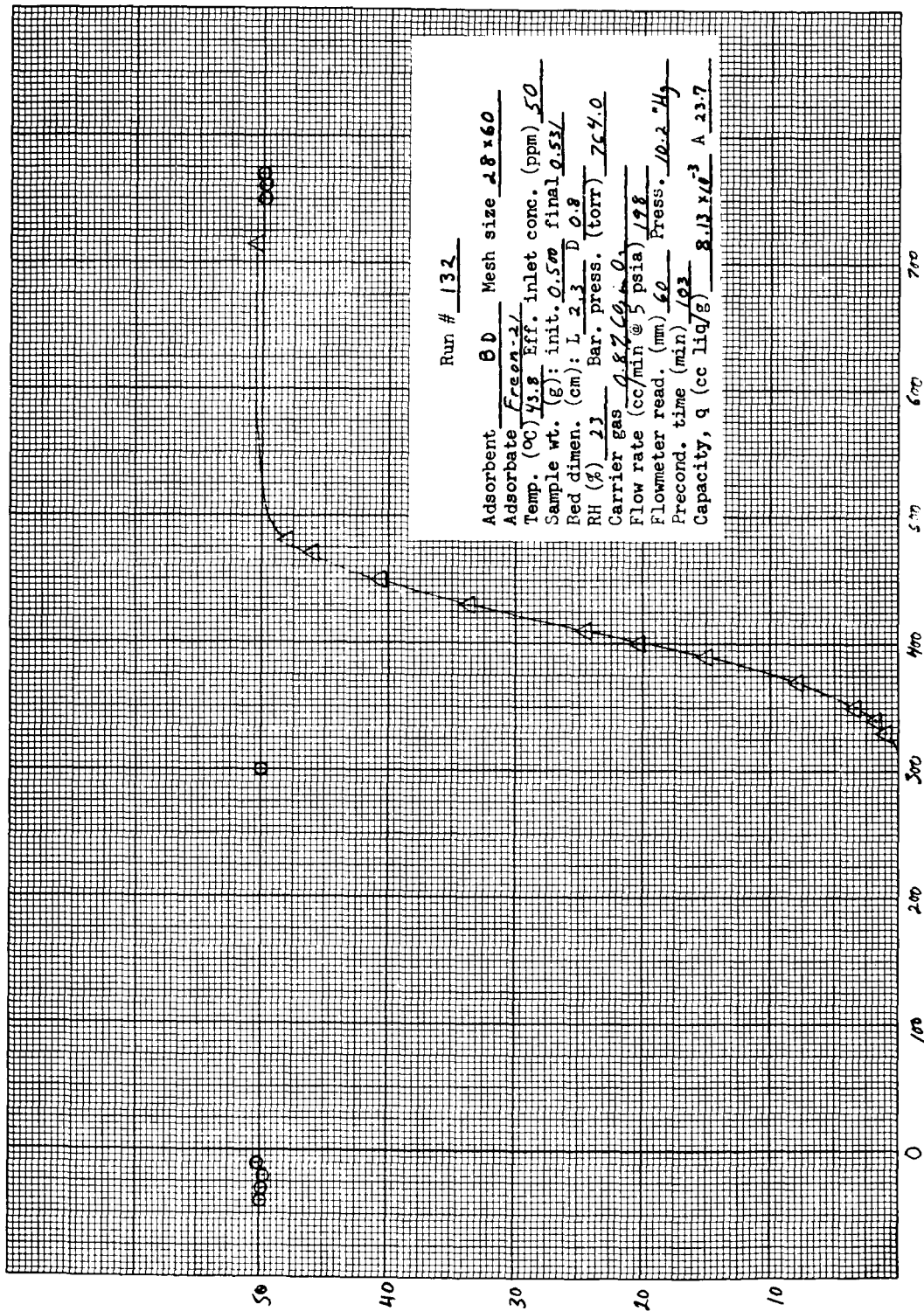


Fig. A-32 Run Number 132

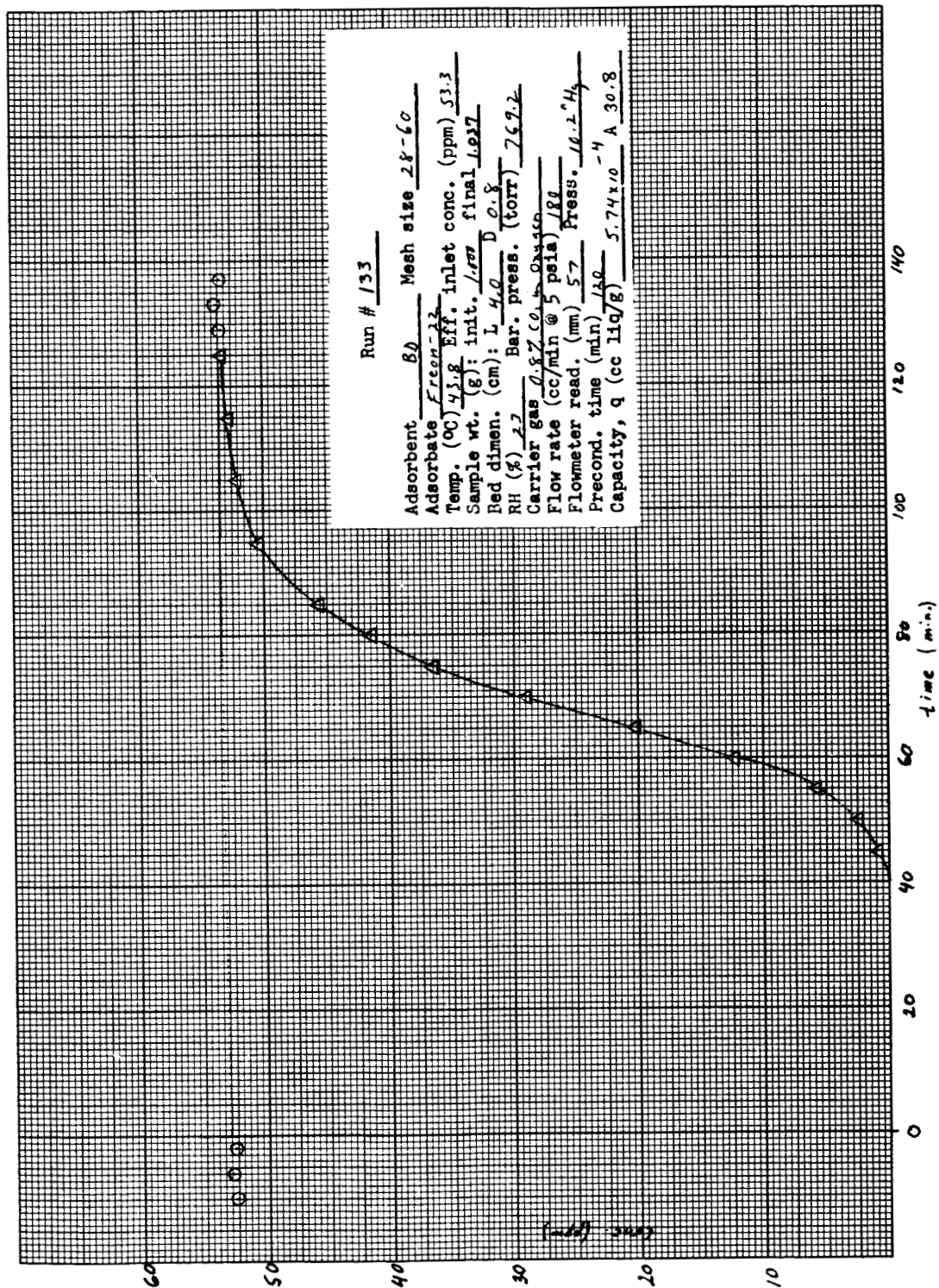


Fig. A-33 Run Number 133

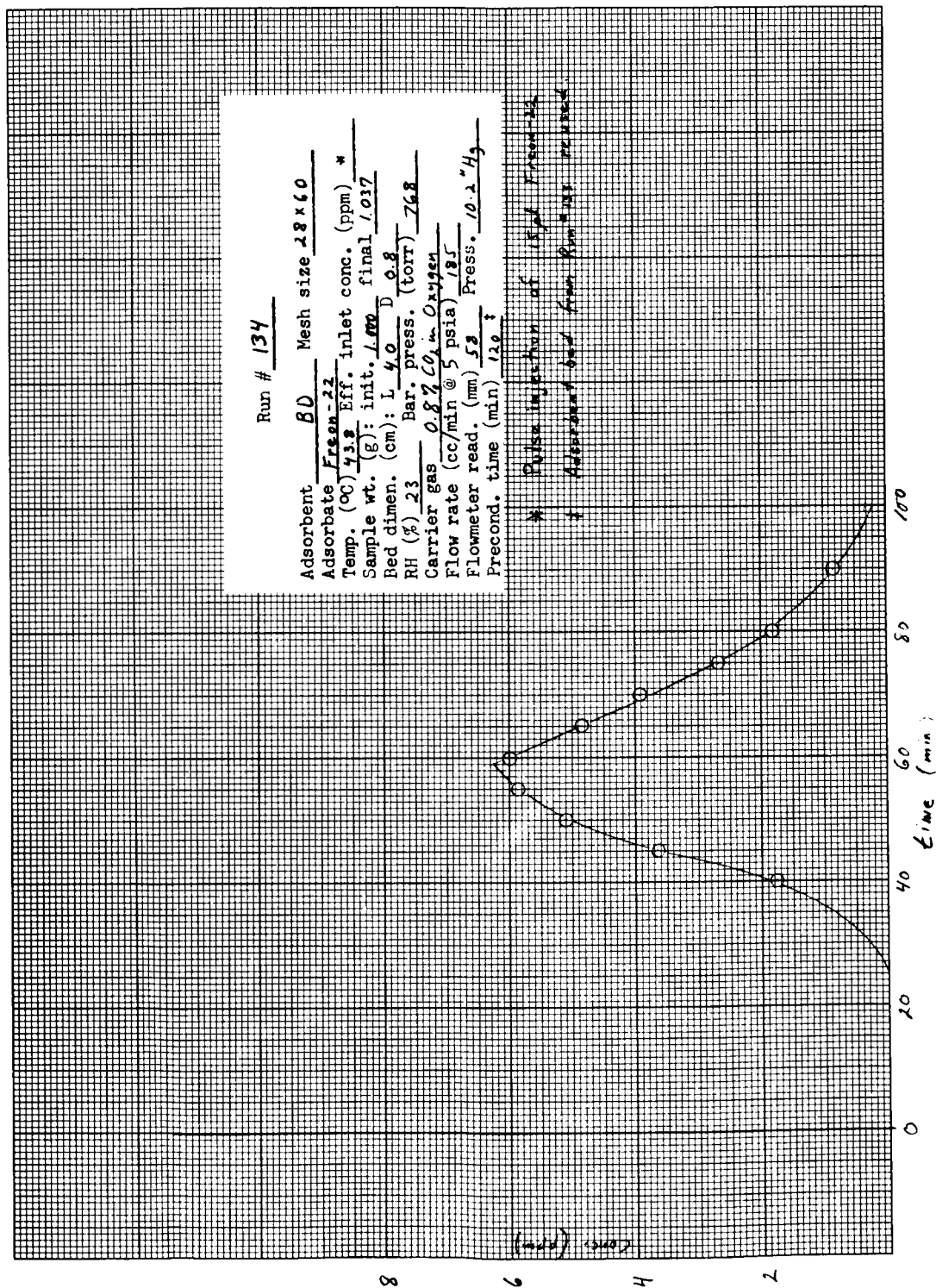


Fig. A-34 Run Number 134

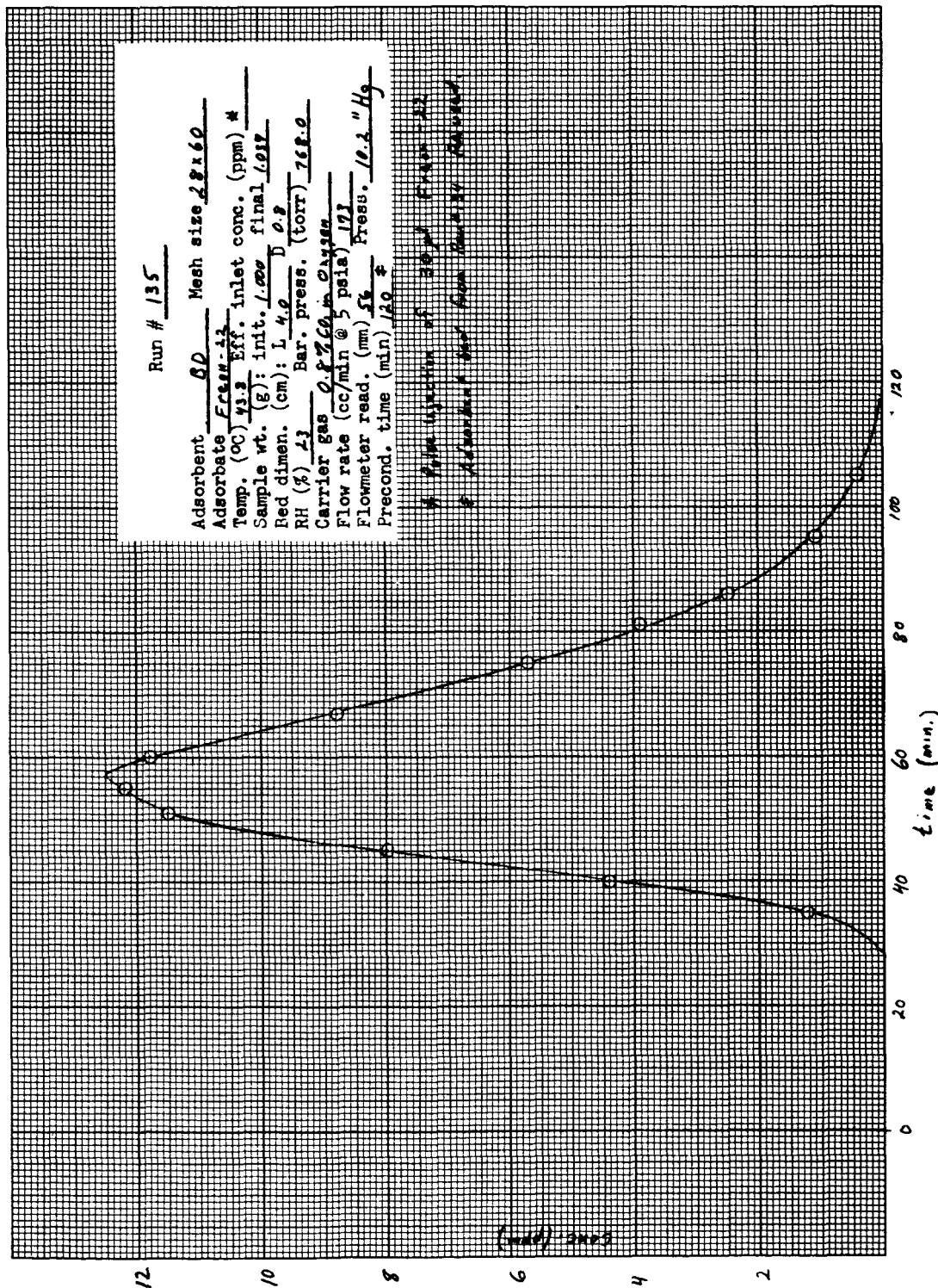


Fig. A-35 Run Number 135

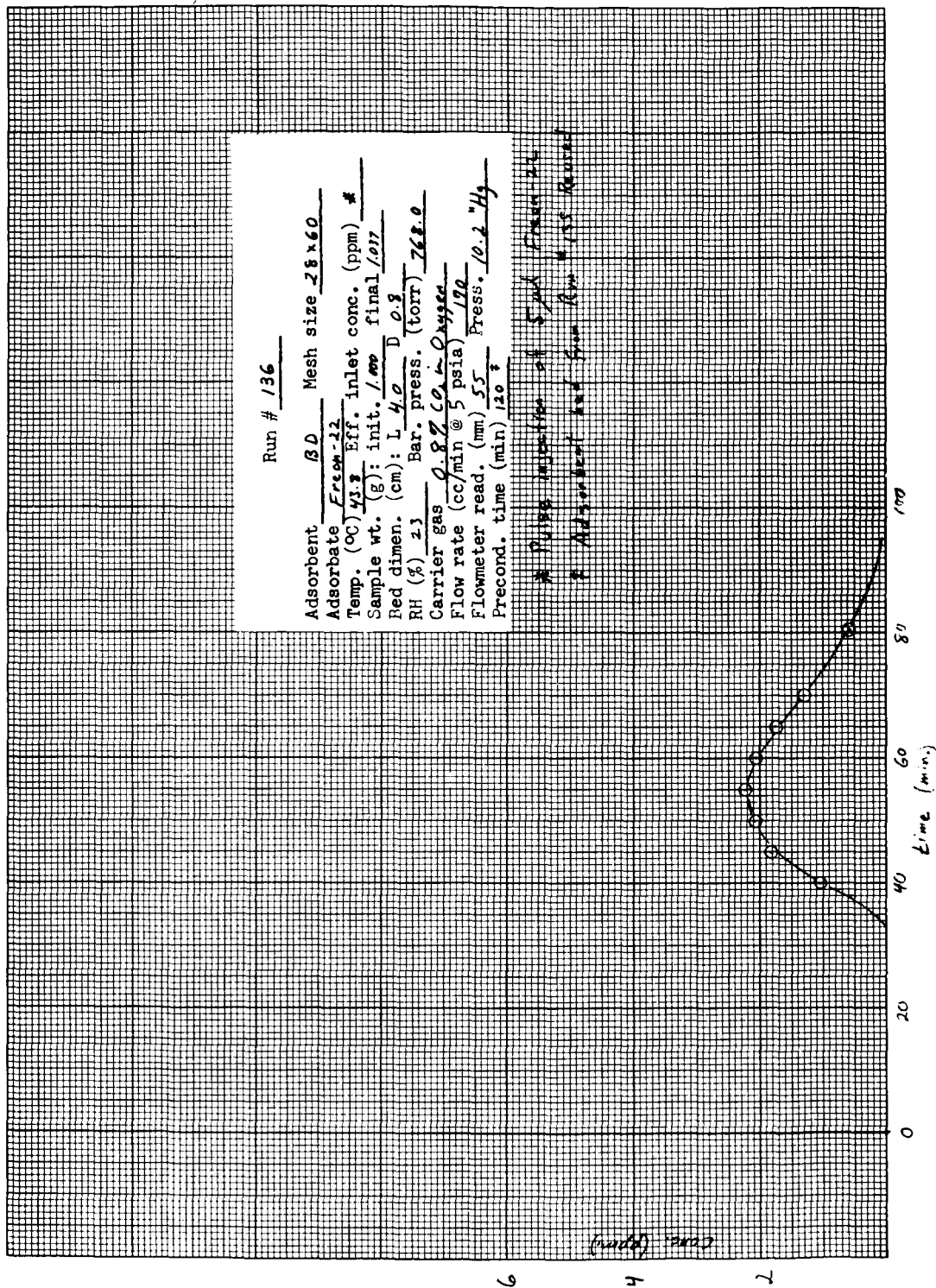


Fig. A-36 Run Number 136

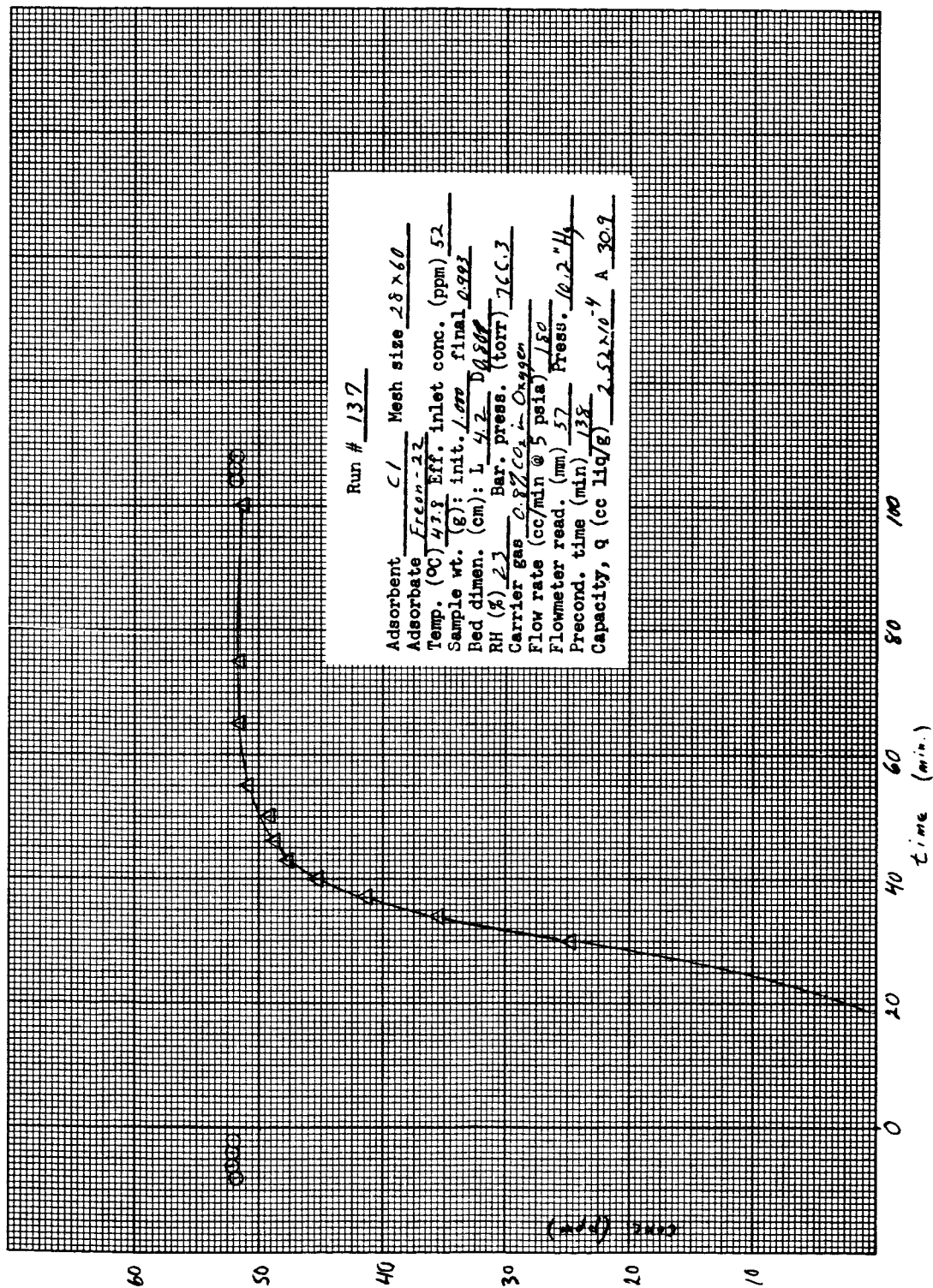


Fig. A-37 Run Number 137

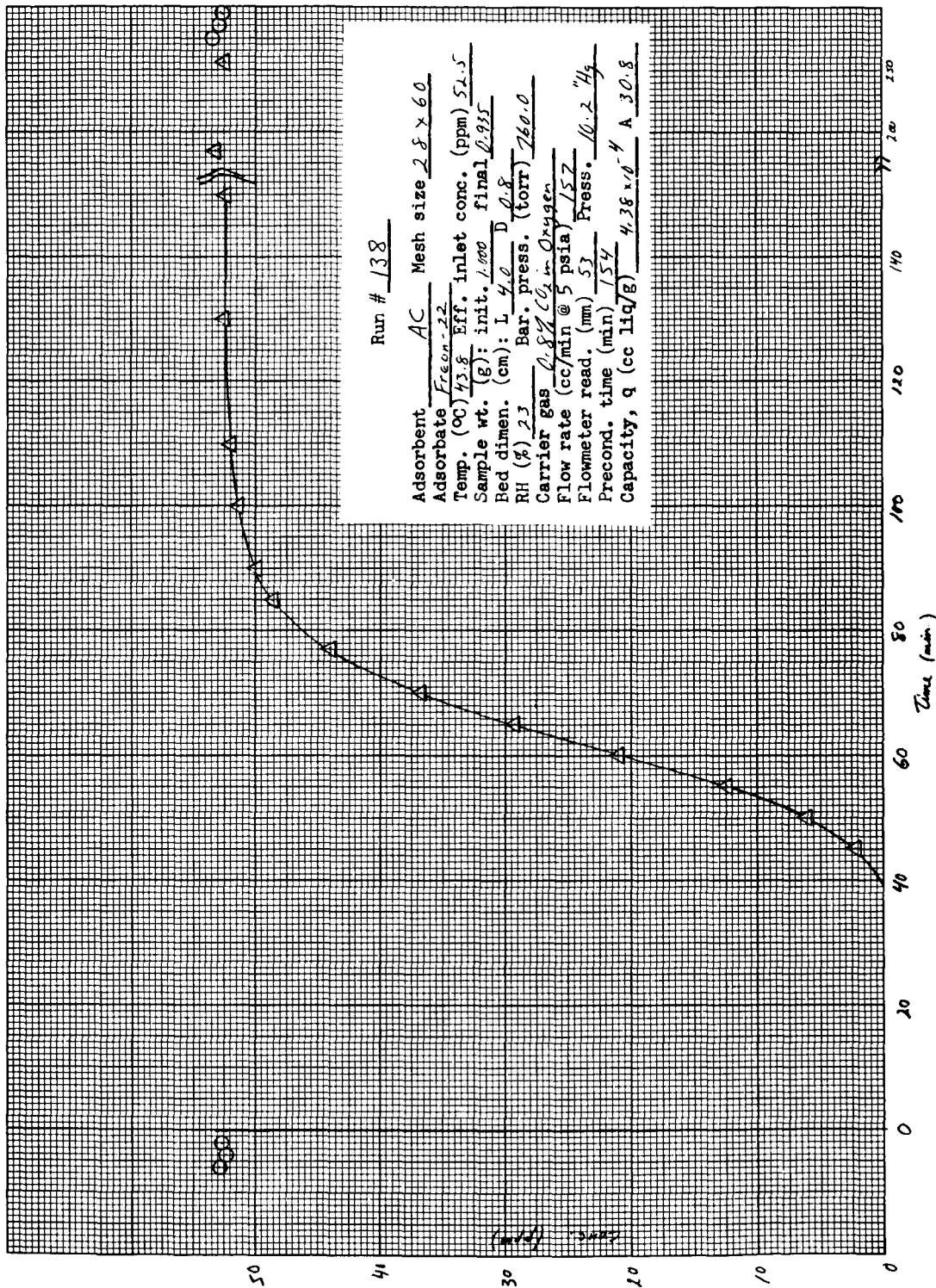


Fig. A-38 Run Number 138

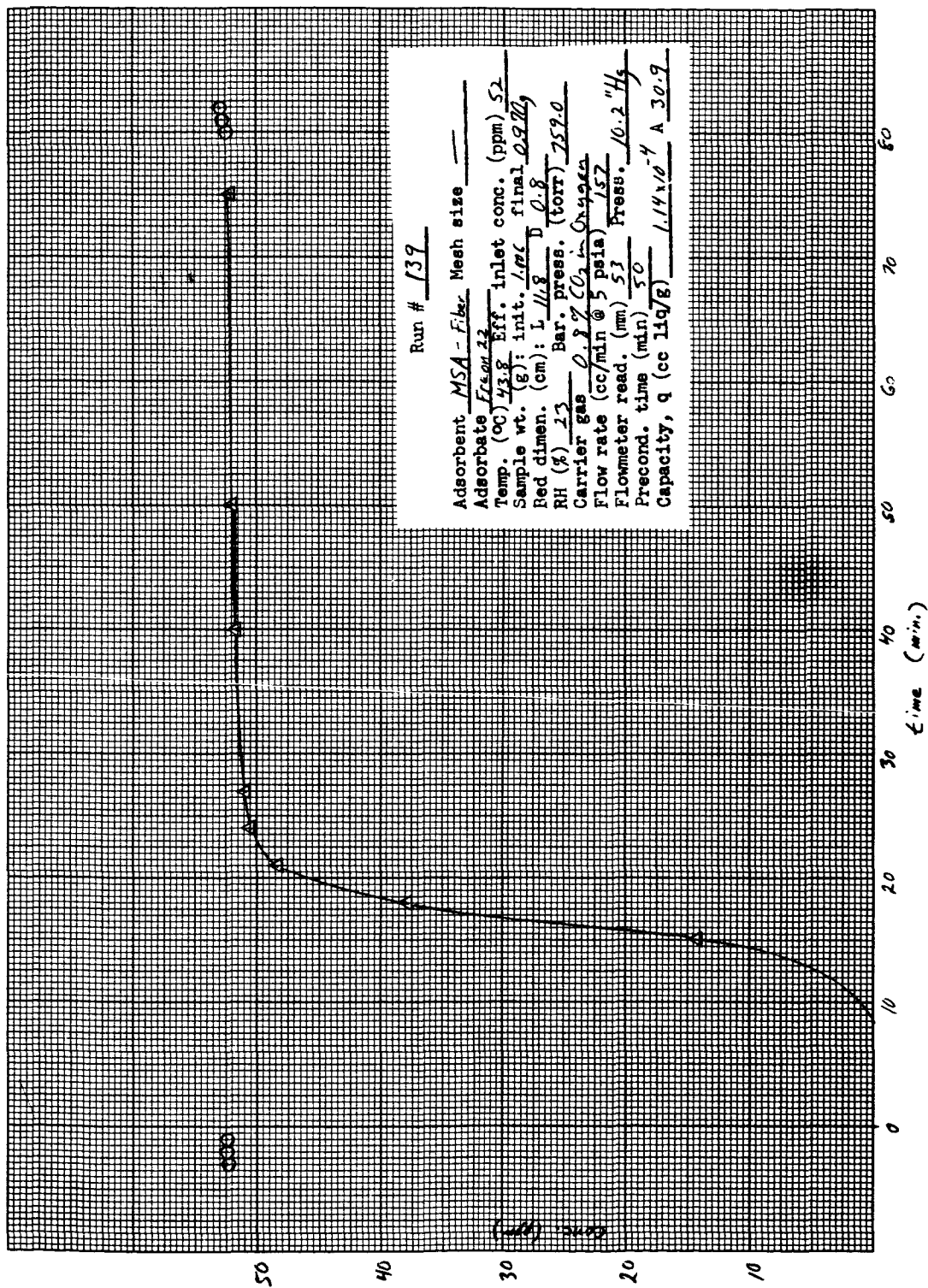


Fig. A-39 Run Number 139

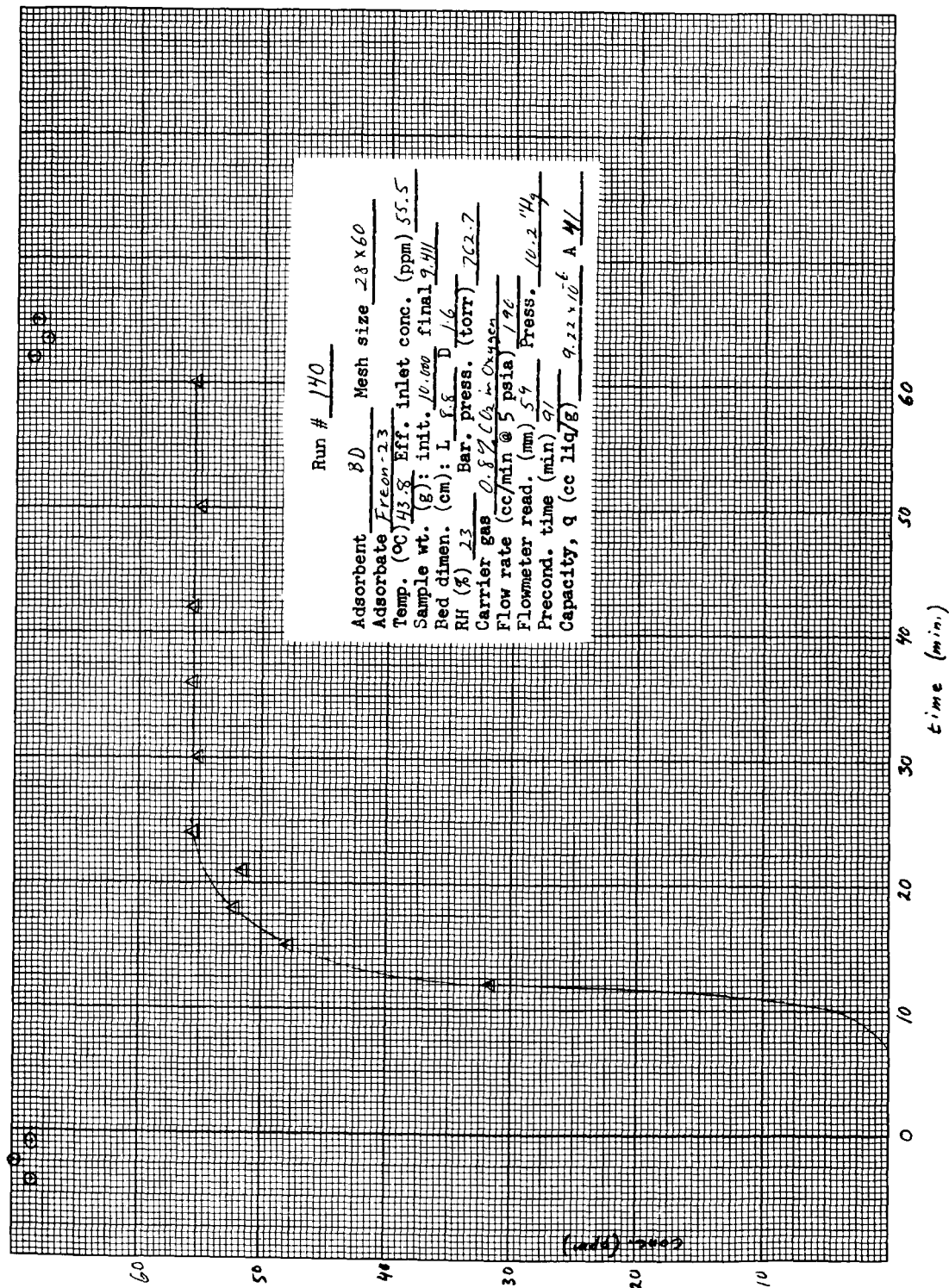


Fig. A-40 Run Number 140

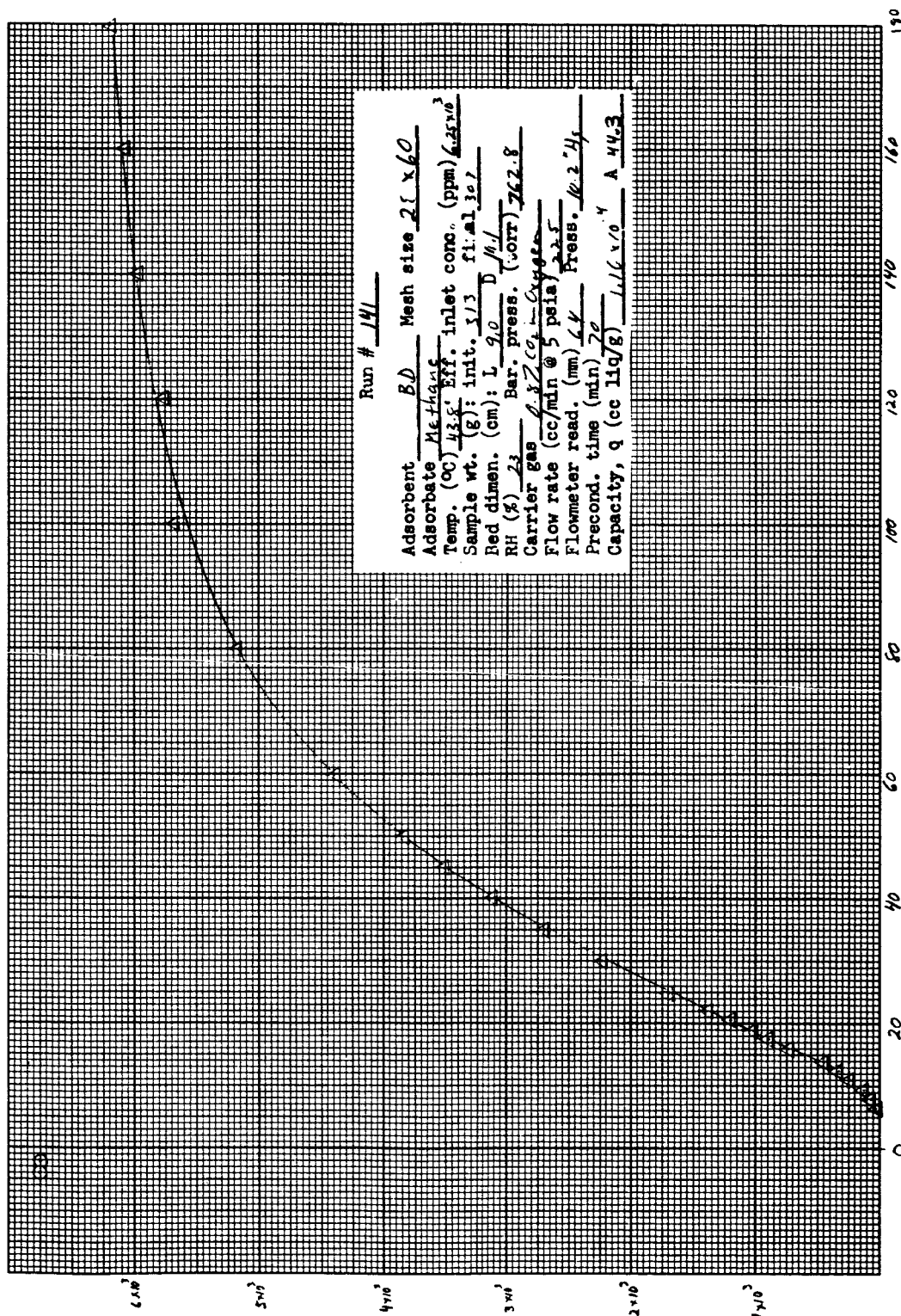


Fig. A-41 Run Number 141

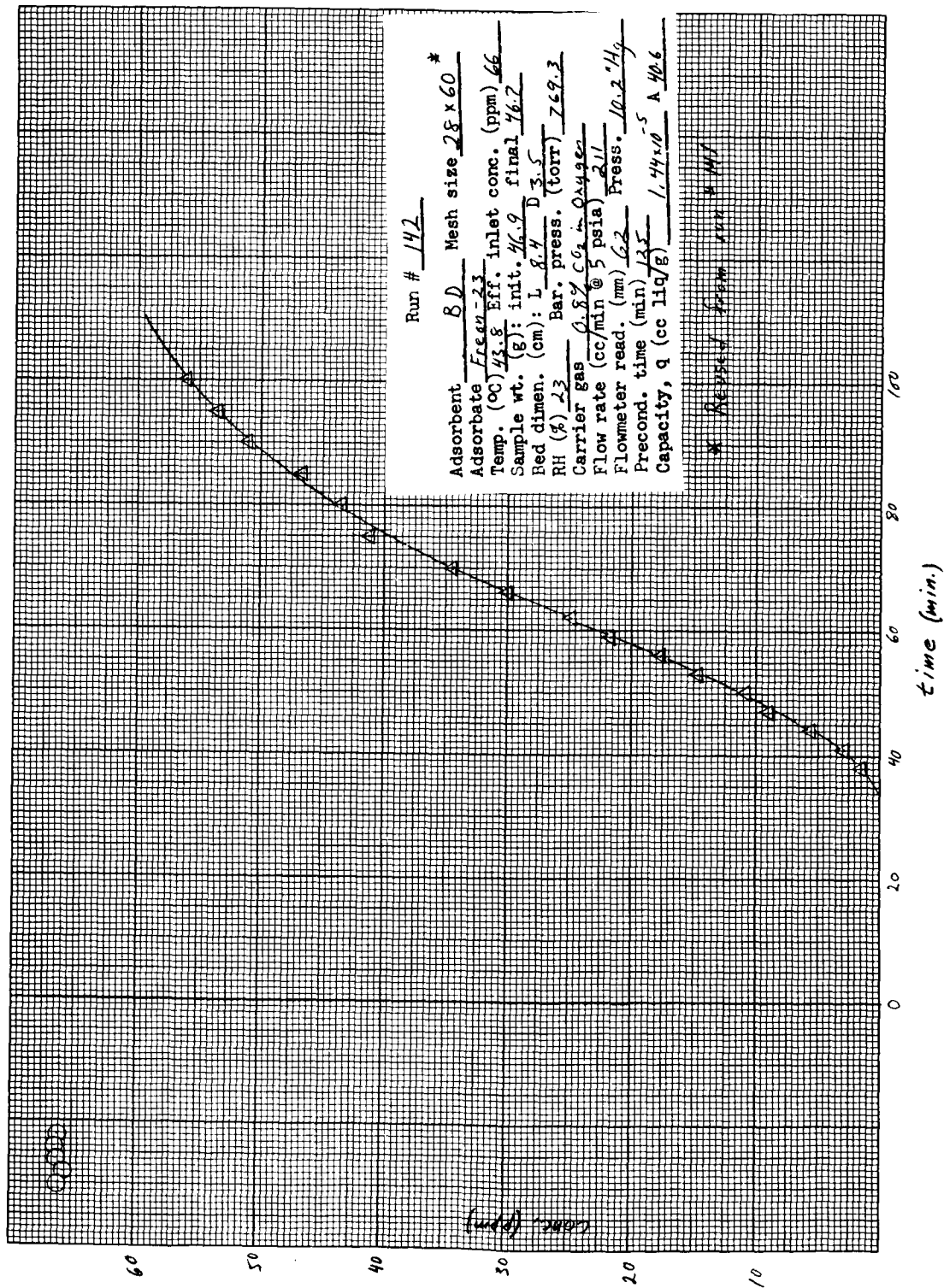


Fig. A-42 Run Number 142

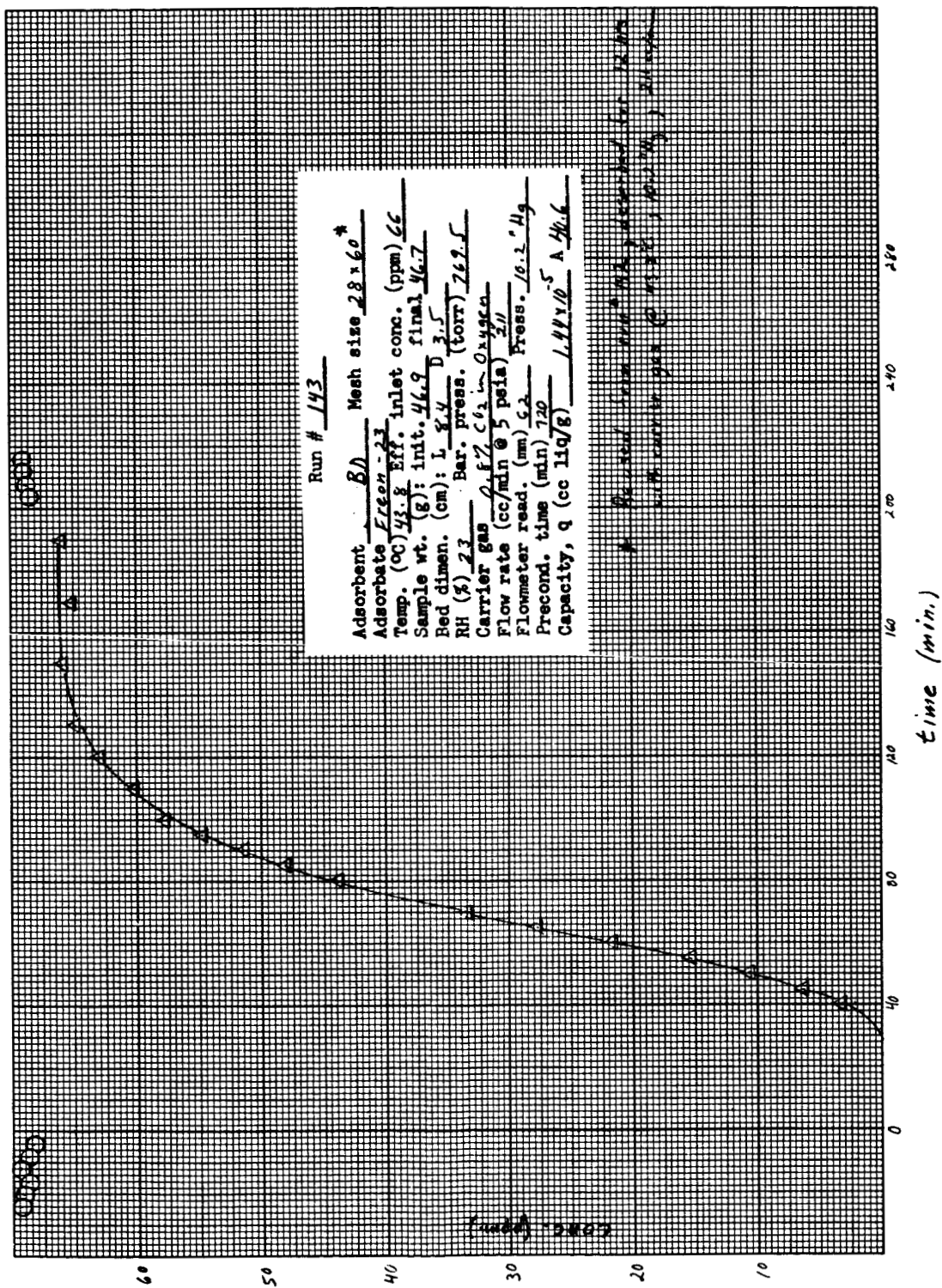


Fig. A-43 Run Number 143

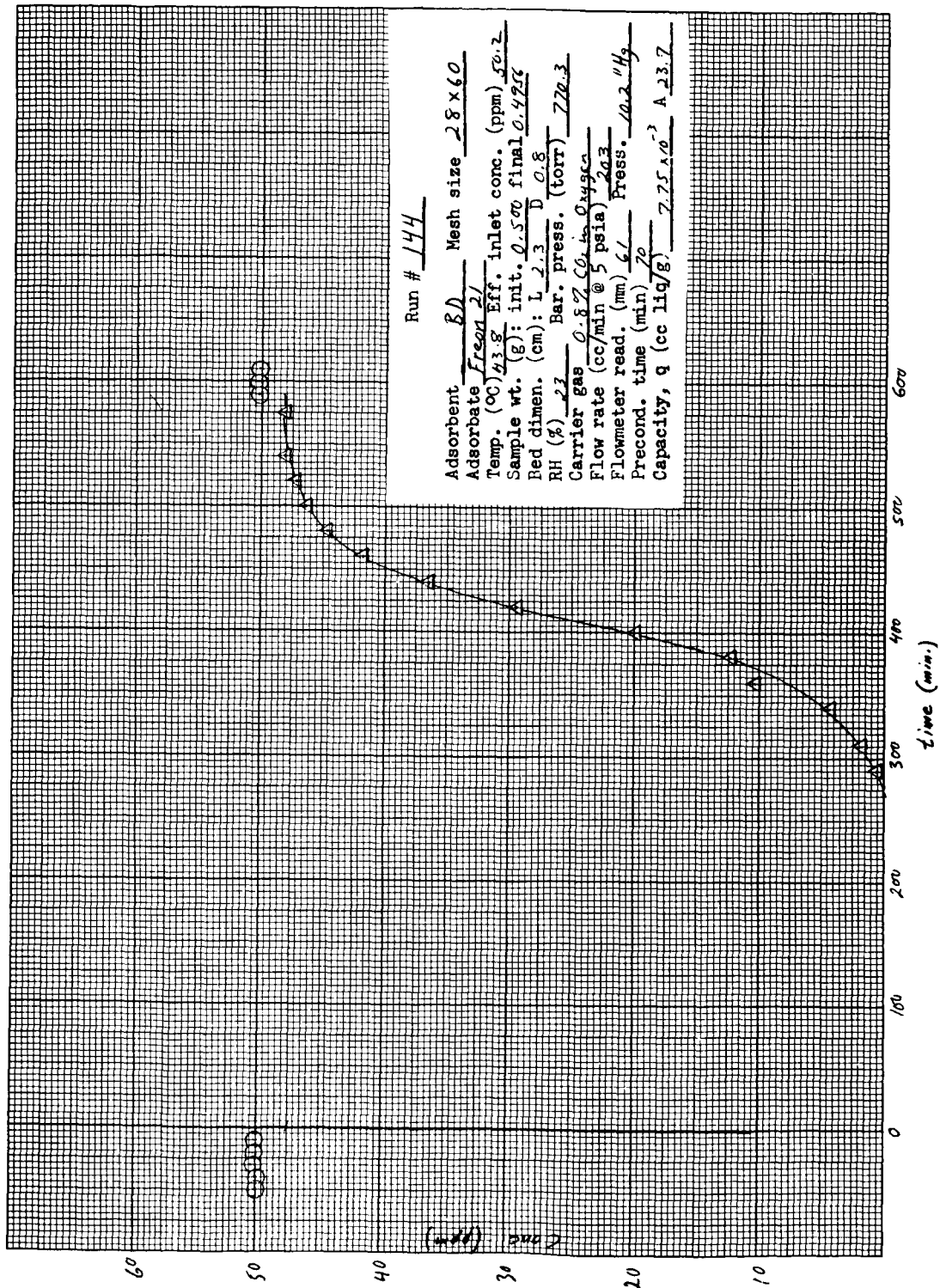


Fig. A-44 Run Number 144

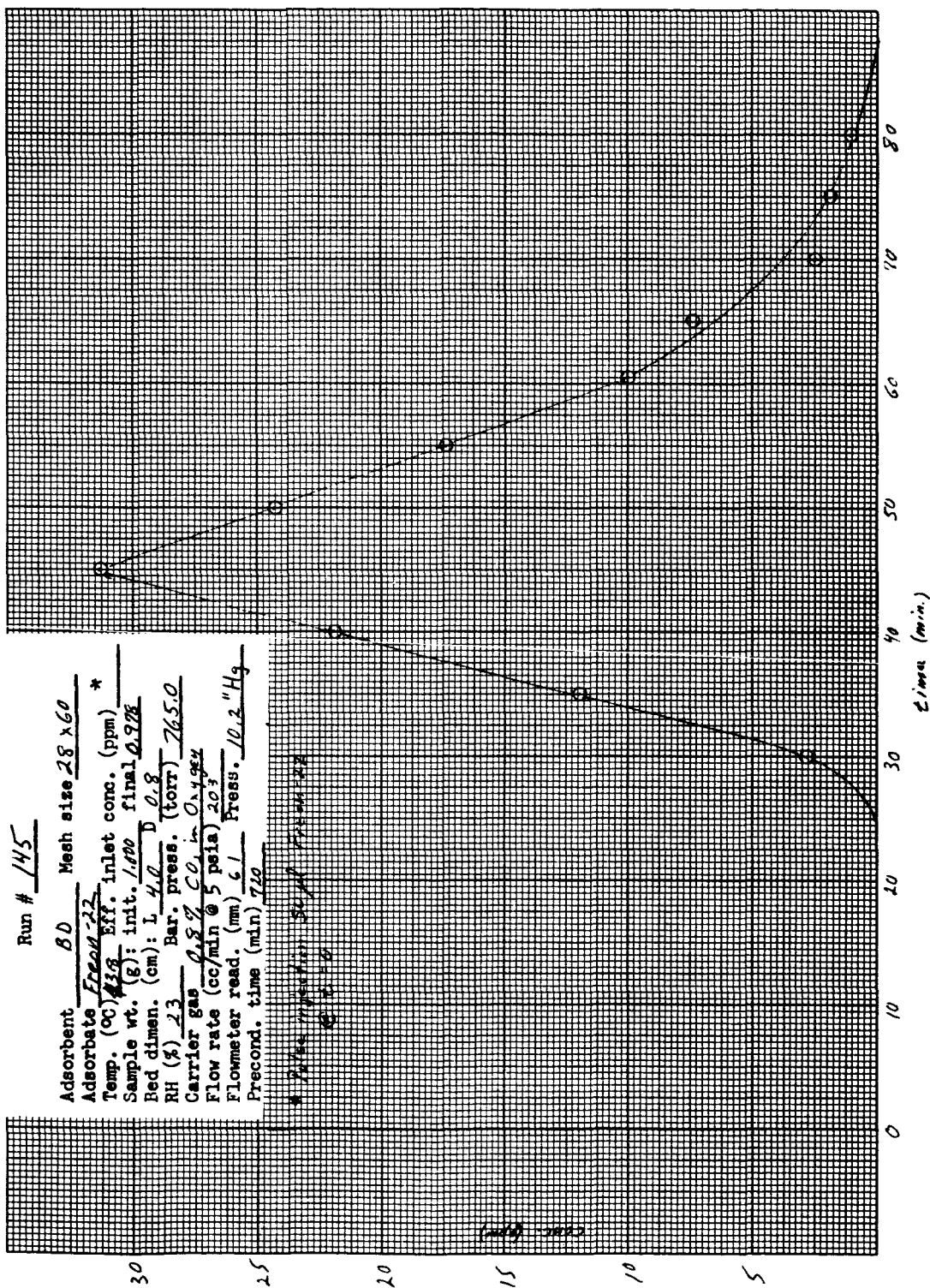


Fig. A-45 Run Number 145

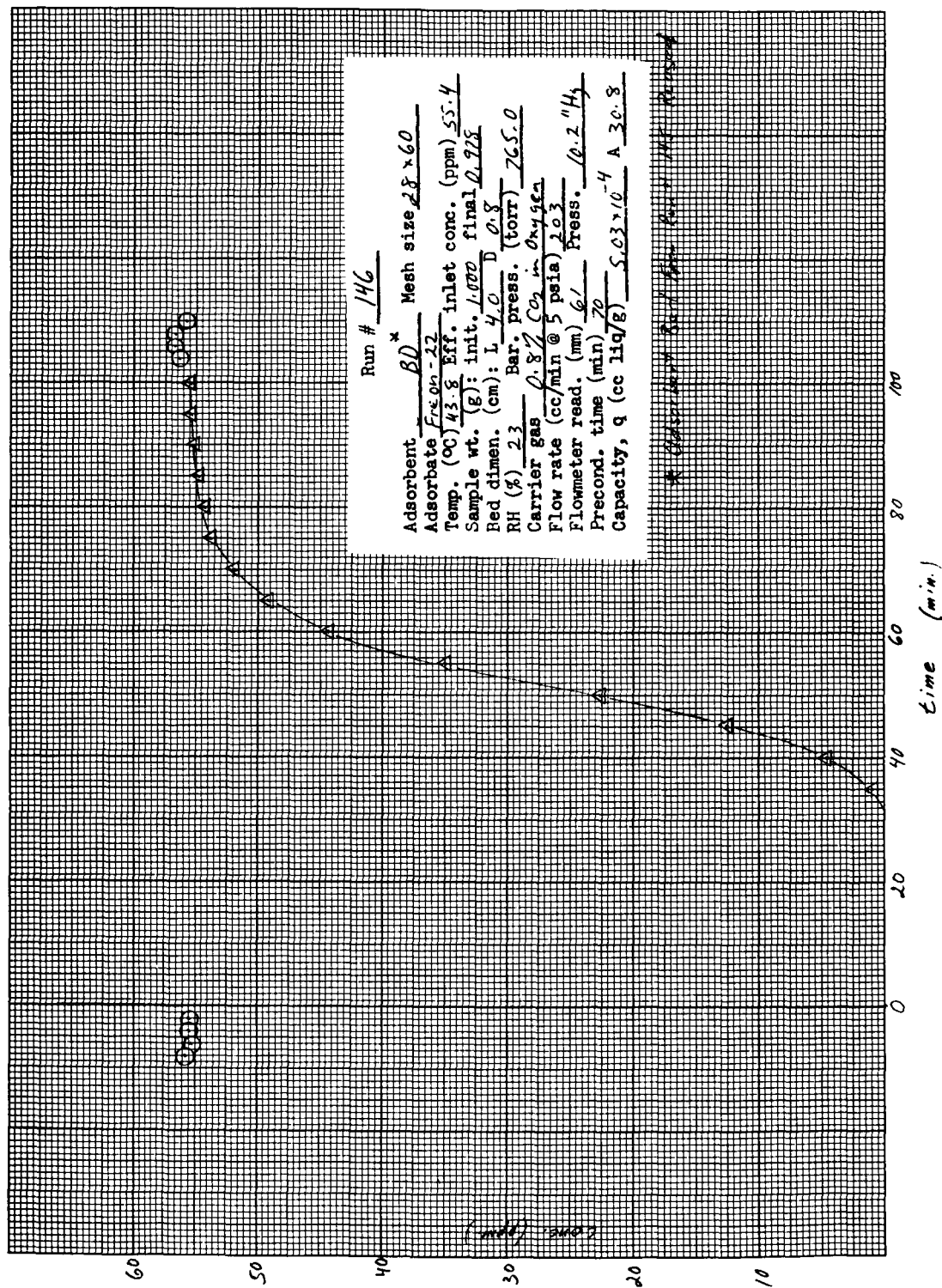


Fig. A-46 Run Number 146

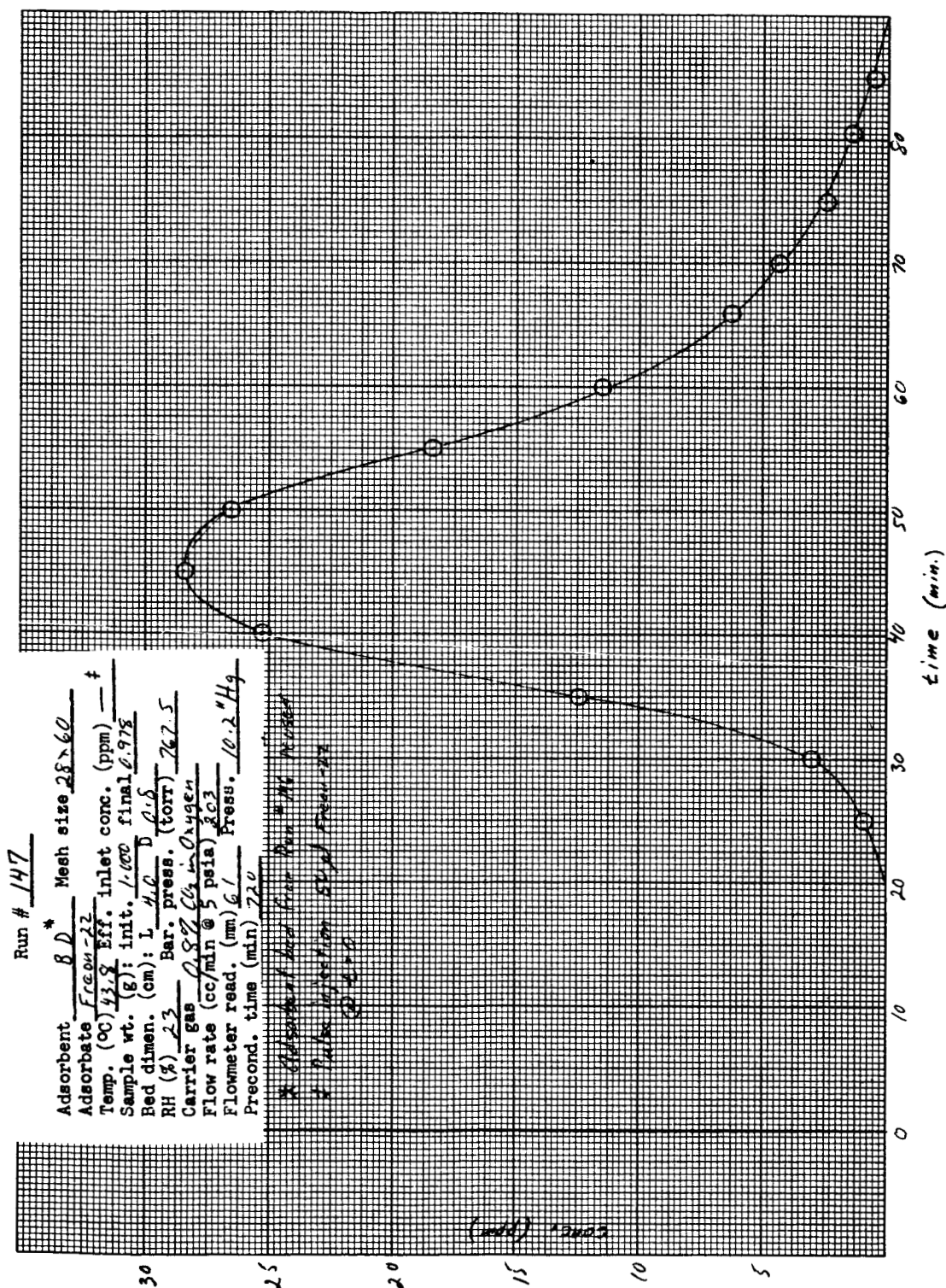


Fig. A-47 Run Number 147